CRANFIELD UNIVERSITY

ZHISONG MIAO

Aircraft Engine Performance and Integration in a Flying Wing Aircraft Conceptual Design

School of Engineering
MSc by Research

MSc Thesis
Academic Year: 2011-2012

Supervisor: Dr. C.P. Lawson
January 2012

CRANFIELD UNIVERSITY

School of Engineering
MSc by Research

MSc Thesis

Academic Year 2011 to 2012

ZHISONG MIAO

Aircraft Engine Performance and Integration in a Flying Wing Aircraft Conceptual Design

Supervisor: Dr. C.P. Lawson
January 2012

ABSTRACT

The increasing demand of more economical and environmentally friendly aero engines leads to the proposal of a new concept – geared turbofan. In this thesis, the characteristics of this kind of engine and relevant considerations of integration on a flying wing aircraft were studied.

The studies can be divided into four levels: GTF-11 engine modelling and performance simulation; aircraft performance calculation; nacelle design and aerodynamic performance evaluation; preliminary engine installation.

Firstly, a geared concept engine model was constructed using TURBOMATCH software. Based on parametric analysis and SFC target, the main cycle parameters were selected. Then, the maximum take-off thrust was verified and corrected from 195.56kN to 212kN to meet the requirements of take-off field length and second segment climb. Besides, the engine performance at off-design points was simulated for aircraft performance calculation.

Secondly, an aircraft performance model was developed and the performance of FW-11 was calculated on the basis of GTF-11 simulation results. Then, the effect of GTF-11 characteristics performance on aircraft performance was evaluated. A comparison between GTF-11 and conventional turbofan, RB211-524B4, indicated that the aircraft can achieve a 13.1% improvement in fuel efficiency by using the new concept engine.

Thirdly, a nacelle was designed for GTF-11 based on NACA 1-series and empirical methods while the nacelle dimensions of conventional turbofan RB211-525B4 were obtained by measure approach. Then, the installation thrust losses caused by nacelle drags of the two engines were evaluated using ESDU 81024a. The results showed that the nacelle drags account for about 4.08% and 3.09% of net thrust for GTF-11 and RB211-525B4, respectively.

Finally, the considerations of engine installation on a flying wing aircraft were discussed and a preliminary disposition of GTF-11 on FW-11 was presented.

Keywords: Geared Turbofan, Simulation, Nacelle, Drag, Installation.

ACKNOWLEDGEMENTS

I would like to thank AVIC and CSC who provided an opportunity for me studying in Cranfield University.

My deepest acknowledgments go to my supervisor Dr C.P. Lawson for his thoughtful assistance and guidance throughout my research.

I also wish to thank the Cranfield staff and AVIC delegates for their friendly support and collaboration during this academic year.

I would like to dedicate this thesis to my parents who worked tirelessly throughout their lives and make all efforts to support me in every possible way. I am here at this stage of my carrier only because of them.

Finally, special thanks to my wife, Qin Jiang, for her endless patience and endurance. Without her encouragement I would have never completed this thesis.

TABLE OF CONTENTS

LIST OF FIGURES

LIST OF TABLES

LIST OF EQUATIONS

LIST OF ABBREVIATIONS

AEO	All Engines Operating
AVIC	Aviation Industry Corporation of China
BFL	Balanced Field Length
BPR	Bypass Ratio
CS	Certification Specification
CSC	China Scholarship Council
EAS	Equivalent Airspeed
ESDU	Engineering Sciences Data Unit
FAR	Federal Aviation Regulatory
FPR	Fan Pressure Ratio
FW	Flying Wing
GDP	Group Design Project
GTF	Geared Turbofan
HPC	High Pressure Compressor
HPT	High Pressure Turbine
ICAO	International Civil Aviation Organization
IRP	Individual Research Project
ISA	International Standard Atmosphere
LFC	Laminar Flow Control
LPC	Low Pressure Compressor
LPT	Low Pressure Turbine
MFR	Mass Flow Ratio
MTOW	Maximum Take-off Weight
MUT	Motor and Turbine Union
NASA	National Aeronautics and Space Administration
NACA	National Advisory Committee for Aeronautics
OEI	One Engine Inoperative
OPR	Overall Pressure Ratio
OEW	Operating Empty Weight
ROC	Rate of Climb
ROD	Rate of Descent
SF	Scaling Factor
SFC	Specific Fuel Consumption
SSC	Second Segment Climb

SQRT	SQuare RooT
TAS	True Airspeed
TET	Turbine Enter Temperature
TOC	Top of Climb

LIST OF NOTATIONS

A	Area	m^2
A_{hl}	Highlight area of nacelle	m^2
A_{th}	Throat area of nacelle	m^2
A_{max}	Maximum area of nacelle	m^2
C_D	Drag coefficient	
C_f	Mean skin-friction coefficient	
C_F	Skin-friction coefficient	
C_L	Lift coefficient	
D	Drag	N
D_f	Fan diameter	m
D_{hl}	Highlight diameter of nacelle	m
D_{th}	Throat diameter of nacelle	m
D_{max}	Maximum diameter of nacelle	m
D_9	Nozzle-exit diameter	m
L	Lift force	N
L_a	After-body length of nacelle	m
L_f	Fore-body length of nacelle	m
L_{ov}	Overall length of nacelle	m
M	Mach number	
M_0	Cruise Mach number	
M_d	Drag-rise Mach number	
$M_{d,a}$	After-body drag-rise Mach number	
MFR_{crit}	Critical mass flow ratio	
P	Standard atmosphere pressure	Pa
P_t	Total or stagnation pressure	Pa
R_a	Ratio of overall length to max nacelle diameter	
Re	Reynolds number	
S	Reference wing area, Distance	m^2, m
T	Thrust, Standard atmosphere temperature	N, K
T_t	Total or stagnation temperature	K
t	Time	s
V	Aircraft speed	m/s
V_1	Decision speed	m/s
V_2	Take-off safety speed	m/s

V_A	Approach speed	m/s
Vs	Stall speed	m/s
V_{EF}	Engine failure speed	m/s
V_{TD}	Touchdown speed	m/s
V_{LOF}	Lift-off speed	m/s
$\dot{m}$	Mass flow rate	kg/s
μ	Friction coefficient	
ρ	Air density	kg/m^3
σ	Relative density	
γ	Ratio of specific heats, Climb gradient	
β	Final boat-tail angle	degree
β_c	After-body chord angle	degree
η_p	Propulsive efficiency	
η_{ov}	Overall propulsion efficiency	
η_{th}	Thermodynamic cycle efficiency	

1 Introduction

1.1 Background

Due to the increasingly stringent environment regulations and economic requirements in aero industry, the commercial aero engines have experienced an evolutionary process in the past decades. The overall pressure ratio (OPR) and turbine enter temperature (TET) have been continually increased and the propulsive cycle has developed from pure turbojets to high bypass ratio (BPR) turbofans, as shown in Figure 1-1 [1, 2]. This process has contributed to significant improvements in engine performance, in terms of fuel efficiency, safety, reliability, and also noise and emissions.

However, conflicts and barriers always accompany the development of new technologies. For instance, the increase of BPR, as one of the effective approaches to improve the propulsive efficiency, will lead to the increase of the engine size and hence higher installation drags which offset the benefit achieved on bare engine. Furthermore, as the diameter of fan increase with the BPR, the rotational speed of fan has to be reduced to protect the fan tip speed from noise and aerodynamic problems. On the other hand, the components which directly drive the fan need a high speed to achieve acceptable thermo efficiency. Therefore, a compromise has to be made to balance them.

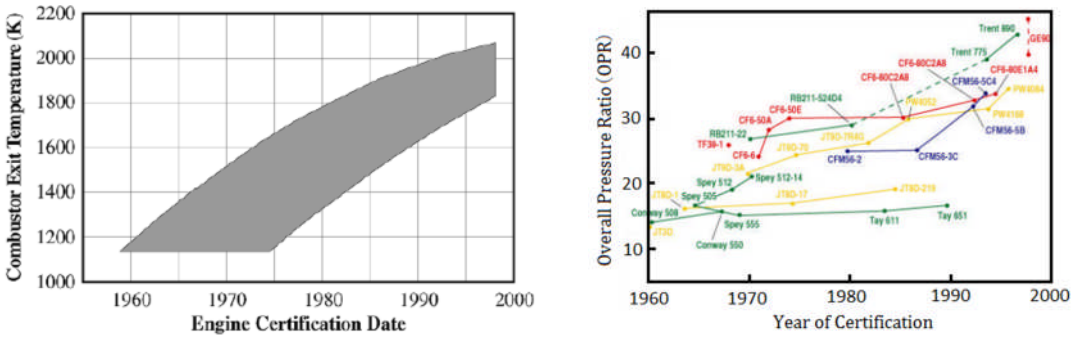

Figure 1-1 Trends of TET and OPR [1, 2]

To solve these conflicts, some approaches have being considered, such as geared turbofan (GTF) concept, which adds a reduction gearbox between the large fan and low pressure shaft to allow them operating at their optimum speed.

It offers the advantages of high BPR and avoids the disadvantages resulted by direct drive. Regarding the higher installation drags, measures could be taken to design aerodynamically efficient nacelles, and a compromise would be achieved between avoiding flow separation on the outer and inner surfaces of inlet lip, minimizing inlet flow distortion, attenuating noise leakage, reducing weight and complexity of nacelle, etc.

Obviously, there are numerous aspects should be considered in integration a high bypass aero engine on aircraft. Since the new concept engine contributes the reduction in specific fuel consumption (SFC) accompanying with the increment in size, the engine installation and improvement in aircraft performance should be evaluated.

1.2 Group Design Project

1.2.1 GDP Objectives

The objective of group design project (GDP) in this academic year 2011 was the conceptual design of a flying wing (FW) configuration aircraft which can contain 250 passengers and cover global airlines. Through the project, the entire process of aircraft conceptual design was developed and the considerations in FW configuration aircraft design were investigated.

1.2.2 GDP Progress

According to the requirements of conceptual design, the main tasks focused on the fundamental questions of configuration arrangement, cabin layout, wing geometry, engine selection, weight estimation, and performance analysis. The project was divided into somewhat distinct three phases: derivation of requirements, design a conventional aircraft as baseline and design a FW configuration aircraft (FW-11) comparing with baseline aircraft, as presented in Figure 1-2. Twenty-three students were assigned in several sub-teams according to their individual tasks in the project. The author’s main assignments were aircraft performance calculation, engine market investigation, engine selection and installation.

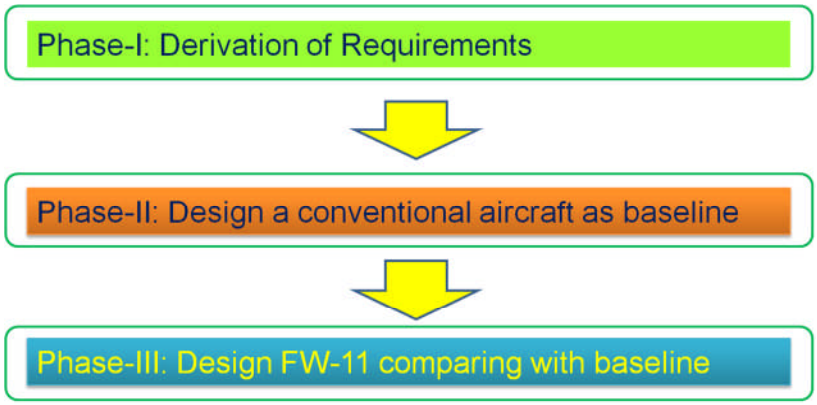

Figure 1-2 General design process in GDP [3]

1.2.3 Issues in GDP

In GDP phase, two geared concept engines (GTF-11) were deployed on FW-11, which aimed to provide sufficient thrust as well as high fuel efficiency, low noise and emission for aircraft.

Due to the time constraint, however, the preliminary dimension of engine and nacelle were sized using empirical equations and the thermodynamic characteristics of engine were only estimated from current aero engines. As far as the author was concerned, these equations just covered the relative low BPR (generally range from 4 to 7) engines, which may be not suitable for very high BPR (over 9) engines. Moreover, further investigation of the thermodynamic parameters related to engine performance and the contribution of the new concept engine to aircraft performance improvement should be developed. Besides, due to the unique concept of the aircraft, the installation of GTF-11 on FW-11 may be different with that on a conventional aircraft. The related issues, such as aerodynamic, flight control and safety should be considered and discussed.

1.3 Aim and Objectives

Based on the issues in GDP, a further research is developed in this thesis. The objectives of the study mainly include following aspects:

- Through the study of preliminary GTF engine modelling, analyze the main considerations in selection of key parameters related to engine performance.

- Through aircraft performance modelling and calculation, verify that the GTF-11 meet the requirements of FW-11 and evaluate the benefits of new concept engine in aircraft performance improvement.
- Through the study of preliminary nacelle design and aerodynamic performance calculation, analyze the key parameters in nacelle design and evaluate the nacelle installation drag.
- Through the study the installation of GTF-11 on FW-11, identify the considerations of engine installation on a FW configuration aircraft.

1.4 Methodology and Thesis Structure

According to the objectives of the research, the thesis was divided into eight chapters and corresponding methodologies were employed to achieve the different objectives.

In Chapter 2, the literature review focus on characteristics of the FW aircraft and GTF engine was presented.

Then the preliminary requirements for engine sizing were estimated in Chapter 3. The thrust requirements of the aircraft and the SFC target for GTF-11 were calculated. Also, the preliminary dimensions of engine were estimated from current very high BPR engines.

Taking cruise condition as a design point, a geared concept GTF-11 engine model was created using the simulation software, TURBOMATCH. The key parameters related to engine performance were analyzed and the main cycle parameters were determined based on the SFC target and fan diameter constraint. Then, the maximum take-off thrust was verified by the second segment climb thrust and take-off field length requirements of the aircraft. After that, the engine performance at off-design points such as take-off and climb were simulated for aircraft performance calculation. These works were presented in Chapter 4.

In Chapter 5, an aircraft performance spreadsheet model was developed based on the methods from Martin E. Eshelby [4] and L. R. Jenkinson [5]. Then, the performance of FW-11 was calculated to verify that the performance

characteristics of the GTF-11 satisfy the design requirements of the aircraft. Meanwhile, the effect of ambient conditions on aircraft field performance was evaluated as well. After that, a comparison between GTF-11 and conventional engine, RB211-524B4, was conducted to identify the benefits of the new concept engine on aircraft performance improvement.

In Chapter 6, the studies of nacelle design were undertaken by NACA and ESDU approaches. A mathematical model of nacelle was developed based on empirical methods and NACA 1-series rules. Then, the sensitivity of key parameters related to nacelle aerodynamic performance was analyzed. Following that, the nacelle of GTF-11 was sized and the drag of nacelle was calculated using ESDU 81024a [6]. Finally, the installation loss of the engine was evaluated.

In Chapter 7, the considerations of engine installation on a FW configuration aircraft were discussed and the preliminary position of the GTF-11 on FW-11 was presented.

Finally, a summarization and a brief discussion of the whole project as well as some suggestions for further research were presented in Chapter 8.

2 Literature Review

2.1 Introduction

The literature review mainly focuses on technologies of FW aircraft and GTF engine. Since the FW is a new concept configuration comparing with conventional aircraft, the associated knowledge should be concerned for further aircraft performance and engine installation analysis. Then the characteristics of GTF engine and basic gas turbine performance simulation theory are investigated, which are necessary in engine modelling and performance analysis.

2.2 Flying Wing

2.2.1 Definition of Flying Wing

What is a FW? Before dealing with the main subject of the thesis, it is considered important to define what is meant by FW.

As we know, a conventional aircraft consists of several parts according to its function in the final aircraft. The fuselage for carry passengers, wing for the production of lift and tails for the production of stability and so on. All of these parts have been optimized by engineers over the years. Although it easy to achieve an improvement in each individual part, these sometimes will conflict with each other. Due to this reason, one may think why not integrate all parts and optimize for a common purpose?

The idea of integrating the several aircraft functions in just one surface, the wing, is not new. Already at the beginning of aviation, many aircraft designers and pilots would have liked to omit all parts that increase the drag, such as fuselage and tails. There are some aircrafts based on this viewpoint can be found in the history of aviation, such as Northrop YB-35 and B-2. Because produce less drag than a conventional aircraft, these all-wing aircrafts always have excellent payload and range capabilities.

There was a primary aircraft classification in relation to its configuration by Lippisch [7]. As shown in Figure 2-1, the aircrafts were classified into four

categories by its planform shape. The obvious characteristic to distinguish these aircrafts is the position of the wing and the stability surface. As a tailless aircraft, it has no stability surface comparing to the conventional aircraft which have wing, fuselage and a rearward tail.

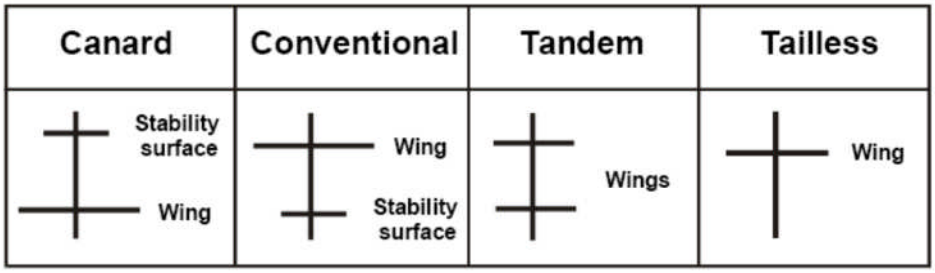

Figure 2-1 Lippisch aircraft classification [7]

Based on Lippisch's classification, there was a further definition of the tailless configuration, as presented in Figure 2-2 [8]. It can be found that a particular kind of tailless aircraft is a purest wing, known as FW. In this configuration there is completely no division between the central body and wing, but all of it is just a wing, and carrying in its interior the entire load.

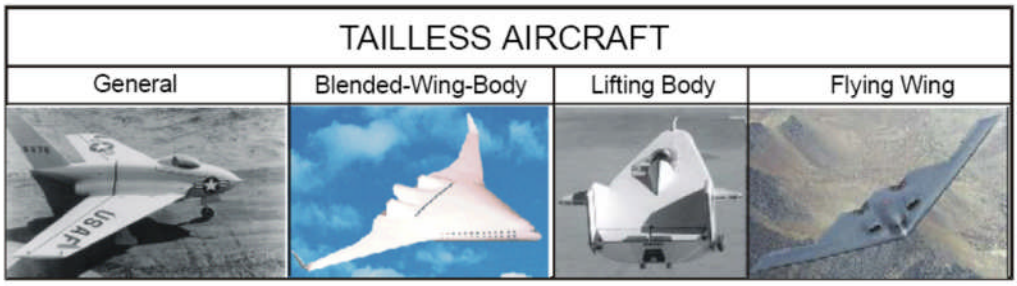

Figure 2-2 Tailless aircraft classification [8]

2.2.2 Characteristics of Flying Wing

Unconventional configurations always appear to possess significant advantages. Compared with a conventional configuration aircraft sized for the same design mission, the FW configuration has substantial improvement in aerodynamic efficiency, structure weight and fuel consumption [9].

The drag reduction contributes to the FW be the most aerodynamically efficient

configuration. Because it eliminates the tail and fuselage, a great deal of drag produced by these components is eliminated. It is also illustrated in Figure 2-3. Integrate a conventional configuration into a tailless configuration can achieve 33% reduction in surface area of the airplane [10]. It in turns leads to drag reduction since the drag is related to the wetted area. Besides; as there is no fuselage which produces very little lift on conventional aircraft and the whole airframe can produces lift, the FW configuration obviously has a high lift. Consequently, these two aspects contrbute to a high curise lift to drag ratio and a advanced aerodynamic efficiency on FW configuration.

Due to the extraordinary configuration, it can put a spar through the entire width of the airplane and distribute the internal weight on span-wise direction. It leads to a light weight of aircraft as the high structural efficiency for a given wing depth. There was a comparison from Liebeck [10] indicate that the blended wing body is 11% lighter than conventional in mean takeoff weight when design for the same capacity and mission.

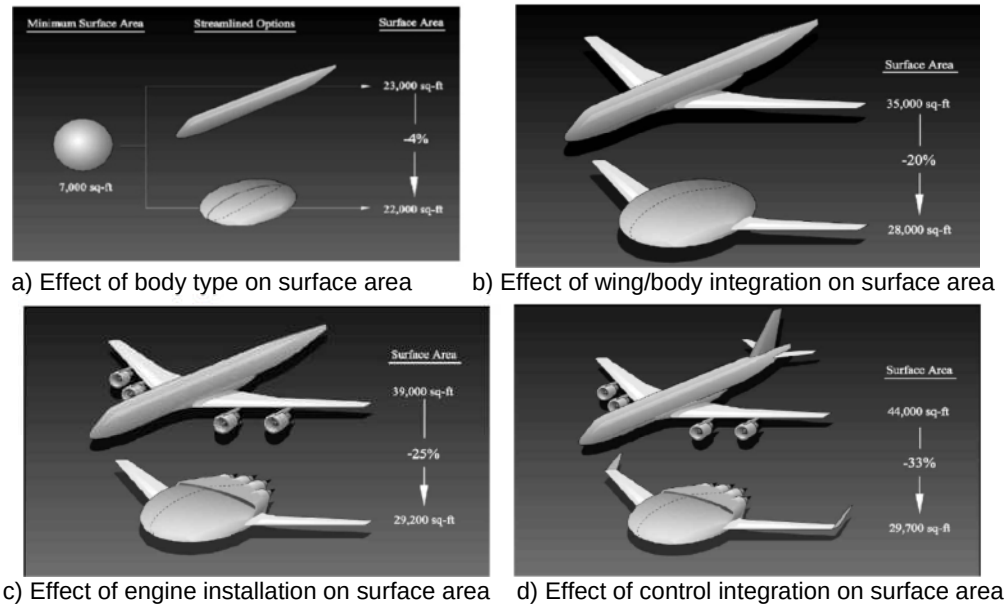

a) Effect of body type on surface area b) Effect of wing/body integration on surface area

c) Effect of engine installation on surface area d) Effect of control integration on surface area

Figure 2-3 Surface area of tailless aircraft concept [10]

It is obvious that increased aerodynamic efficiency plus reduced weight results in a lower power required of the aircraft. Thus, the propulsion system for a FW will be lighter and this contributes to a reduction of aircraft weight again. The fuel efficiency of the aircraft is also improved due to the lower SFC of the engine.

Besides, another benefit is it tends to place the engine on the rear fuselage of the FW and a laminar flow control (LFC) technology may be deployed. It enhances the aircraft aerodynamic efficiency as the engine take in the layer of air on the wing surface [11].

A new concept like the FW obviously brings some challenges to the table. Stability control is one of the challenges facing the FW. Since there is no vertical tail, the lateral-directional control always couple with the longitudinal control. It complicates the control system. Due to the smaller moment arm, larger and more control surfaces will be needed as well. However, moving the fins to the tip of the wings and advanced fly-by-wire systems that controlled by computer allowed for these drawbacks to be minimized, making for a stable aircraft [12], B-2 is a successful example. Cabin pressurization is another challenge. Due to the unique configuration, it requires a special approach to satisfy pressurization and structural needs of FW. In NASA's project, the internal space was divided into several bays by chord-wise ribs, from front to back of the aircraft. Each bay likes a fuselage of conventional aircraft that easy for pressurization. Moreover, advanced composite material was used to minimize the amount of structure needed to withstand the pressurization loads and deflections in the skins [11].

2.3 The Geared Turbofan

2.3.1 Environmental Challenges of Aviation Industry

Since the introduction of the first passenger aircraft, there has been considerable growth in air traffic, and it is predicted to increase further. Along with this generally development of the aviation industry it come serious problems for the environment. There was an increasing volume of complaints from the people that affected by aircraft noise, especially the local residents around airports. Meanwhile, the emissions of the aircraft, such as carbon dioxide, oxides of nitrogen and oxides of sulphur, impacted the atmosphere and change the climate gradually.

In order to minimize these impacts, the local governments and aviation organizations have been defining increasingly stringent regulations for aircraft engine emissions and noise. The International Civil Aviation Organization (ICAO) Chapter 4 is such an example. In 2001, the ICAO adopted this tighter noise limitation regulation on all new aircraft types certificated from January 2006. And it implied that only aircrafts with high bypass ratio engines can meet this regulation [13]. Consequently, all of these regulations proposed challenges for the further aircrafts and engines.

2.3.2 Next Generation Engine Requirements

Over the past decades, the aero-engine has gone through an evolutionary process and numerous technical and conceptual innovations were produced. These innovations brought significant improvements in engine performance, in terms of fuel consumption, safety and reliability and also noise and emissions reduction. A historical trend in aircraft noise was presented in Figure 2-4. It can be seen that a reduction of approximately 20dB since the 1960s due to the adoption of high bypass and advanced materials [13].

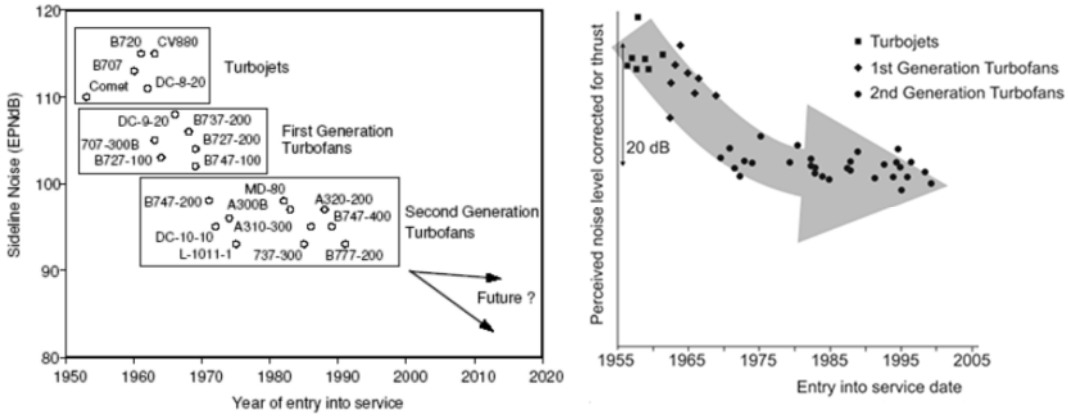

Figure 2-4 Historical trends in aircraft noise [13]

However, due to the increasingly stringent regulations and economic requirements, there is a high demand for low noise and high fuel efficiency aircrafts and engines, and the purchasing decisions of airline companies are also influenced by these issues. The Figure 2-5 summarizes mid-term requirements for the next generation aero engines of MTU.

Criteria	Existing Engine	Objective
Fuel Burn	Base	> -12%
Noise	-2 to -4 dB rel. ICAO stg. 4	> - 20dB rel ICAO stg. 4
Emissions	-40% rel ICAO96	-60% rel ICAO 96
Maintenance Cost	Base	> - 30%
Reliability	Base	Zero Target (no IFSDs)

Figure 2-5 Mid-term objectives for aero engines [14]

It is convinced that further new engine concepts plus advanced engine components will provide fuel consumption reduction up to 12% combined with extensive noise and emission reduction up to 20dB and 60% respectively [14].

2.3.3 Characteristics of Geared Turbofan

2.3.3.1 High Bypass Ratio Turbofans

As presented in Chapter 2.3.3, the mainly objective for the next generation engine is to reduce noise and fuel consumption. According to Cumpsty [15], the overall propulsion efficiency can be expressed as in Equation 2-1.

$$\eta_{ov} = \eta_{th} \times \eta_{p} \quad \textbf{(2-1)}$$

Note that the overall propulsion efficiency η_{ov} directly relate to the specific fuel SFC, so reduction in SFC can be achieved by enhancing thermodynamic cycle efficiency η_{th} and/or propulsive efficiency η_{p}.

The thermodynamic cycle efficiency can be improved by the increase of TET, OPR and component efficiencies, which are always limited by available materials and/or cooling techniques [15].

The propulsive efficiency is related to the engine exhaust velocity. As presented in Equation 2-2.

$$\eta_{p} = 2/(1 + c/v) \quad \textbf{(2-2)}$$

Where c is the exhaust velocity, and v is the velocity of the aircraft. It can be easy find that getting exhaust velocity closer to the flight speed will improve the

propulsive efficiency. There was a general trend of the fan pressure ratio (FPR) with the BPR [14], as shown in Figure 2-6. Since a low velocity of bypass flow can be got by the low fan pressure ratio, an increase in BPR will slow the exhaust velocity and consequently a high propulsive efficiency which leads to lower SFC.

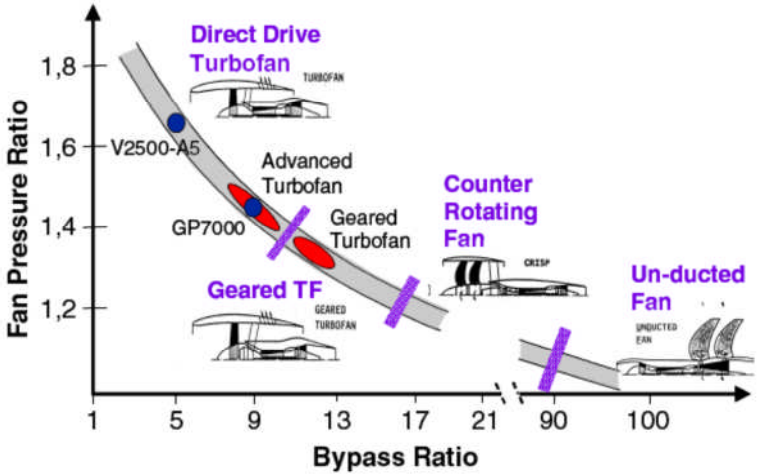

Figure 2-6 Trend of FPR with BPR [14]

Besides, according to D. Crichton [16], the noise of the engine is related to the velocity of the exhaust gases as well, approximate being proportional to the eighth power of the jet velocity. Therefore, a noise reduction can be also achieved by high BPR.

Though the high BPR can achieve a reduction in SFC and noise, there are some barriers in front of it. As a high BPR means a larger fan diameter required for a given thrust demand, the rotation speed of the fan has to be reduced to protect the fan tip speed from aerodynamic problems and transonic loss. Also, the big fan spin quickly makes more noise. Since the fan is directly derived by the low pressure compressor (LPC) and low pressure turbine (LPT), this leads to the latter two turbo components suffer from a “low” speed. In order to keep the pressure ratio and thermal efficiency, it has to increase the stage count for LPC and LPT. In addition, the torque of low rotor will increase as the speed decreases. It has to enlarge the LP-shaft diameters to tolerate the core engine discs. Obviously, it increases the length, weight and cost of the engine [14].

2.3.3.2 The Geared Turbofan Concept

Fortunately, this problem can be overcome by adding a fan drive reduction gear system between the fan and low pressure shaft. This enables the fan and the other two low pressure components operate at their optimum speed. Consequently, reduces the weight and cost of the low pressure components for a same specific thrust requirement. [17]

As presented in Figure 2-7. The GTF concept offers the advantages of a high bypass ratio turbofan engine with correspondingly slow fan speed and low fan noise and jet noise but avoids the disadvantages of low LPC and LPT efficiency and increased engine weight and maintenance cost [17].

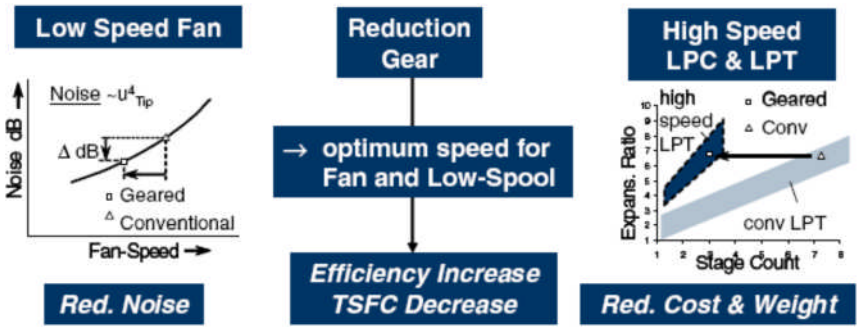

Figure 2-7 The Geared Turbofan concept [17]

Furthermore, the first generation GTF was successfully demonstrated by NASA and P&W partnership, and P&W will enter it into service with aircraft manufacturers in 2013. According to P&W's prospection, the GTF concept can achieve 12% to 15% fuel burn reduction and 20dB reduction in noise compared to direct drive turbofan engines [18].

Despite the GTF engine brings numerous benefits in terms of fuel burn and noise reduction, there is a potential physical limitation for it applications. Because the GTF engine typically features a larger fan diameter than the direct drive turbofan for the given thrust class, it require enough ground clearance for under wing installation. It is especially a challenge for small business jet that focuses on weight instead of SFC. However, for most existing long range wide body and mid-range single aisle airplanes this is not a limitation though.

2.4 Gas Turbine Simulation Theory and Tools

2.4.1 Performance Prediction of Gas Turbine

Gas turbine performance prediction usually begins with choosing a design point, which is defined as a particular point when the engine is operating at a specific condition for which its components are designed. From preliminary cycle calculation, it is possible to determine the thermodynamic parameters, such as mass flow, OPR and TET, for the maximum overall thermal efficiency and given power output. After determining these parameters, other suitable design parameters for a particular gas turbine system may be chosen. Then the individual engine components can be designed in detail to enable the complete system provide the required performance when operating at design point. [19]

Apart from the design point, the overall performance of engine over the whole operating range of speed and power output needs to be estimated as well. To predict the performance variation of engine over this range is defined as off design performance [19].

Previous experience or experimental data from actual tests can be very useful in estimating the performance characteristics of individual engine components. Basically, the components are able to operate over a wide range of operating conditions. When individual components are linked together, however, the operating range for each component is reduced significantly. When the engine is operating at a steady state or in equilibrium, corresponding operating points of each component can be plotted for a series of speeds and joined up to generate an equilibrium running lines, and the whole lines forming an equilibrium diagram. As shown in Figure 2-8, once the operating conditions of an engine have been determined, then various performance outputs of thrust or power, and SFC can be gained [19, 20].

According to Figure 2-8, the equilibrium running diagram also provides the compressor surge margin which is the proximity of the operating line to the surge line. When the running line is displaced beyond the surge line, the operation of gas turbine will become unstable. Furthermore, the program also

presents the region of compressor efficiency with respect to engine's operation. Ideally, the equilibrium running line should be lie close to the region where locus of maximum efficiency [19].

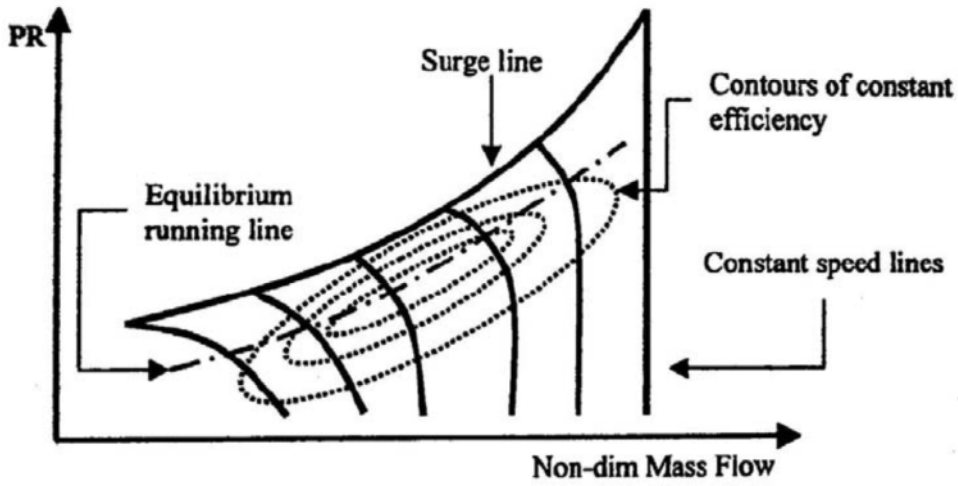

Figure 2-8 Typical compressor map [20]

Another important aspect should be considered in engine performance prediction is the ambient condition. The variations of ambient condition in terms of pressure and temperatures have significant impacts on performance of gas turbine. It can affect the payload and runway length required of the same aircraft at different geographic locations around the globe. As aero engines have to operate over a wide range of inlet temperature and pressure, the variation of engine performance with operating conditions is clearly important safety and economics issues of an aircraft. Hence, the effects of ambient condition should be taken into account for an accurate gas turbine modelling and performance simulation [20].

2.4.2 Gas Turbine Performance Simulation Tools

2.4.2.1 Introduction

It is obvious that to develop an aero engine is a complex progress and need innumerable calculations and iterations. In aviation industry, these calculations would be carried out using sophisticated software. There are a large number of in-house and commercially successful software available for gas turbine performance simulation, such as GasTurb, GateCycle and TURBOMATCH.

Through these tools have been developed by different people and delivered in different years, most of them share similar features and capabilities [21].

In this thesis, TURBOMATCH is selected as simulation tool for engine modelling and performance analysis, as which is developed by Cranfield University itself and required little experience of computer programming. The lecture review mainly focuses on the scheme of this software.

2.4.2.2 TURBOMATCH Scheme for Gas Turbine [22]

The TURBOMATCH has been developed by Cranfield University for gas turbine engines performance calculation at design and off design conditions using a digital computer. For a specific engine model, engine components and the connections between them are defined by means of “codewords”. The simulation progress results in output of thrust, specific thrust, SFC, etc., together with the thermodynamic properties at each stage within the engine.

In TURBOMATCH, any specific engine is constructed on modular fashion by using various pre-programmed units named “Bricks”. Most of Bricks contain the information about definition of physical engine components, such as COMPRE (compressor) and TURBIN (turbine), while others are used to perform some specific operations such as ARITHY (arithmetical operation), PERFOR (for final calculation of performance) and PLOTBD (for plotting brick data on screen).

Since most bricks define an individual component and only concern the thermodynamic processes in themselves, they have to be linked in order to perform a complete engine. In engine simulation, the properties and thermodynamic state of gases at the entry of every Brick can be collected as Station Vector (SV) to connect each brick. Each of SV consists of following eight items.

- Fuel-air ratio
- Mass Flow
- Static Pressure
- Total Pressure
- Static Temperature
- Total Temperature
- Velocity
- Area

Figure 2-9 presents a Brick and its various inputs and outputs as some discussed above. Generally, some other input data required by Brick do not form part of the SV. These items, such as the pressure loss and component efficiencies, which are different for each Brick, are grouped separately as Brick Data (BD). Additionally, some Bricks produce outputs such as engine thrust or power, which are different with the items of SV, are grouped separately as Engine Vector Results (EVK). Moreover, some Bricks need the outputs of other Bricks to be used as inputs; this set of data is known as Engine Vector Data.

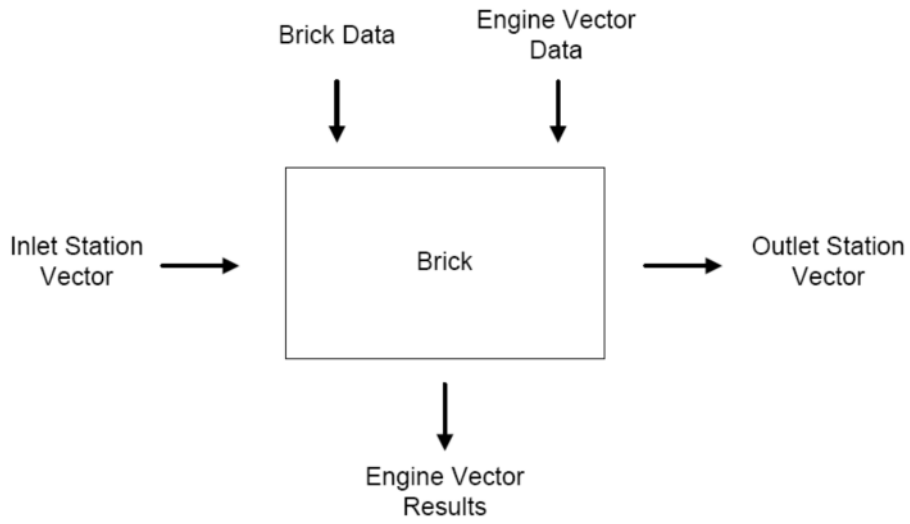

Figure 2-9 Schematic diagram of a brick inputs and outputs [22]

2.5 Conclusion

It is obvious that the aero industry experienced a greater improvement in the past several decades. To meet the environment requirements and economic issues, all of evolutions mainly focused on performance enhancement, in terms of fuel burn, noise and emissions reduction. In the same time, new concepts and technologies brought numerous opportunities and challenges for the next generation aero engines and aircrafts. Two typically concepts, FW for aircraft and GTF for engine respectively, attracted more interests in this field. As a tailless configuration, FW had lower drag and high aerodynamic efficiency compared to conventional aircraft. On the other hand, GTF offers advantages of the high bypass ratio engine but avoided problems from speed mismatching

between the large fan and other low spool components.

It should be noted that there is a large number of sophisticated software available for gas turbine performance simulation and prediction. Since TURBOMATCH requires little or no experience of programming and easy gets access to, it is selected as simulation tool for further study in this thesis.

3 Requirements for Engine Sizing

3.1 Introduction

The factors for engine sizing are investigated in this section. Firstly, the thrust requirements for FW-11 at different flight phases are calculated, since GFT-11 has prescribed ratings to meet these demands. Then, the preliminary dimensions and SFC target of GTF-11 are estimated from current high BPR engines base on P&W's perspective of the geared concept engine. These parameters will be used for engine cycle selection in engine modelling.

3.2 Thrust Requirements for FW-11

3.2.1 Take-off Thrust Requirement

According to constraint analysis, Wang Faliang [23] suggested that the reasonable thrust weight ratio for FW-11 was 0.226. Meantime, the estimated aircraft maximum take-off weight provided from Zhang Jin [24] was 176469kg. Then, the total thrust required for take-off of 391.12kN can be conducted and the take-off thrust required for each engine is 195.56kN, detailed calculation process is presented in Appendix A.1.1.

3.2.2 Second Segment Climb Thrust Requirement

For two engines aircraft, second segment climb (SSC) and en-route climb are often the critical design requirements affecting the engine size. The SSC is based on the situation with one engine of the aircraft inoperative. It is assumed to start at gear retraction, and completed at a height of 400 feet (122m) above the take-off surface. The configuration for SSC for all airplanes is defined as follow:

- gear completely retracted;
- flaps at the take-off position;
- one critical engine inoperative;
- other engines (remaining operating at maximum T/O thrust)

According to the regulation in FAR25.121 [23], the steady gradient of climb may be not less than 2.4% for two-engine airplanes. It is means that each engine

should have an ability to provide enough thrust for aircraft to maintain a no less than 2.4% gradient climb. From the equilibrium condition, two equations can be got as below:

$$T = D + W \times \sin\gamma \tag{3-1}$$

$$L = W \times \cos\gamma \approx W \tag{3-2}$$

Since these equilibrium conditions have to be achieved with one engine inoperative. The thrust required for SSC can be estimated as:

$$T_{req\_sec} = \left(\frac{1}{L/D} + \sin\gamma\right) \times W_{req\_sec} \tag{3-3}$$

According to the detailed calculation that presented in Appendix A.1.2, the thrust required for SSC is 159.31kN.

3.2.3 Maximum Climb Thrust Requirement

Aircraft initial cruise altitude capability is another critical design requirement for engine sizing. It defined as the ability to sustain a certain rate of climb (ROC) at this attitude, at typical cruise speed and with the engines operating at maximum climb rating. Aircraft arrives at this altitude at top of the climb (TOC). Usually, the aircraft will require a 300ft/min ROC at this condition. This enables the aircraft at this altitude with engines at cruise thrust to have a margin over the maximum cruise thrust. Therefore, the climb gradient at the initial cruise altitude of 35000ft can be got as:

$$\gamma = \frac{ROC}{V} \tag{3-4}$$

Based on the aircraft equilibrium equations, the thrust required at top of climb can be calculated as:

$$T_{req\_toc} = \left(\frac{1}{L/D} + \sin\gamma\right) \times W_{req\_toc} \tag{3-5}$$

W_{req_toc} is the aircraft weight at the top of climb. It can be estimated as 97-98% of the maximum take-off weight. The calculation result indicates that the maximum climb thrust required is 46.51kN, and detailed calculation process is presented in Appendix A.1.3.

3.2.4 Cruise Thrust Requirement

According to Jenkinson [5], the cruise thrust is about 7% to 8% less than the climb thrust. In this thesis, assume that the cruise thrust is 8% less than the climb thrust. Then the thrust requirement for FW-11 at the condition of cruise can be conducted as:

$$T'_{req\_cruise} = (1 - 8\%)T'_{req\_toc} = 42.79\text{kN}$$

3.3 Specific Fuel Consumption Target

As presented in Chapter 2.3.3.2, the GTF concept is designed focusing on low SFC and noise. A prediction from P&W indicates that SFC of this new concept engine can achieve a 12% reduction compared to the current engines that have the similar thrust. Thus, the SFC of GTF-11 can be estimated from this viewpoint. According to the maximum take-off thrust requirement of GTF-11, PW2043 and RB211-535E4B are selected as reference engines for SFC survey. Table 3-1 shows the parameters of these two engines.

Table 3-1 SFC investigation of reference engines [2, 26]

	PW2043	RB211-535E4B	Average
Company	Pratt & Whitney	Rolls & Royce	-
Application Aircraft	B757-200	B757-200	-
Certificate Time	1995	1989	-
Maximum Take-off Thrust	191.29kN	192kN	-
SFC@Take-off	9.014mg/Ns	9.952mg/Ns	9.483mg/Ns
SFC@Cruise	16.92mg/Ns	17.58mg/Ns	17.25mg/Ns

It can be seen that the average SFC of reference engines at take-off and cruise are 9.483 mg/Ns and 17.25mg/Ns respectively. Then the SFC of GTF-11 can be estimated as a 12% reduction.

At sea level take-off condition: $(1-12\%)\times 9.483 = 8.345\mathrm{mg/Ns}$

At cruise (H=10668m, M=0.82) condition: $(1-12\%)\times 17.25 = 15.18\mathrm{mg/Ns}$

3.4 Preliminary Engine Sizing

3.4.1 Scaling Factor

There is a theoretical method for sizing a baseline engine from a mature engine that have the similar configuration and thrust (not excess 20%). A scaling factor (SF) is defined as the thrust required of baseline engine divided by the thrust of the reference engine.

$$\mathrm{SF} = \frac{\mathrm{T_{req}}}{\mathrm{T_{ref}}} \tag{3-6}$$

Then the dimentions of baseline engine can be scaled by square root of SF while engine mass scale by SF, as following:

$$\mathrm{D_{req}} = \sqrt{\mathrm{SF}} \times \mathrm{D_{ref}} \tag{3-7}$$

$$\mathrm{L_{req}} = \sqrt{\mathrm{SF}} \times \mathrm{L_{ref}} \tag{3-8}$$

$$\mathrm{W_{req}} = \mathrm{SF} \times \mathrm{W_{ref}} \tag{3-9}$$

3.4.2 Reference Engine Survey

According to P&W's prospective, the BPR of incoming GTF engines ranges from 8 to 12. However, it seems no turbofans have the similar BPR with required thrust of GTF-11 in the current market. In order to gain reasonable dimensions of candidate engine, a survey of existing very high BPR engines is developed, as shown in Table A-1. The fan diameter, overall length and weight of these high bypass engines are investigated to seek trends between these parameters with take-off thrust.

As illustrated in Figure 3-1, it finds that the relationship between fan diameter and SQRT of the take-off thrust is almost linear, which same as the equation presented in pervious. Despite there are no apparent relationships between length, weight with thrust. It can be understood as the investigation just includes

a very small number of engines and many of these engines have different systems and components, such as reduction gear system and de-rated system. Therefore, the preliminary geometry of GTF-11 can be sized from these baseline engines which have the similar configuration. Since the Trent1000 has the closest value of take-off thrust with GTF-11, it is selected as reference engine for calculation. Detailed calculation progress refers to Appendix A.2.

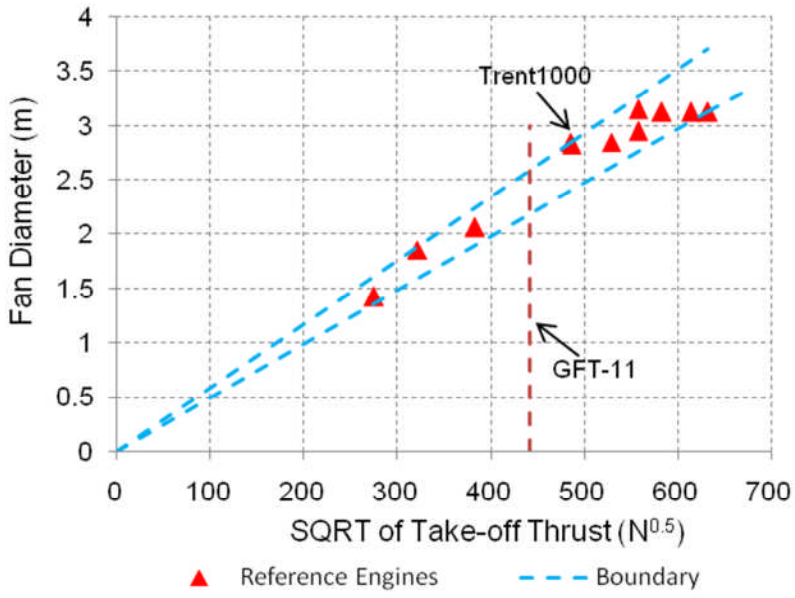

Figure 3-1 Relationship between fan diameters and take-off thrust

3.5 Technology Parameters of GTF-11

Based on above analysis, the preliminary technology parameters of GTF-11 can be conducted, as presented in Table 3-2.

Table 3-2 Technology parameters of GTF-11

Maximum Take-off Thrust@ISA+15℃, Sea Level	195.56kN
Cruise Thrust@35000ft, M=0.82	42.79kN
SFC@Take-off	8.35mg/N.s
SFC@Cruise	15.18mg/N.s
BPR	8~12
Fan Diameter	2.562m
Overall Length	3.523m
Weight	4870.8kg

4 Engine Performance Simulation

4.1 Introduction

The performance simulation of GTF-11 is aimed to deeply understand the main considerations in key parameters related to engine performance. Besides, the performance simulation also provides results for further investigation of FW-11 aircraft performance since the engine performance data plays a significant role in aircraft performance calculation.

Firstly, in this chapter, a preliminary performance model of GTF-11 engine is developed using TURBOMATCH software. Then, the effects of thermodynamic parameters on engine performance are investigated and optimum cycle parameters for GTF-11 at design point are decided. Finally, the off design performance of engine at different operating conditions are simulated.

4.2 GTF-11 Performance Modelling

4.2.1 Design Point

The cruise conditions is always chosen as design point for a long range aircraft engine modelling, because it covers the most time of whole flight. During this period, a minimum SFC is desired for a lower aircraft operation cost. The optimization of engine components in this phase is useful for the whole mission. The design point for GTF-11 modelling is defined in Table 4-1.

Table 4-1 Design point of GTF-11

Flight Mach Number	0.82
Altitude	10,668m (35,000ft)
Pressure	23,843.2Pa
Temperature	218.81K
ISA Deviation	0K
Density	0.376kg/m^3

4.2.2 Mass Flow

As the fan diameter was estimated from current high BPR engine, the mass flow for GTF-11 at design point can be estimated by one-dimensional isentropic

equations [27]. The result is 372.1kg/s and detailed calculation process refers to Appendix B.1.

4.2.3 Thrust Requirement

According to Chapter 3.2.4, the net thrust required for FW-11 at design point is 42.79kN.

4.2.4 Components Efficiency and Pressure Losses

According to the typical design values of current commercial aero-engine components, and also taking into account of technology development in the next decade since the GTF-11 is designed to apply on FW-11 in 2020. The component efficiencies and pressure losses for engine modeling are set as Table 4-2.

Table 4-2 Components efficiency and pressure Losses [28]

Intake Pressure Recovery	0.995
Fan Isentropic Efficiency	0.915
Boost Isentropic Efficiency	0.91
HPC Isentropic Efficiency	0.87
Combustion Efficiency	0.99
Combustor Pressure Loss	0.03
HPT Isentropic Efficiency	0.91
LPT Isentropic Efficiency	0.93
Inter Compress or Duct Pressure Loss	0.02

4.2.5 Engine Performance Model

In present study, the GTF-11 is supposed as a typical two spools, separated nozzles turbofan engine, with the LPT driving the fan and the boost and the high pressure turbine (HPT) driving the high pressure compressor (HPC). A reduction gearbox system is added between the fan and the boost to allow them operating at their optimum speed. Since the fan speed is constrained by the fan diameter, and a larger reduction factor can allow for a lower fan speed and larger fan diameter which contributes to a higher BPR, a larger reduction factor

will be favourable. However, a larger factor will increase the weight and the complexity design of the gearbox system as well. In present study, the factor of three that was used on P&W's first generation GTF [18] is assumed for preliminary engine performance analysis. Since TURBOMATCH does not work with absolute values of rotational speed but only with relative speeds, there is no need to consider the reduction gear in engine modelling. Detailed description of the engine model and codes refer to Appendix B.2.

4.3 Design Point Parameters Analysis

With the required performance of engine determined previously, the next step is to select proper cycle parameters which generate the required performance at design point. Basically, the parameters include FPR, BPR, OPR and TET. In this section, the effects of these parameters on engine design point performance are analyzed and optimum design parameters are decided. Table 4-3 presents ranges of these parameters.

Table 4-3 Thermodynamic cycle parameters

Bypass Ratio	10~12
Overall Pressure Ratio	30~45
Turbine Enter Temperature (K)	1400~1650
Fan Pressure Ratio	1.2~1.65

4.3.1 Effects of BPR on Engine Performance

Firstly, OPR and TET are set as fixed values to analyze the effects of BPR on engine performance in terms of specific thrust and SFC. According to the simulation results, as shown in Figure 4-1 and Figure 4-2, following characteristics can be obtained:

- For fixed OPR and TET configurations, there is an optimum FPR for each BPR and this value decreases as BPR increases.
- For fixed OPR and TET configurations, the maximum specific thrust at optimum FPR improves dramatically with BPR decreases.
- For fixed OPR and TET configurations, the minimum SFC at optimum FPR increases lightly with the BPR decreases.

It can be found that, for OPR is 35 and TET is 1400K, the optimum FPR (for maximum specific thrust and minimum SFC) is 1.50, 1.47 and 1.45 for BPR of 10, 11 and 12, respectively. For OPR is 35 and TET is 1450K, it is 1.55, 1.52 and 1.47, respectively. The optimum FPR and corresponding specific thrust and SFC are presented in Table 4-4. Besides, more simulation results are presented in Appendix B.3.

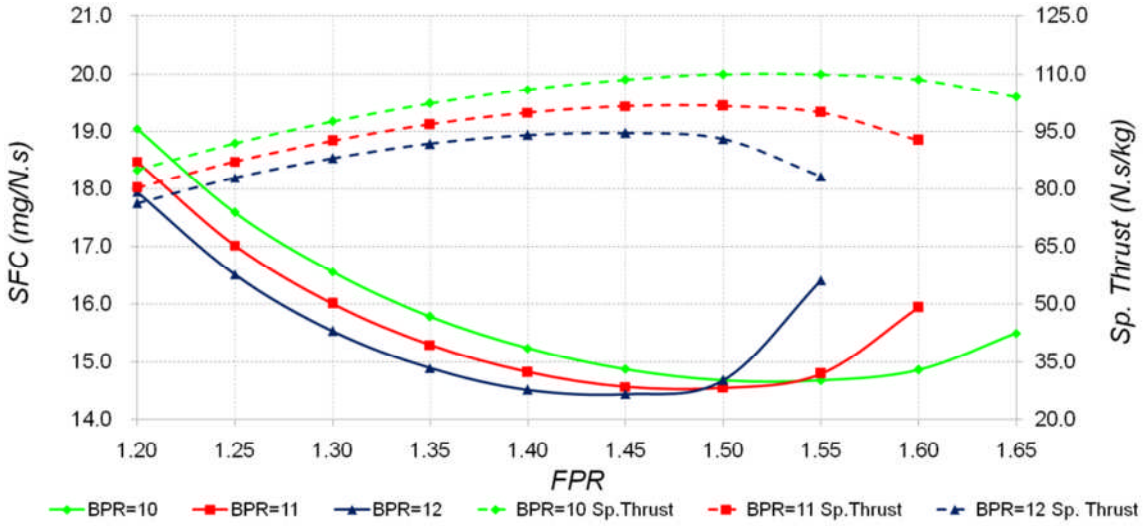

Figure 4-1 Effects of BPR on engine performance (OPR=35, TET=1400K)

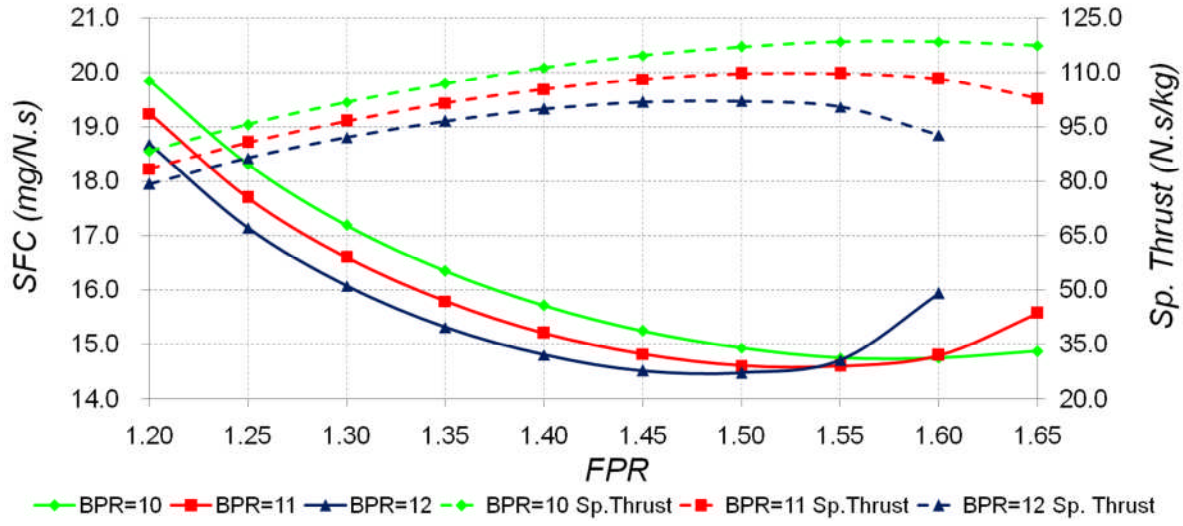

Figure 4-2 Effects of BPR on engine performance (OPR=35, TET=1450K)

Table 4-4 Optimum FPR of different BPR

OPR	TET (K)	BPR	FPR	SFC (mg/N.s)	Sp. Thrust (N.s/kg)
35	1400	10	1.50	14.67	110.00
		11	1.47	14.55	101.72
		12	1.45	14.44	94.61
	1450	10	1.55	14.75	118.43
		11	1.52	14.61	109.67
		12	1.47	14.48	102.10

4.3.2 Effects of TET on Engine Performance

Then, BPR and OPR are set as fixed values to analyze the effects of TET on engine performance in terms of specific thrust and SFC. According to the simulation results, as shown in Figure 4-3 and Figure 4-4, following characteristics can be obtained:

- For fixed BPR and OPR configurations, there is an optimum FPR for each TET and this value increases as TET increases.
- For fixed BPR and OPR configurations, the maximum specific thrust at optimum FPR improves dramatically with TET increases.
- For fixed BPR and OPR configurations, the minimum SFC at optimum FPR increases lightly with the TET increases.

It can be found that, for BPR is 11 and OPR is 35, the optimum FPR (for maximum specific thrust and minimum SFC) is 1.47, 1.52, 1.57 and 1.62 for TET is 1400K, 1450K, 1500K and 1550K, respectively. For BPR is 12 and OPR is 35, it is 1.45, 1.47, 1.52 and 1.57, respectively. The optimum FPR and corresponding specific thrust and SFC are presented in Table 4-5. Besides, more simulation results are presented in Appendix B.3.

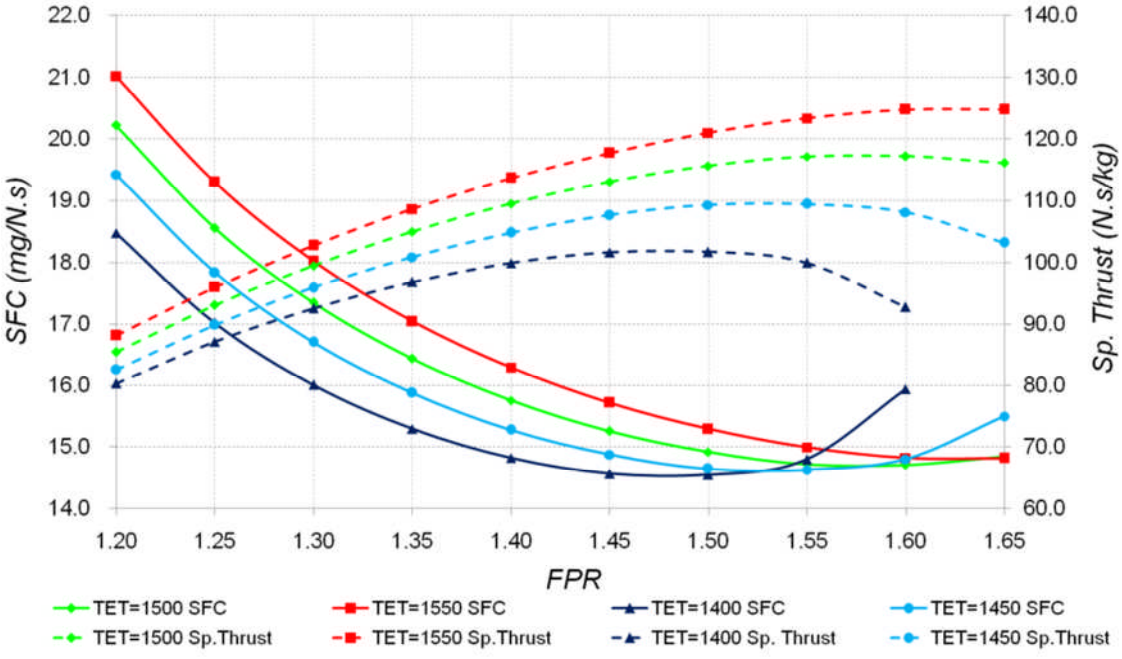

Figure 4-3 Effects of TET on engine performance (BPR=11, OPR=35)

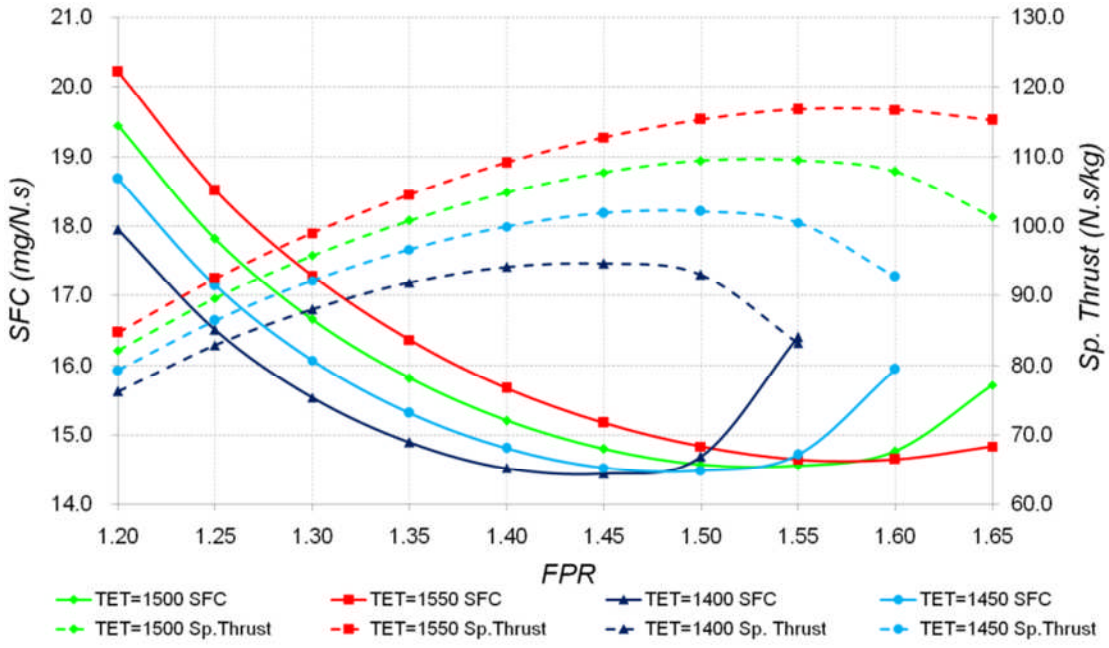

Figure 4-4 Effects of TET on engine performance (BPR=12, OPR=35)

Table 4-5 Optimum FPR of different TET

OPR	BPR	TET (K)	FPR	SFC (mg/N.s)	Sp. Thrust (N.s/kg)
35	11	1400	1.47	14.55	101.72
		1450	1.52	14.62	109.40
		1500	1.57	14.70	117.19
		1550	1.62	14.81	124.82
	12	1400	1.45	14.44	94.61
		1450	1.47	14.48	102.10
		1500	1.52	14.55	109.45
		1550	1.57	14.64	116.72

4.3.3 Effects of OPR on Engine Performance

Finally, effects of OPR on engine performance are investigated based on fixed BPR and TET. According to the simulation results, as presented in Figure 4-5, Figure 4-6 and Figure 4-7, following characteristics can be obtained:

- For fixed BPR and TET configurations, there is an optimum FPR for each OPR and this value decreases as OPR increases.
- For fixed BPR and TET configurations, the maximum specific thrust at optimum FPR decreases as OPR increases.
- For fixed BPR and TET configurations, the minimum SFC at optimum FPR decreases apparently with the OPR increases.

It can be found that, for BPR is 10 and TET is 1400K, the optimum FPR (for maximum specific thrust and minimum SFC) is 1.55, 1.52, 1.50 and 1.47 for OPR of 30, 35, 40 and 45, respectively. For BPR is 11 and TET is 1400K, it is 1.50, 1.48, 1.47 and 1.45 respectively. For BPR is 12 and TET is 1400K, it is 1.47, 1.45, 1.43 and 1.42 respectively. The optimum FPR and corresponding specific thrust and SFC are presented in Table 4-6. Besides, more simulation results are presented in Appendix B.3.

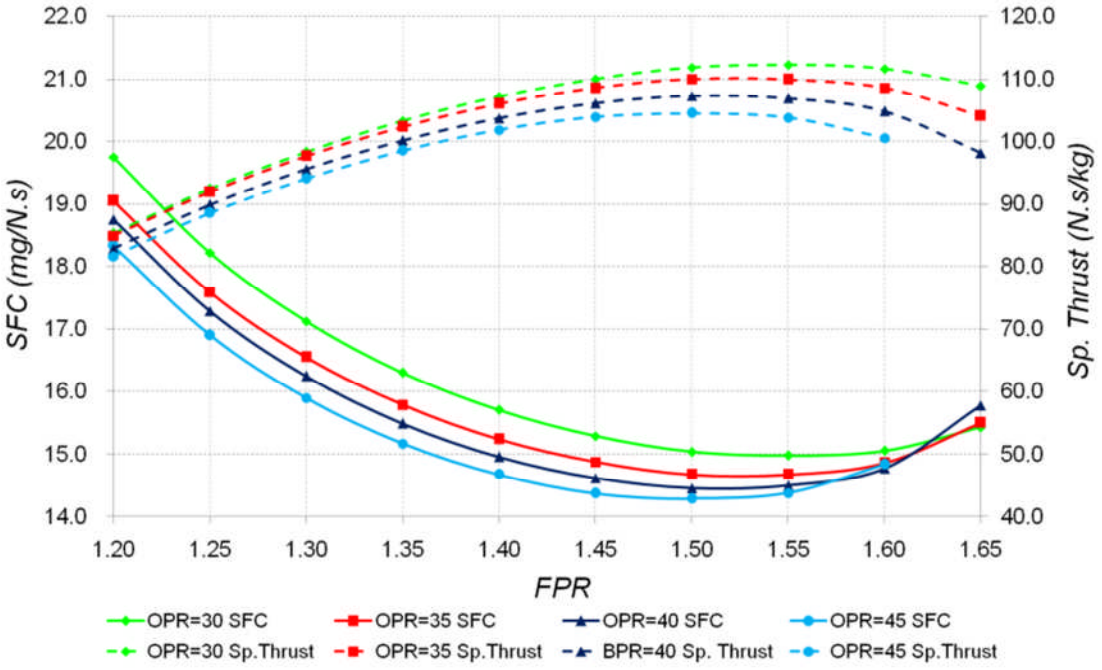

Figure 4-5 Effects of OPR on engine performance (TET=1400K, BPR=10)

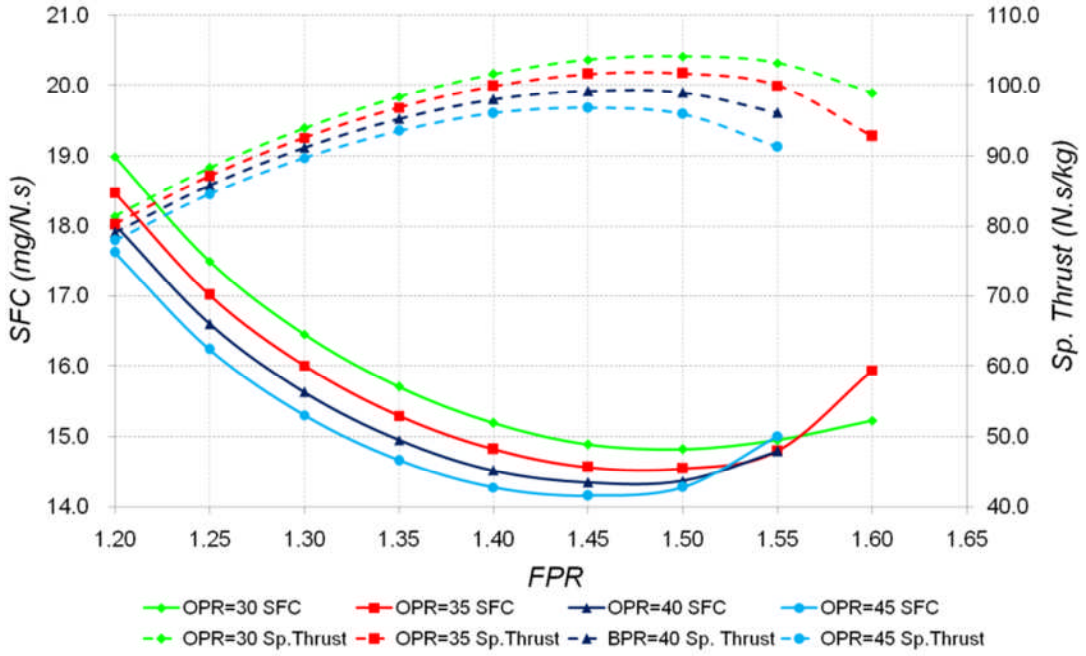

Figure 4-6 Effects of OPR on engine performance (TET=1400K, BPR=11)

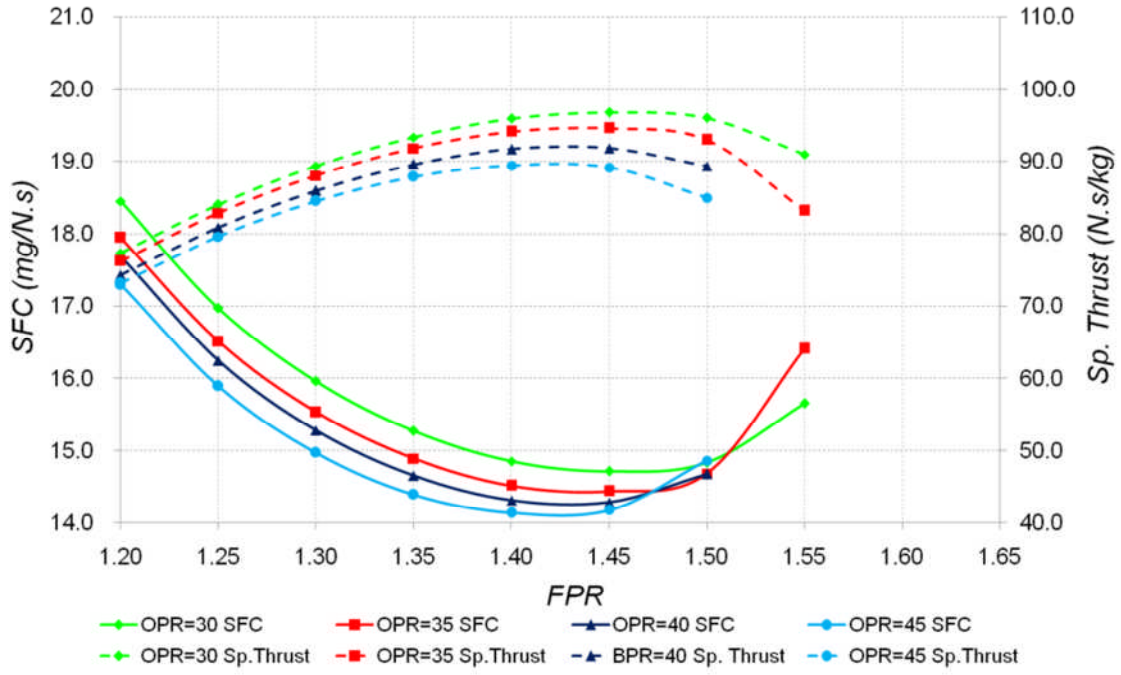

Figure 4-7 Effects of OPR on engine performance (TET=1400K, BPR=12)

Table 4-6 Optimum FPR of different OPR

TET (K)	BPR	OPR	FPR	SFC (mg/N.s)	Sp. Thrust (N.s/kg)
1400	10	30	1.55	14.98	112.27
		35	1.52	14.67	110.00
		40	1.50	14.45	107.27
		45	1.47	14.28	104.51
	11	30	1.50	14.82	104.15
		35	1.48	14.55	101.92
		40	1.47	14.34	99.19
		45	1.45	14.16	96.81
	12	30	1.47	14.71	96.82
		35	1.45	14.44	94.61
		40	1.43	14.28	91.83
		45	1.42	14.13	89.42

4.3.4 Combination Effects of Parameters

According to above investigations, it can be found that each parameter has its corresponding optimum FPR and a proper FPR for complete engine should be a compromise result of BPR, OPR and TET.

The combination effects of cycle thermodynamic parameters on engine performance are studied as shown in Figure 4-8.

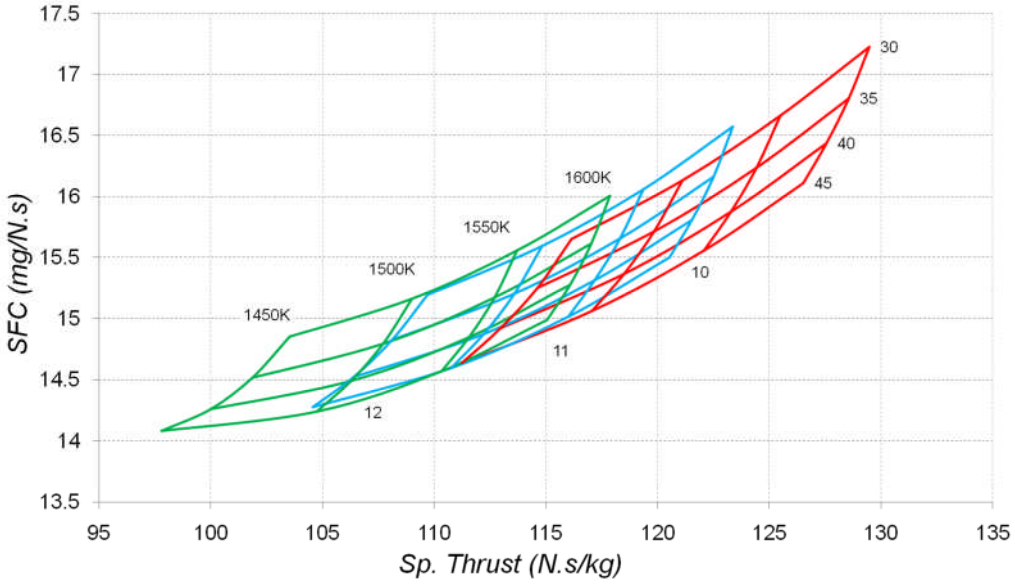

Figure 4-8 Combination effects on engine performance

From simulation results, following characteristics can be gained:

- In all configurations the SFC decreases as the OPR increases.
- An increment in BPR leads to reduction in SFC and specific thrust.
- Increase the TET results in specific thrust increment.

4.3.5 Design Point Parameters Selection

Since the optimum FPR decreases as the BPR increases, a low FPR will be required by ultra-high bypass turbofan. It is especially for GTF configuration turbofan which has a high bypass ration and a lower fan rotation speed due to the reduction gear system. As sub-sections analysis indicates that the optimum FPR mainly ranged from 1.40 to 1.55 and a low FPR will also reduce the design complexity of the fan, the FPR is selected as 1.45 for GTF-11.

In present study, there are two constraints for cycle parameters selection. One is the fan diameter. As presented in previous chapter, the fan diameter of GTF-11 is 2.562m and corresponding mass flow at design point is 372.1kg/s. Then the specific thrust required can be estimated as net thrust divided by mass flow

and the calculation result is 115Ns/kg. Another one is the SFC target, which was estimated from current turbofans being 15.18mg/Ns at cruise.

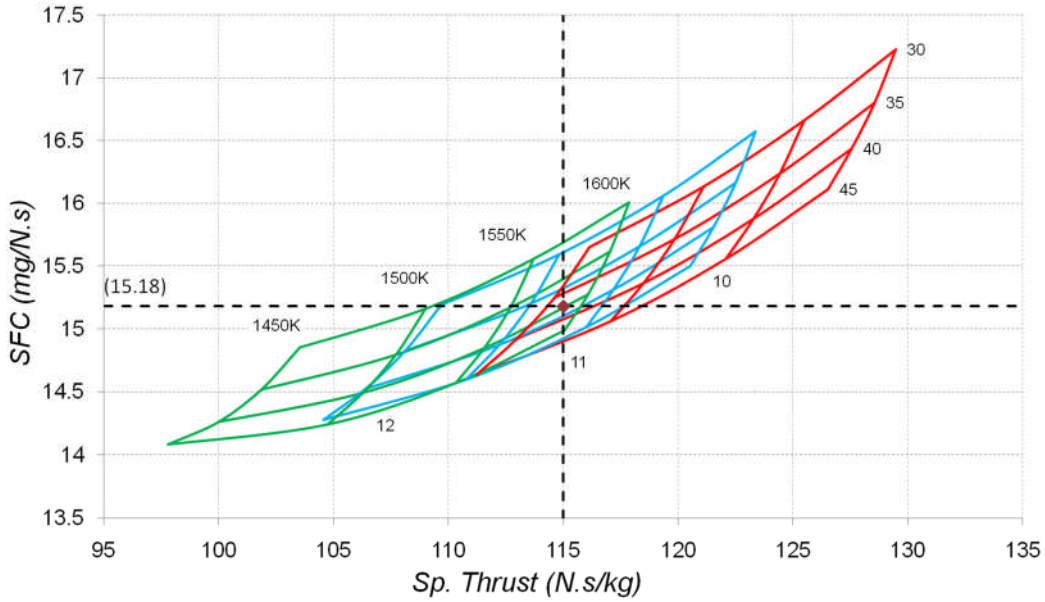

Figure 4-9 Design point parameters selcetion

Based on the SFC target and fan diameter constraint, the cycle parameters can be selected for design point, as shown in Figure 4-9.

As presented in table 4-7, there are two groups of parameters can be used for engine design. Comparisons of these parameters are listed as following.

Table 4-7 GTF-11 engine cycle parameters

BPR	FPR	OPR	TET (K)	SFC (mg/Ns)	Sp. Thrust (Ns/kg)	Mass flow (kg/s)
11	1.45	38.2	1517	15.18	115	372.1
12	1.45	39.8	1581	15.18	115	372.1

For BPR selection, a high BPR contributes to both SFC and noise reduction, therefore, BPR of 12 is preferred for a fixed fan diameter configuration.

For OPR selection, a high OPR can bring an improvement in engine thermodynamic performance but would result in the boost and HPC too complex and expensive to be practical. Besides, the OPR for most of current high bypass engines are between 30 and 40 and some even achieve 50 due to

the introductions of multi-spool and improvements in materials and compressor blades. According to these viewpoints, OPR of 38.2 is appropriate for GTF-11.

For TET selection, a high TET would enhance the thermodynamic efficiency as well. However, a high temperature would reduce the service life of component blade. As TET of 1517K can meet the required engine performance, it is practicable for engine component design.

According to the above considerations, it is easily to draw a conclusion that the thermodynamic parameters for GTF-11 on design point should be BPR of 11, OPR of 38.2 and TET of 1517K.

4.4 Take-off Thrust Verification

Before conducting the off design performance simulation, the take-off thrust is verified by aircraft requirements of second segment climb and take-off field length.

4.4.1 Second Segment Climb Requirement

As presented in Chapter 3.2.2, the engine should provide enough thrust for SSC. Assuming that the aircraft speed at SSC equals the take-off safety speed which is estimated by 1.2 times of the stall speed. Detailed calculation process of take-off safety refers to Appendix C.1. According to the simulation result, as shown in Figure 4-10, the uninstalled thrust of engine for SSC 152.31kN when maximum take-off thrust is 195.56kN. Taking account of 3% installation thrust loss, the installed thrust at this condition is 147.74kN. Obviously, it cannot meet the thrust required for SSC, which should be 159.31kN. Therefore, the maximum take-off thrust should be corrected to satisfy this critical requirement.

In order to get a correct value, different values of take-off thrust are set as input for simulation in TRUBOMATCH. The results indicate that the climb grade required in FAR25/CS25 can be satisfied when maximum take-off thrust is 209.08kN, as shown in Figure 4-11.

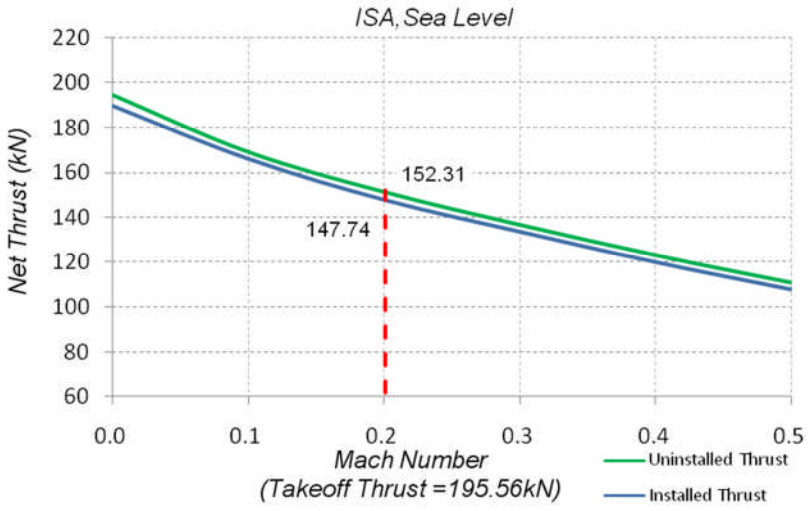

Figure 4-10 Thrust available for SSC at take-off thrust of 195.56kN

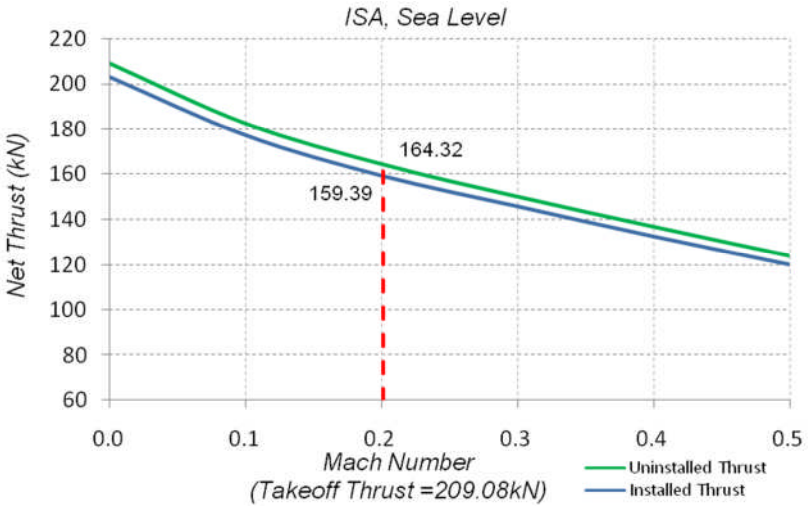

Figure 4-11 Thrust available for SSC at take-off thrust of 209.08kN

4.4.2 Take-off Field Length Requirement

Besides, the engine also has to provide sufficient thrust to meet the required take-off field length of 1900m of FW-11. In present study, the take-off field length is estimated using ESDU 76011a [29] on the basis of engine simulation results. Detailed calculation process refers to Appendix C.2 and the results are presented in Table 4-8.

It can be found that the take-off field length is 1940m, 1895m and 1850m when take-off thrust is 209.8kN, 212kN and 215kN, respectively. Therefore, the required take-off thrust of FW-11 should be corrected to 212kN as which satisfy

the field length requirement, and corresponding thrust to weight ratio is 0.245.

Table 4-8 Take-off field length for different take-off thrust

Take-off Thrust	Cases	Field Length
209.08kN	AEO (Unfactored)	1640m
	AEO (Factored)	1886m
	OEI (BFL)	1940m
	FAR/CS Required	1940m
212kN	AEO (Unfactored)	1610m
	AEO (Factored)	1852m
	OEI (BFL)	1895m
	FAR/CS Required	**1895m**
215kN	AEO (Unfactored)	1580m
	AEO (Factored)	1817m
	OEI (BFL)	1850m
	FAR/CS Required	1850m

4.5 Off Design Performance Simulation

The off design point performance of engine in take-off, climb and cruise are simulated based on the design point, as shown in Figure 4-12 to Figure 4-18.

4.5.1 Take-off Performance Simulation

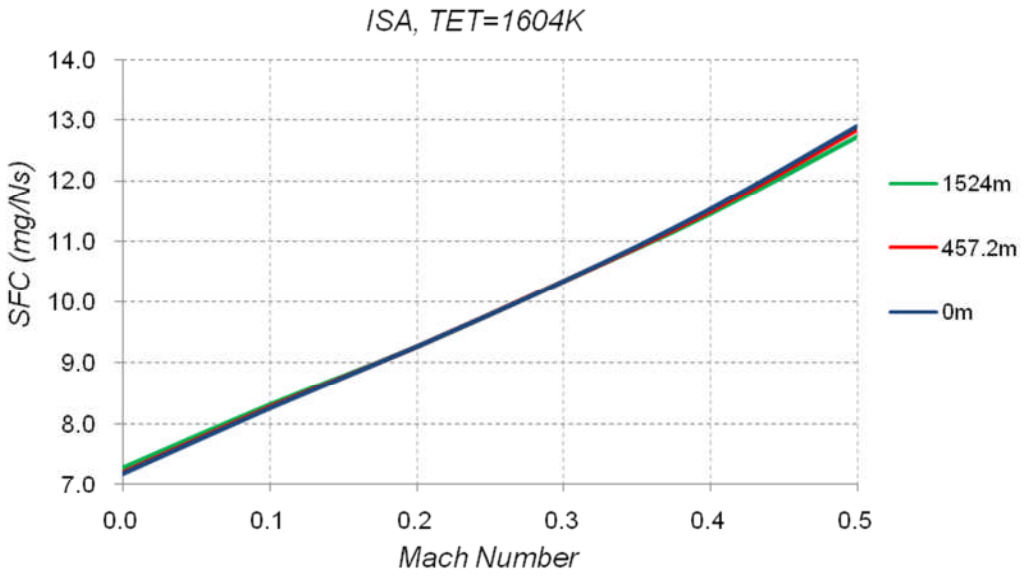

Figure 4-12 SFC at take-off

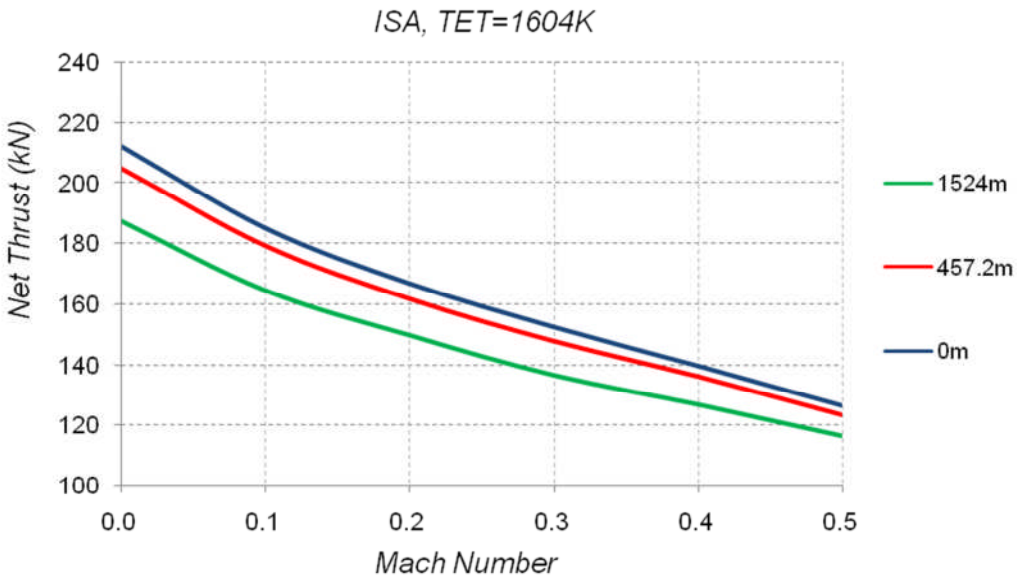

Figure 4-13 Net thrust at take-off

Since the temperature and altitude have significant effects on engine performance, these two factors should be considered to ensure the engine has the capacity of taking off from high altitude airport at hot day. The simulation results about the influence of the two factors are presented in Figure 4-14.

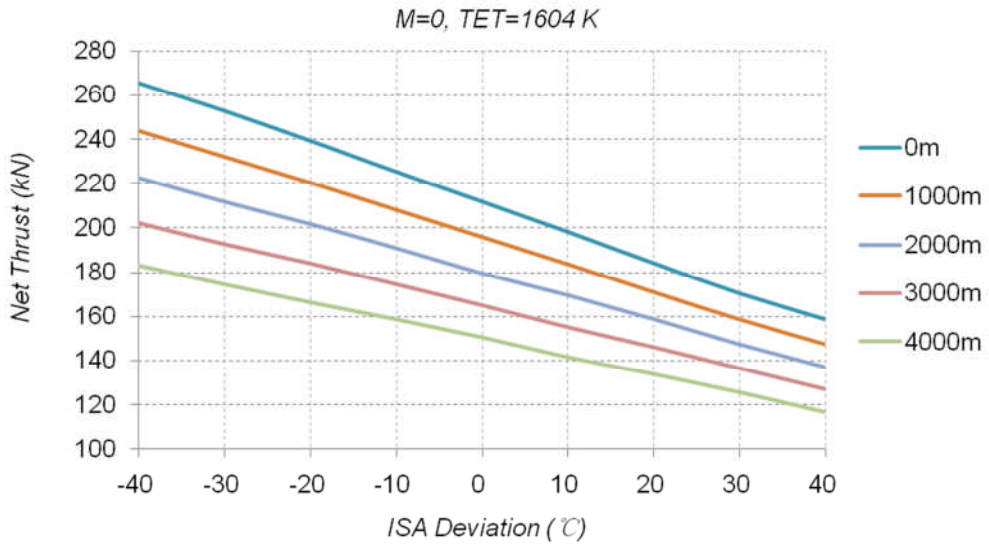

Figure 4-14 Take-off thrust versus temperature deviation at different altitudes

It can be found that, from Figure 4-14, for the same temperature deviation, the net thrust decreases as the altitude increases, which is the result of reducing air density and hence the mass flow. For the same altitude, the net thrust drops as

day temperature increases. The reason is that for a given TET and OPR the compressor consumes more work during hot day as ambient temperature goes up and hence less useful work could be output to produce thrust.

4.5.2 Cruise Performance Simulation

To evaluate the engine performance through the whole operating process, the engine off-design performance at cruise condition are simulated as well, as presented in Figure 4-15 and Figure 4-16.

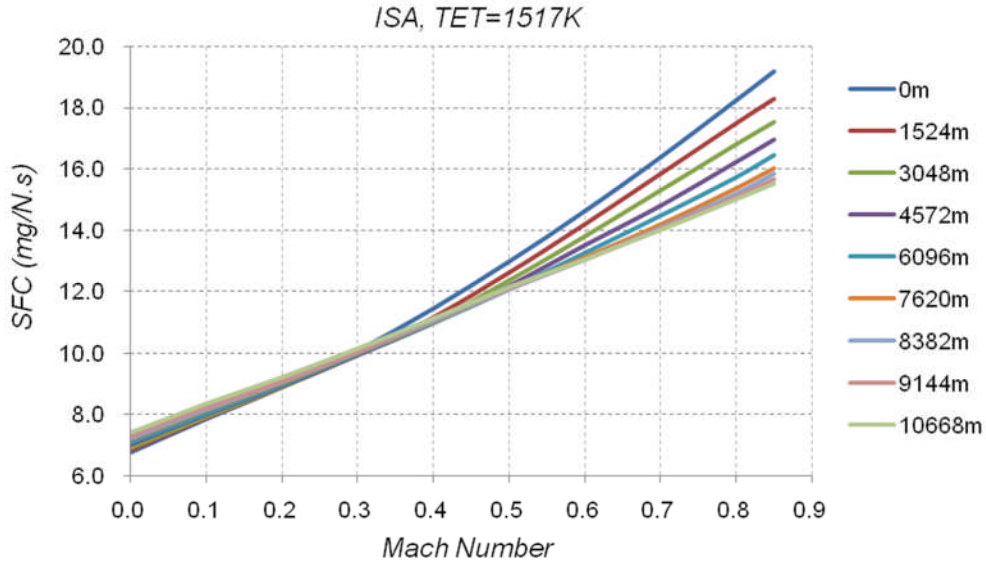

Figure 4-15 SFC in cruise

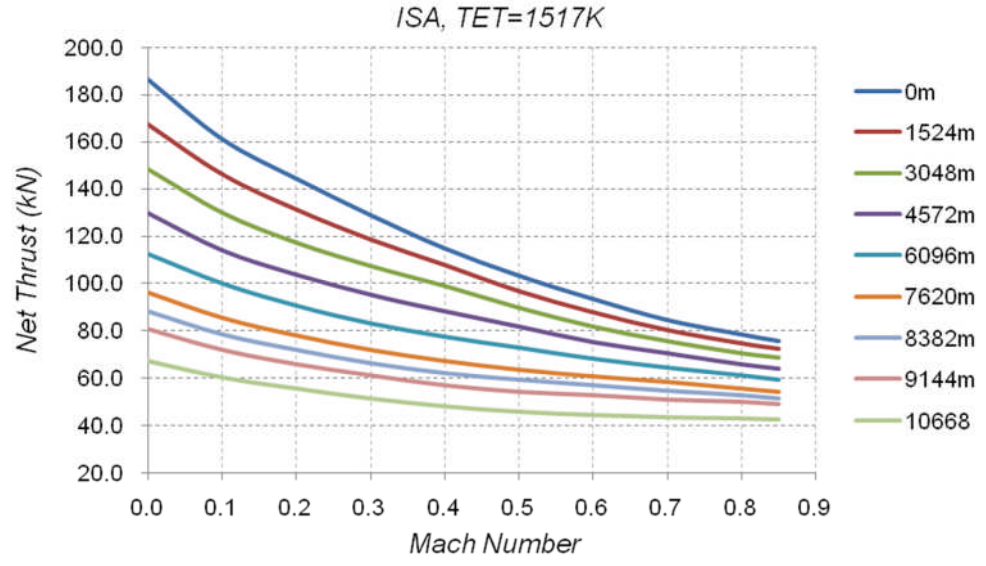

Figure 4-16 Net thrust in cruise

4.5.3 Climb Performance Simulation

Climb performance is a key factor based on which desired climb path can be scheduled. In Figure 4-17 and Figure 4-18, the SFC and net thrust of the engine against flight Mach number and altitude in climb are illustrated.

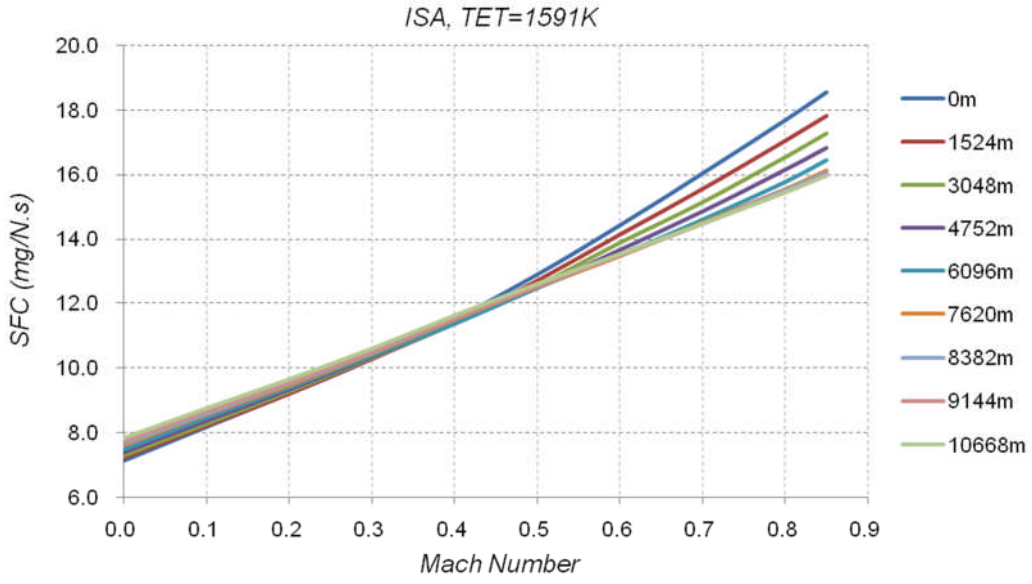

Figure 4-17 SFC in climb

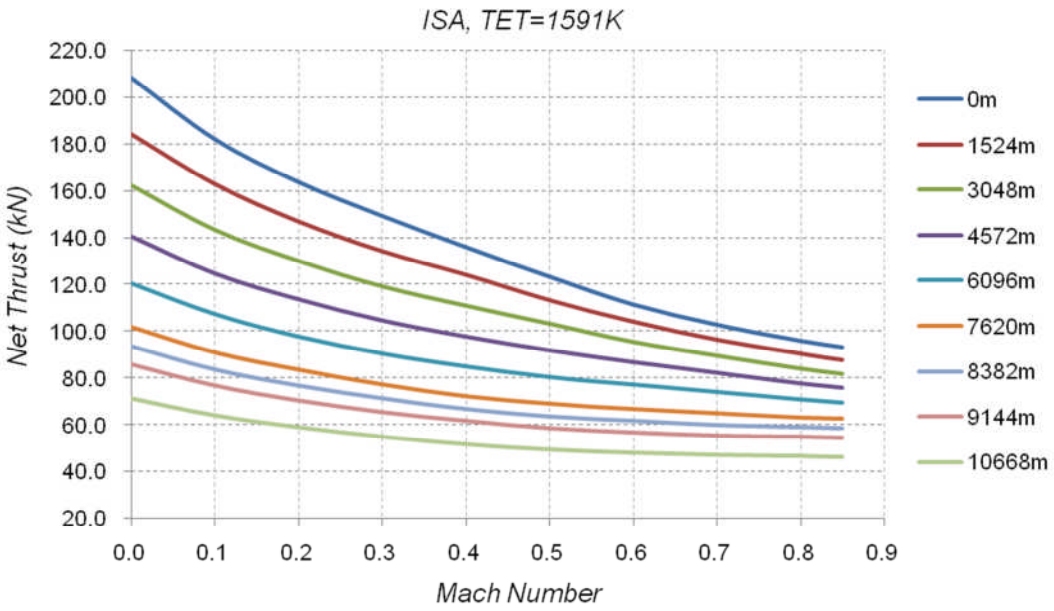

Figure 4-18 Net thrust in climb

5 Aircraft Performance Calculation

5.1 Introduction

Since the performance of GTF-11 is simulated using TURBOMATCH, the performance matching between aircraft and engine is analyzed in this chapter. Firstly, an aircraft performance calculation model is constructed using empirical methods. Then, the aircraft performance with typical mission profile is analyzed on the basis of GTF-11 simulation results. Finally, a comparison between GTF-11 and conventional turbofan is conducted to evaluate the benefits of new concept engine in aircraft performance improvement.

5.2 Aircraft Performance Calculation Model

The aircraft performance calculation model includes five modules: specification data module, atmosphere module, mission profile module, engine data module and performance calculation module.

5.2.1 Specification Data Module

The specifications of FW-11 are provided in GDP specification report [3]. Data related to aircraft performance calculation are presented below.

A. Geometry
   - Wing area: 647m^2
   - Span: 65m
   - Aspect ratio: 6.33
   - Taper ratio: 0.11
   - Mean thickness: 0.14
   - Leading edge sweep angle: 39°
   - 1/4 chord sweep angle: 34.3°

B. Masses
   - Maximum take-off mass: 176469kg
   - Maximum landing mass: 162351kg
   - Operating empty mass: 75044kg
   - Maximum payload: 41320kg

- Design payload: 28686kg
- Design fuel load: 72740kg

C. Aerodynamic

- Lift characteristics
  - Maximum lift coefficient of basic wing: 0.8
  - Maximum lift coefficient of take-off configuration: 1.35
  - Maximum lift coefficient of landing configuration: 1.45
- Drag characteristics
  - Cruise condition (Ma=0.82, 35000ft):

$$C_D = 0.00848 + 0.0535{C_L}^2$$

  - Take-off at sea level, undercarriage and flaps deployed:

$$C_D = 0.01443 + 0.05617{C_L}^2$$

  - Landing at sea level, undercarriage and flaps deployed:

$$C_D = 0.02434 + 0.05955{C_L}^2$$

  - Landing gear increment: $\Delta C_d = 0.0075$

D. Performance

- Design cruise speed: Mach 0.82
- Minimum cruise ceiling from MTOW take-off: 35000ft
- Design Range: 7500nm

Above data are collected in specific data module as inputs for aircraft performance calculation.

5.2.2 International Atmosphere Module

The International Standard Atmosphere (ISA) is the foundation of aircraft performance calculation as it is presented in ESDU 68046 [30]. In this thesis, the aircraft performance analyses are accomplished under ISA conditions. The atmosphere model, used to calculate the characteristics of the ISA, is developed on the basis of ESDU 77022b [31].

5.2.3 Mission Profile Module

The mission profile module includes two parts: main mission flight profile and reserve profile, as shown in Figure 5-1 and Figure 5-2.

The main flight profile defined for FW-11 aircraft performance calculation include following segments:

- Take-off and initial climb to1500ft
- Climb from 1500ft to initial cruise altitude
- Stepped cruise
- Descent to 1500ft
- Approach and landing

The climb segment is scheduled as following for performance calculation:

- 1500ft~10000ft: climb at 250KEAS
- 10000ft~26460ft: climb at 320KEAS
- 26460ft~35000ft: climb at 0.82M

The descent segment of FW-11 is scheduled as the aircraft speed decreases from cruise speed at 39000ft to 250KEAS at sea level. Since the maximum ROD of the aircraft is limited by the maximum ROD of the cabin which is 300ft/min for passengers comfort, the minimum time required for the aircraft to descent can be determined by the cabin pressure height. Assuming the cabin altitude of the FW-11 is 7000ft, the minimum descent time can be calculated as 7000/300=23.3min.

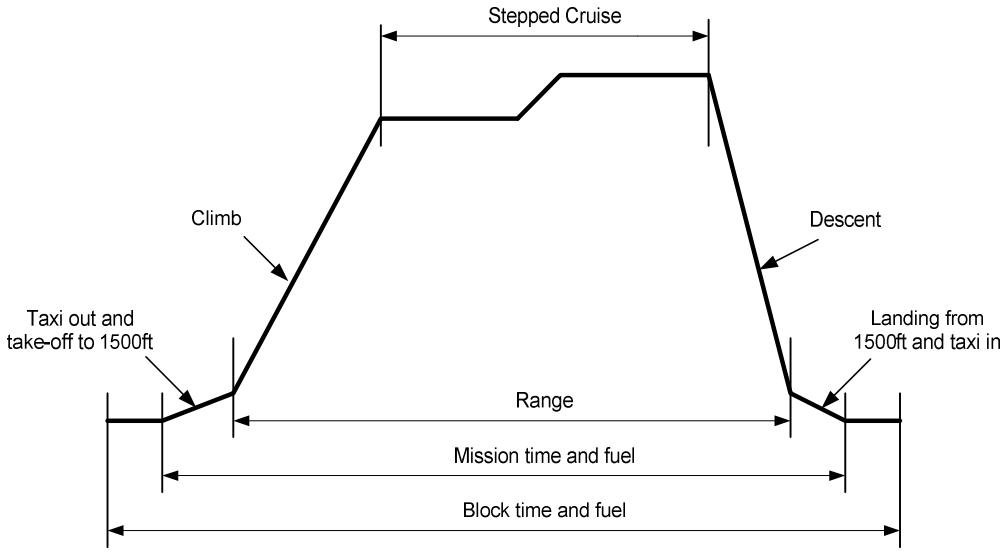

Figure 5-1 Main mission profile definition [5]

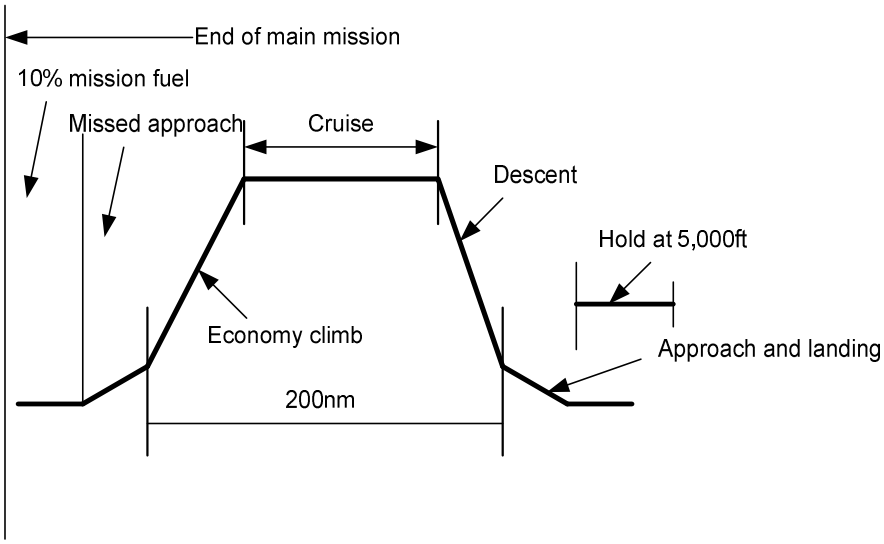

Figure 5-2 Reserve fuel profile definition [5]

The typical reserve fuel flight profile includes following segments:

- Missed approach and climb to diversion cruise altitude 1,0000ft
- Cruise at speed for maximum range
- Descent to 1000ft
- Approach and landing
- Hold for a specified time at speed for minimum fuel consumption
- Contingency of 10%fuel used in the main mission profile.

According to Jenkinson's Civil Jet Aircraft Design [5], a typical set of allowances for take-off, division distance and fuel reserves is defined for FW-11 performance calculation, as shown in Table 5-1.

Table 5-1 Typical set of allowances [5]

	Typical flights
Allowances	
Take-off	2min
Approach and landing	6min
Reserves	
Block fuel	45min
Division	200nm

5.2.4 Engine Data Module

This module is developed on the basis of engine performance simulation results, as presented in Chapter 4. The engine data used for performance calculation includes following aspects:

- Engine thrust and corresponding fuel consumption during take-off
- Engine thrust and corresponding fuel consumption during climb
- Engine thrust and corresponding fuel consumption during cruise
- Engine thrust and corresponding fuel consumption during descent

5.2.5 Performance Calculation Module

There are many empirical methods available for aircraft performance calculation. In this thesis, the calculation module is developed mainly using the methods from Jenkinson's Civil Jet Aircraft Design [5] and Eshelly's Aircraft Performance: Theory and Practice [4]. The methods are presented in Appendix D. The aircraft performance characteristics, such as filed performance, en-route performance and payload-range can be estimated in this module on the basis of inputs from other modules.

5.3 Mission Analysis

5.3.1 Field Performance

The take-off and landing performance of FW-11 are summarized in Table 5-2. Detailed calculation process refers to Appendix E.

Table 5-2 Filed performance of FW-11

		Field Length (m)	Time (min)	Fuel Burn (kg)
Take-off	AEO(unfactored)	1332	2	368
	AEO(factored)	1532	-	-
	OEI(BFL)	1780	-	-
Landing	Unfactored	1044	6	607
	Factored	1734	-	-

It can be found that, from Table 5-2, the take-off field length and landing field length of FW-11 is 1780m and 1734m respectively.

In order to analyze the aircraft capability of take-off from high altitude airport, cases with different altitudes are calculated and corresponding results are presented in Table 5-3. It can be found that the required field length for aircraft take-off with maximum weight increases significantly as the altitude increases. It means the aircraft has to select a more powerful engine or reduce the weight to meet the field length requirement when take-off from a high altitude airport. Otherwise, a longer field length will be required to allow the aircraft take-off with maximum weight at high altitude airport.

Table 5-3 Take-off field length at different altitudes

	AEO(Unfactored)	AEO(Factored)	OEI(BFL)
MTOW, ISA, Sea Level	1332m	1532m	1780m
MTOW, ISA, 1000m	1440m	1656m	1960m
MTOW, ISA, 2000m	1563m	1797m	-
MTOW, ISA, 3000m	1688m	1941m	-
MTOW, ISA, 4000m	1830m	2105m	-

5.3.2 En-route Performance

The detailed calculation process of FW-11 en-route performance is presented in Appendix F and results are summarized in Table 5-4.

It should indicate that following assumptions are adopted in en-route performance calculation:

- The segments are broken down into 1000ft steps to keep the error of the calculation small.
- The values of each step are calculated by using the results of the previous step.

Table 5-4 En-route performance of FW-11

	Distance (nm)	Time (min)	Fuel Burn (kg)
Climb Segment	155.7	21.9	3266.7
Cruise Segment	7000	878.1	58182.0
Descent Segment	160.4	28.7	343.9
Total	7316.1	928.7	61792.6

5.3.3 Division and Reserve Performance

The division performance is calculated using the same model for main mission. The results are summarized in Table 5-5.

Table 5-5 Division performance calculation

	Distance (nm)	Time (min)	Fuel (kg)
Climb to 10000ft from Decision Height	12.8	2.8	561.7
Cruise at 10000ft	147.5	28.2	2160
Descent from 10000ft to Landing	39.7	8.9	132.2
Totals	200.0	39.9	2853.9

Taking account of 45min regulatory fuel reserve and 10% contingency of trip fuel reserve, the fuel reserves required for FW-11 is then estimated as presented in Table 5-6.

Table 5-6 Fuel reserves for FW-11

45min Regulatory Reserve Fuel (kg)	2281
Diversion Fuel (kg)	2854
10% Contingency Fuel (kg)	6216
Total (kg)	11351

5.4 Payload-Range Analysis

To show the ability of the aircraft to perform different missions, a typical payload-range diagram for FW-11 is constructed on the basis of mission analysis at critical points. The range and payload at three critical points are calculated and presented in Table 5-7. The corresponding diagram is plotted in Figure 5-3. It can be found that the design payload range for FW-11 is 7821nm.

Table 5-7 Critical points parameters for payload-range diagram

	Maximum Payload	Maximum Fuel	Ferry
Take-off Weight(kg)	176469	176469	167544
OEW(kg)	75044	75044	75044
Payload available(kg)	41320	8925	-
Total Fuel Available(kg)	60105	92500	92500
45 min Reserve Fuel(kg)	2281	2281	2281
Diversion Fuel(kg)	2854	2854	2854
Total Trip Fuel(kg)	54970	87365	87365
10% Contingency Fuel(kg)	5497	8737	8737
Trip Fuel Available(kg)	49473	78629	78629
Take-off Fuel(kg)	368	368	368
Climb Fuel(kg)	3267	3267	3267
Descent Fuel(kg)	344	344	344
Landing Fuel(kg)	607	607	607
Cruise Fuel Available(kg)	44888	74043	74043
R(nm)	5857	10839	11488

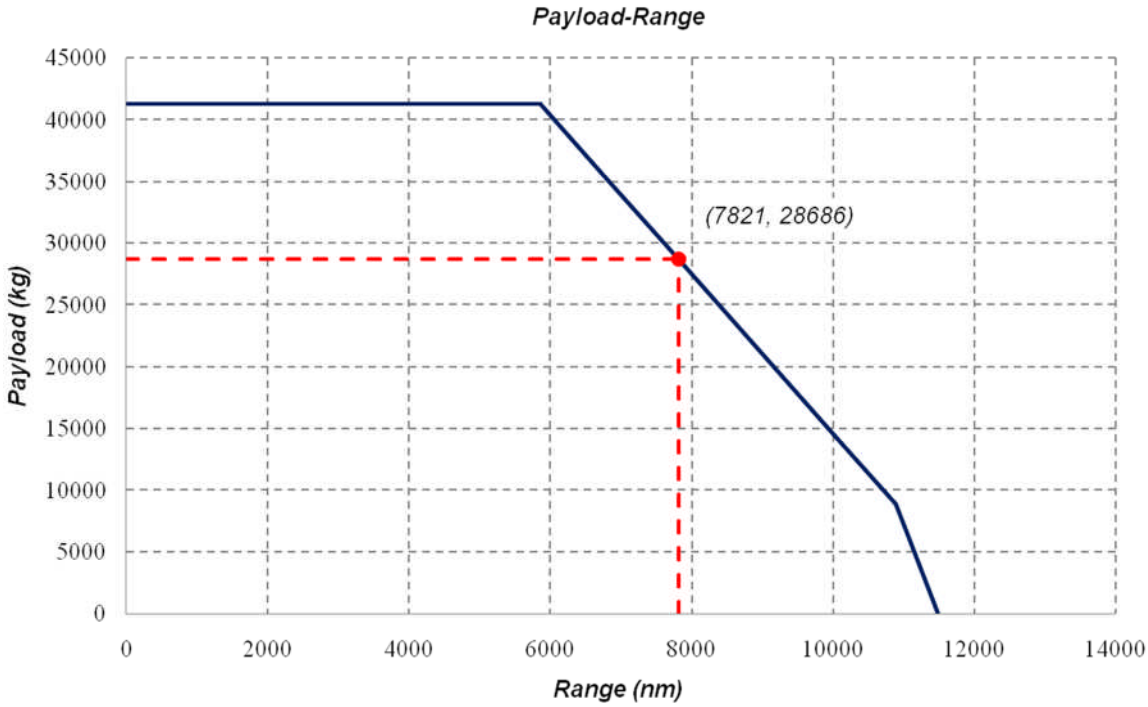

Figure 5-3 Payload range diagram of FW-11

5.5 Comparison with GDP

A comparative study between the aircraft performance of GDP and IRP is conducted, as presented in Table 5-8. It notes that the biggest deviation is 8.4% in maximum fuel range and all deviations are less than 10%. Taking account of different methods are used in aircraft performance prediction, these deviations are negligible in conceptual design phase. Consequently, the aircraft performance calculation model, constructed herein, is validated. Besides, it also can be found that the performance of aircraft, powered by GTF-11, meet the requirements of the FW-11 which are given in GDP specification report.

Table 5-8 Comparison with GDP

	GDP	IRP	Deviation
MTOW(kg)	176469	176469	-
OEW(kg)	75044	75044	-
Design Payload(kg)	28686	28686	-
Maximum Payload(kg)	41320	41320	-
Maximum Fuel Capacity(kg)	92500	92500	-
Take-off Field Length @MTOW, SL(m)	1853	1780	-3.9%
Landing Field Length @MTOW, SL(m)	1852	1734	-6.4%
Maximum Payload Range(nm)	6256	5857	-6.4%
Maximum Fuel Range(nm)	10003	10839	8.4%
Ferry Range(nm)	10594	11488	8.3%
Design Range(nm)	7772	7821	0.6%

5.6 Comparison with RB211-524B4

To investigate the benefits of geared concept engine in aircraft performance improvement, a comparative study between aircraft performance of using GTF-11 and conventional turbofan RB211-524B4 is conducted. As shown in Table 5-9 and Figure 5-4, the range for aircraft with GTF-11 at design payload is 13.1% larger than that with RB211-524B4, which means the fuel efficiency (fuel used per passenger per nautical mile) of the aircraft can achieve a 13.1% improvement by using new concept engine.

Table 5-9 Comparison with conventional turbofan RB211-524B4

	GTF-11	RB211-524B4	Deviation
Maximum Payload Range (nm)	5857	5179	-
Maximum Fuel Range (nm)	10893	9633	-
Ferry Range (nm)	11488	10159	-
Design Payload Range(nm)	7821	6916	13.1%

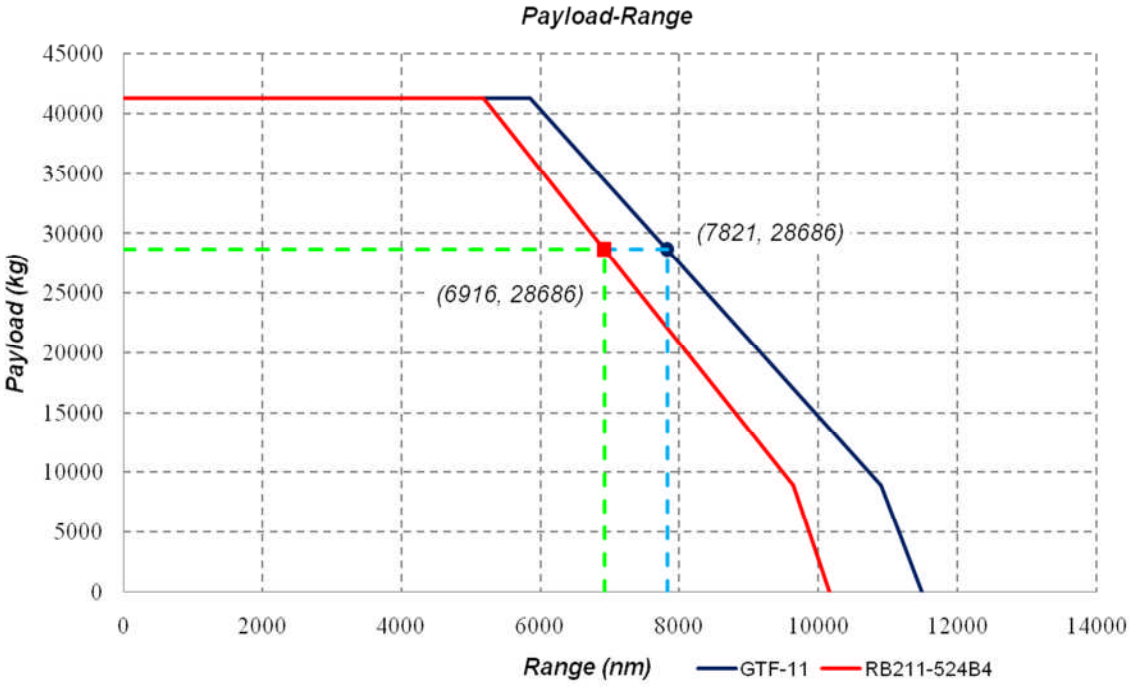

Figure 5-4 Comparison between GTF-11 and RB211-524B4

6 Nacelle Sizing

6.1 Introduction

The aero engine nacelle plays an important role on engine and aircraft performance. Since the high BPR which contributes to a significant improvement in engine performance results in an increment in engine size, the nacelle drag and weight for high BPR turbofans will increase. To keep the benefits of high BPR engines, it is necessary to design a nacelle of optimum aerodynamic performance and minimum weight. In this chapter, the processes of nacelle geometry design and drag calculation for GTF-11 engine are presented.

6.2 Functions and Types of Nacelle

For high BPR engine, nacelle mainly has following functions [32]:

- A container for engine and add-on accessories, device and components;
- An intake to deliver air to the engine with high efficiency and minimum inlet distortion;
- A nozzle to exhaust gases getting thrust efficiently;
- A thrust reverser to provide backward thrust which can relieve the brake burden and reduce the required run way length during landing.
- A noise suppressor or absorber to keep the engine noise on an acceptable level.

Basically, the nacelle can be categorized in two kinds: separate exhaust nacelle and mixed exhaust nacelle, as shown in Figure 6-1. For the former kind, the fan duct flow and core duct flow exit separately. For the latter kind, the flows mixed before leave nacelle [33].

Since the flows are mixed before leaving, the mixed nozzle nacelle provides a lower jet velocity and better performance. However, these advantages are at the expense of increased weight and surface friction drag. It is particular for high BPR engine, the higher the BPR is, the severer the penalties will become. Therefore, almost all of current high BPR turbofans employ the separate

exhaust nacelle which has a simple structure and low friction drag. In present study, a separate exhaust nacelle is selected for GTF-11.

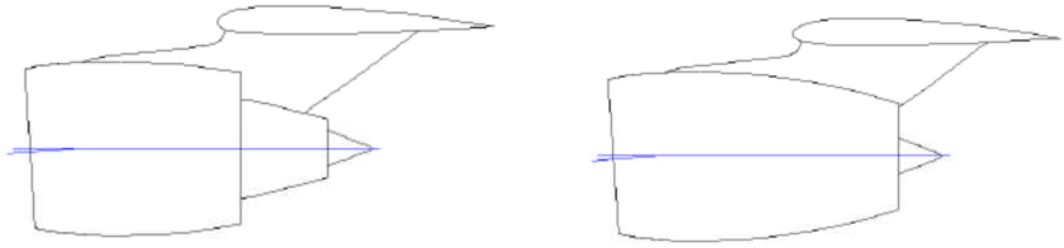

a) Separate exhaust nacelle b) Mixed exhaust nacelle

Figure 6-1 Types of nacelle

6.3 Nacelle Design Methods [33]

Generally, the engine nacelle design can be divided into three parts: fore-body design, mid-body design and after-body design. The fore-body is from intake tip to maximum diameter; the middle-body connects the fore-body and after-body and the after-body is the last part and forms a nozzle of the nacelle. Since the mid-body is usually just a cylinder, no detailed information will be presented here.

6.3.1 Fore-body Design Method

The nacelle fore-body design is a compromise to fulfil all the aerodynamic performance requirements. It is suggested to design the fore-body using well-know NACA-1 cowl design rules. As shown in Figure 6-2, the geometry parameters of fore-body can be determined using this method.

In practice, the fore-body sizing can be divided into following steps:

1) Decide the throat diameter, D_{th}, and highlight diameter, D_{hl}

The throat area of the inlet is sized to meet the maximum flow demand of the engine during the whole flight envelope. Typically, this occurs at TOC. Knowing the inlet Mach number and mass flow rate at TOC, the throat diameter, D_{th}, can be estimated using one-dimensional equations presented in Appendix B.1. The intake maximum throat Mach number, M_{th}, typically, ranges from 0.7 to 0.75 [33].

Then, the highlight diameter, D_{hl}, can be estimated with throat diameter, D_{th}, and the empirical value of lip contraction ratio (Equation 6-1), which typically ranges from 1.2 to 1.35 [33].

$$\text{contraction ratio} = \frac{\text{highlight area}}{\text{throat area}} = \frac{A_{hl}}{A_{th}} = \left(\frac{D_{hl}}{D_{th}}\right)^2 \quad \textbf{(6-1)}$$

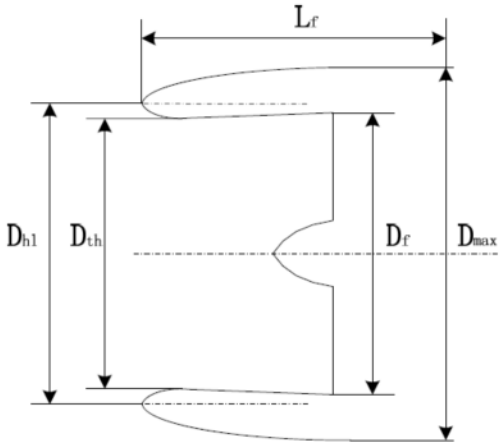

Figure 6-2 NACA 1-series nacelle fore-body

2) Decide the fore-body length, L_f, and maximum diameter, D_{max}

The fore-body length, L_f, and maximum diameter, D_{max}, can be obtained from D_{hl}/D_{max} and L_f/D_{max} which are chosen to avoid the onset of significant spillage drag and wave drag during flight.

According to reference [33], the D_{hl}/D_{max} and L_f/D_{max} are correlated approximately against the critical mass flow ratio, MFR_{crit}, and drag rise Mach number, M_d, as following equations.

$$\text{MFR}_{\text{crit}} = [1 - 4(1 - D_{hl}/D_{max})^2/(L_f/D_{max})]^{5/2} \quad \textbf{(6-2)}$$

$$M_d = 1 - 1/8\left[\sqrt{1 - (D_{hl}/D_{max})^2}/(L_f/D_{max})\right] \quad \textbf{(6-3)}$$

Once the design values of MFR_{crit} and M_d are selected, the leading dimensions of the fore-body can be estimated by these equations, as shown in Figure 6-3.

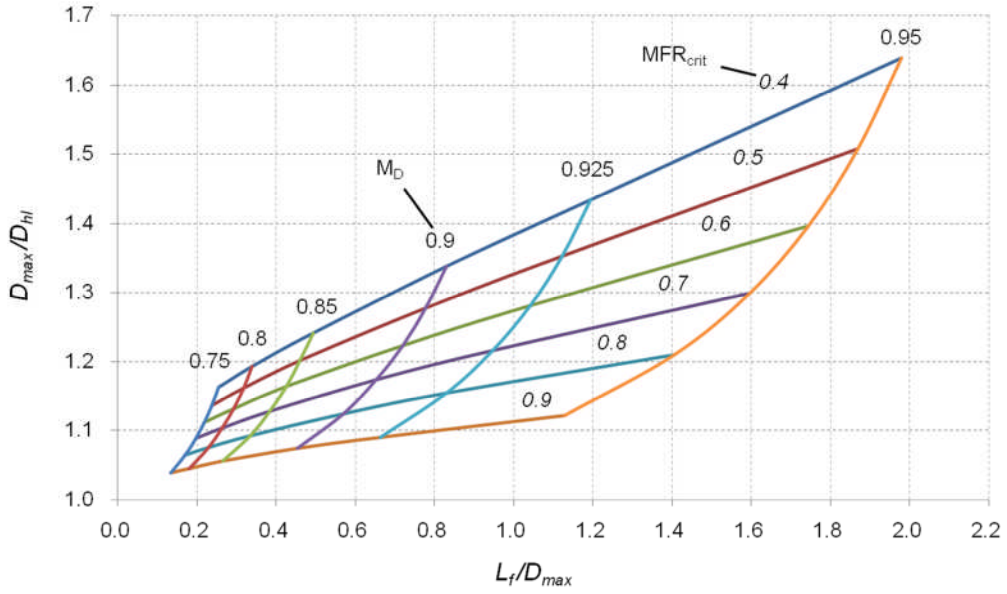

Figure 6-3 Critical MFR and Drag-rise Mach number of NACA-1 Series

As shown in Figure 6-4, the MFR_{crit} and M_d give a brief overview of the fore-body aerodynamic performance. For a given free stream Mach number, when the intake operating MFR is lower than MFR_{crit}, the flow over fore-body will separate and results in spillage drag. While for a given MFR, severe wave drag will take place when the free stream Mach number, M_0, is higher than M_d. Theoretically, the lower the MFR_{crit} and the higher the M_d, the better the nacelle performance will be.

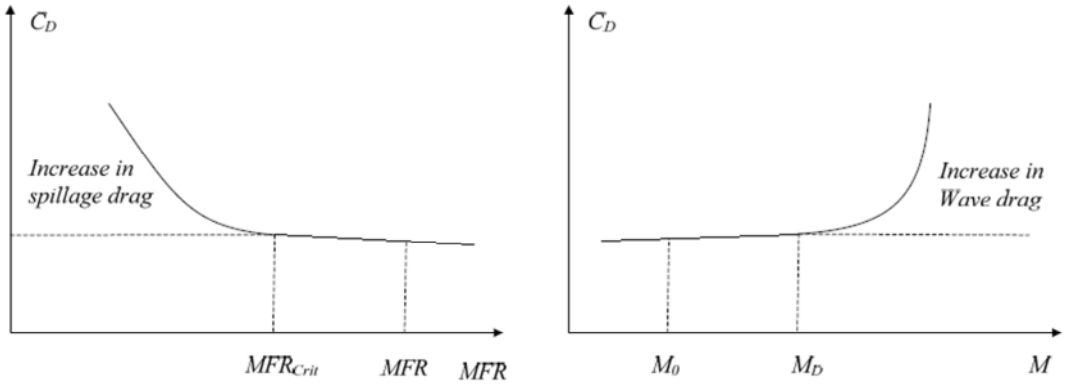

Figure 6-4 Effect of MFR_{crit} and M_d on nacelle performance

4) Decide the shape of inlet lip

The inlet lip connects the highlight area to the throat plane, which is suggested sizing as elliptical or super-ellipse shape to improve low speed characteristics of the nacelle. [34]

For elliptical inlet lip, the profile is a quarter of ellipse which can be expressed as following equation.

$$\left(\frac{x}{a}\right)^n + \left(\frac{y}{b}\right)^n = 1 \tag{6-4}$$

where:

a is the major super-ellipse axis;

b is the minor super-ellipse axis;

n is the elliptic exponent.

According to Albers and Miller [35], the axis ratio and elliptic exponent can be all selected as 2 for the sake of better performance during take-off and landing. Then the Equation 6-4 can be rewritten as:

$$\left(\frac{x}{2b}\right)^2 + \left(\frac{y}{b}\right)^2 = 1 \tag{6-5}$$

where,

$$b = \frac{D_{hl} - D_{th}}{2} \tag{6-6}$$

5) Decide the external contour

The external contour should be a smooth surface that has an acceptable drag level during flight. To design a smooth external contour, an approach presented in ESDU 94013 [36] can be employed as following.

$$\frac{y}{Y} = c\left(\frac{x}{X}\right)^{0.5}\left[\frac{1}{c} - \frac{1}{2c}\left(\frac{x}{X} - 1\right)\right] + \left[\left(1 - \frac{1.5}{c}\right)\left(\frac{x}{X} - 1\right)^2\right] + \left[\sum_{n=0}^{7}(-1)^{n+1}A_n\left(\frac{x}{X}\right)^n\right]\left[\frac{\left(\frac{x}{X}\right)^{1.5}\left(1 - \frac{x}{X}\right)^2}{\left(b + \frac{x}{X}\right)^2}\right] \tag{6-7}$$

In which, b=0.05, c=1.044988 and:

$$X = L_f \tag{6-8}$$

$$Y = \frac{D_{max} - D_{hl}}{2} \tag{6-9}$$

n	0	1	2	3	4	5	6	7
A_n	0.009466	0.378874	1.709298	7.731339	22.79108	40.64622	38.05716	14.23322

6) Decide the internal contour

The internal contour from throat plane to fan entry face forms the duct diffuser. It also needs a smooth surface to ensure that separation will not take place even in engine transient operation, because the flow separation along the diffuser will result in unacceptable engine thrust or engine surge [37].

In practice, the empirical value of diffuser ratio, fan entry area to throat area ratio, is in range of 1.25 to 1.35 [33].

Besides, the practical minimum intake length, proposed by Leynaert [38], should be 0.62 times of the fan diameter required for a subsonic transport. This value is defined as minimum for acoustic treatment and also suitable to design a convenient aerodynamic intake shape for cruise Mach number of about 0.80.

6.3.2 After-body Design Method

The design of nacelle after-body is to fair the maximum diameter section and the final nozzle. Normally, the shape of boat-tail is circular-arc, sketched in Figure 6-5.

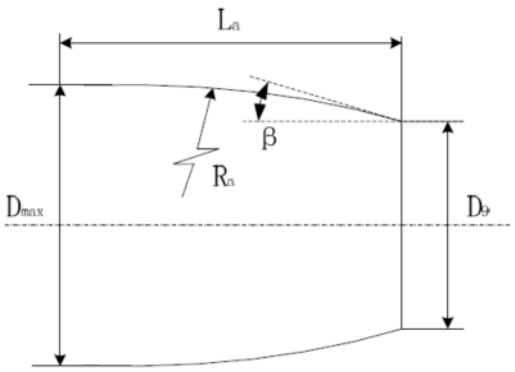

Figure 6-5 After-body dimensions

where:

L_a=after-body length;

R_a=boat-tail radius;

D_9=nozzle-exit diameter;

β =final boat-tail angle.

The after-body ratio, R_a/D_{max}, is related to free stream drag rise Mach number, $M_{d,a,}$ as Equation 6-10.

$$R_a/D_{max} = 0.04/(1 - M_{d,a})^2 \quad \textbf{(6-10)}$$

It indicates that the ratio of R_a/D_{max} will verge to infinity when $M_{d,a}$ moves toward Mach number 1. Therefore, a bigger R_a is preferable for drag-rise Mach number. Moreover, if the radius ratio is too small, the boundary layer will grow rapidly and the flow separation will occur at the rear of the boat-tail. However, if the ratio is too large, the higher skin friction drag will arise caused by too much wet surface area.

The final boat-tail angle, β , has to be set to minimize the possibility of boundary-layer grow and flow separation. The after-body chord angle, β_c, half of the β , is defined as the equation:

$$\tan\beta_c = (D_{max} - D_9)/2L_a \quad \textbf{(6-11)}$$

In which, the nozzle-exit diameter D_9 can be decided in engine performance simulation.

Typically, the value of β is less than 16 degrees and corresponding chord angle, β_c, for a circular-arc design is less than 8 degrees.

6.4 Nacelle Drag Estimation Methods [33]

They are many approaches available for nacelle drag evaluation, such as wind tunnel testing, CFD simulation and ESDU calculation program. In present study, a brief drag assessment method from Darrell Williams [33] is reviewed and employed for further key parameters analysis.

Basically, the nacelle drag is given by profile drag plus any spillage drag or/and wave drag. So, the estimation of the drag of a nacelle can be divided into two parts:

- Design conditions: for MFR, M_0 are within MFR_{criti} and M_d limits, the nacelle drag is given by profile drag.
- Off-design conditions: for MFR, M_0 are outside the MFR_{criti} and M_d limits, in which spillage drag and wave drag become increasingly significant.

As a discussion of the latter part would take us far away, the methods presented here are just limited to the former part.

6.4.1 Fore-body Drag

In the range of $MFR>MFR_{crit}$ and $M_0<M_d$, the NACA-1 nacelle drag coefficients, C_D, can be calculated by empirical Equation 6-12 presented in reference [33].

$$\left(\frac{C_D}{C_F}\right)^{0.6} = 1 + \frac{1}{3}\left[\left(1 - \frac{D_{hl}}{D_{max}}\right)\Big/\left(\frac{L_f}{D_{max}}\right)\right]\left[1 + \frac{7}{4}(1 - MFR)\Big/\left(\frac{A_{max}}{A_{hl}} - 1\right)\right] \quad \textbf{(6-12)}$$

In which, C_F is the skin-friction coefficient of the flat-plate having the same wetted surface area as the nacelle. It can be calculated by M_0 and Reynolds number R_e based on L_f.

$$C_F = C_f \frac{S_{wet}}{A_{max}} \quad \textbf{(6-13)}$$

Where, S_{wet} is the fore-body wetted area and A_{max} is the maximum cross area. The mean skin-friction coefficient, C_f, can be estimated as Equation 6-14.

$$C_f = \frac{0.455}{(\log R_e)^{2.58}} \quad \textbf{(6-14)}$$

The calculation process of Re is presented in Appendix G.1.

For Equation 6-14, there is a datum conditions when MFR=1, then:

$$\frac{C_{D,0}}{C_F} = \left[1 + \frac{1}{3}\left(1 - \frac{D_{hl}}{D_{max}}\right)\Big/\left(\frac{L_f}{D_{max}}\right)\right]^{\frac{5}{3}} \quad \textbf{(6-15)}$$

Or, more simply:

$$\frac{C_{D,0}}{C_F} = \left(1 + \frac{2Y}{3L_f}\right)^{\frac{5}{3}} \quad \textbf{(6-16)}$$

where:

$$Y = \frac{D_{max} - D_{HL}}{2} \quad \textbf{(6-17)}$$

Then, in the range of MFR_{crit}<MFR<1, C_D can be expressed in terms of the cowl drag at datum conditions as:

$$\frac{C_D}{C_{D,0}} = [1 + K(1 - MFR)]^{\frac{5}{3}} \quad \textbf{(6-18)}$$

The value of constant K that depends on the geometry of the nacelle can be calculated as:

$$K = 1.75\left\{\left(\frac{D_{max}}{D_{hl}} + 1\right)\left[\left(1 + 3\frac{L_f}{D_{max}}\right)\frac{D_{max}}{D_{hl}} - 1\right]\right\}^{-1} \quad \textbf{(6-19)}$$

Finally, the fore-body drag is estimated using:

$$D = \frac{1}{2}\rho V^2 A_{max} C_D \quad \textbf{(6-20)}$$

6.4.2 After-body Drag

Similarly, the after-body drag can be calculated on an equivalent flat-plate basis, as for the fore-body, within the design domain, M_0<$M_{d,a}$.

6.5 Sensitivity Analysis of Parameters

The nacelle design not only has to meet the performance requirements of engine, but also needs to seek a better aerodynamic performance. In present research, the effects of key parameters on nacelle aerodynamic performance are analyzed to seek optimum nacelle geometry.

Based on above nacelle design and drag assessment methods, a spreadsheet calculation model is constructed for parameters sensitivity analysis. The variables, such as lip contraction ratio, MFR_{crit}, M_d and $M_{d,a}$, are set as input to calculate the geometry and drag of the nacelle as output. The typical ranges of

input variables for analysis are listed in Table 6-1. In which, the R_{ld} is the ratio of overall length L_{ov} to maximum diameter D_{max}.

Table 6-1 Typical range of input variables

Input Variable	Minimum	Maximum
A_{hl}/A_{th}	1.2	1.35
MFR_{crit}	0.55	0.65
M_a	0.875	0.925
$M_{d,a}$	0.875	0.925
β_c	6°	8°
R_{ld}	1.3	1.5

The effects of input variables on nacelle maximum diameters D_{max} and drags in terms of fore-body drag, d_f, after-body drag, d_a, and total drag, d_t are calculated and plotted in Figure 6-6 to Figure 6-11.

It can be found that, from Figure 6-6, the MFR decreases as the contraction ratio increase. The reason is that for fixed A_0 and A_{th}, an increment in contraction ratio will lead to an increment in A_{hl}, in turns, the reduction of MFR (A_0/A_{hl}). It also means the margin of mass flow ratio △MFR decreases for a fixed MFR_{crit}.

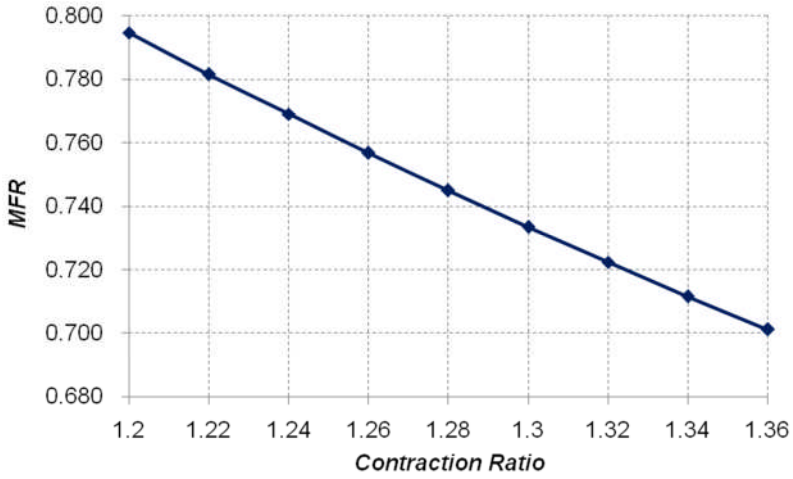

Figure 6-6 MFR against contraction ratio

As shown in Figure 6-7 and Figure 6-8, the D_{max} and nacelle drags increase as the contraction ratio increase. Besides, the reduction in MFR_{crit} results in an

increment in D_{max} and nacelle drags while the M_d has the reverse effects. It also should note that, the nacelle fore-body drag, d_f decrease with the M_d increase.

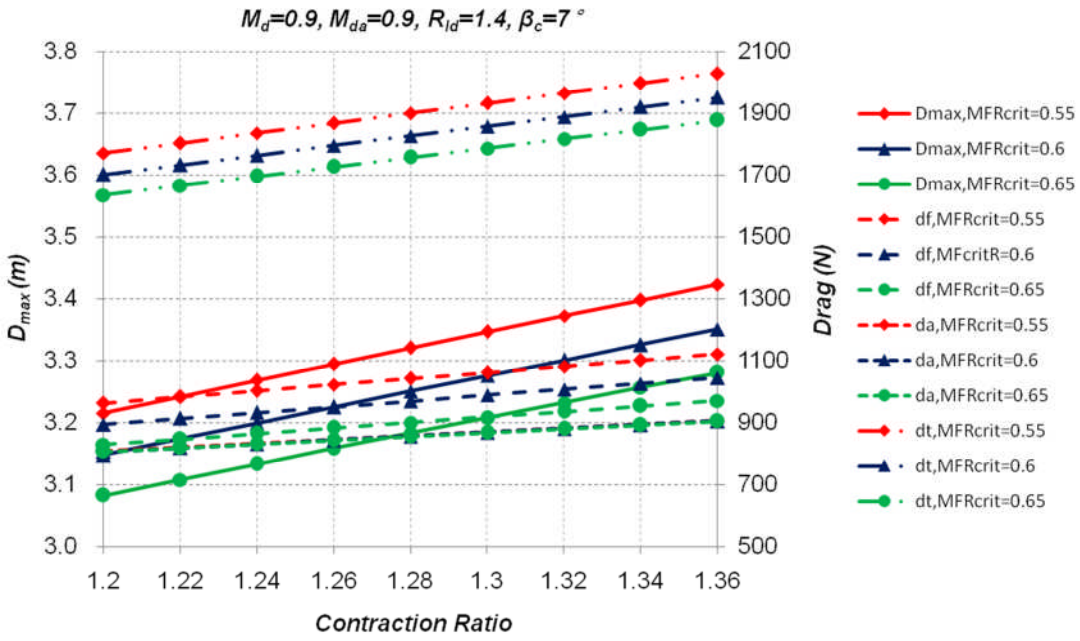

Figure 6-7 Effects of MFR_{crit} on D_{max} and drags

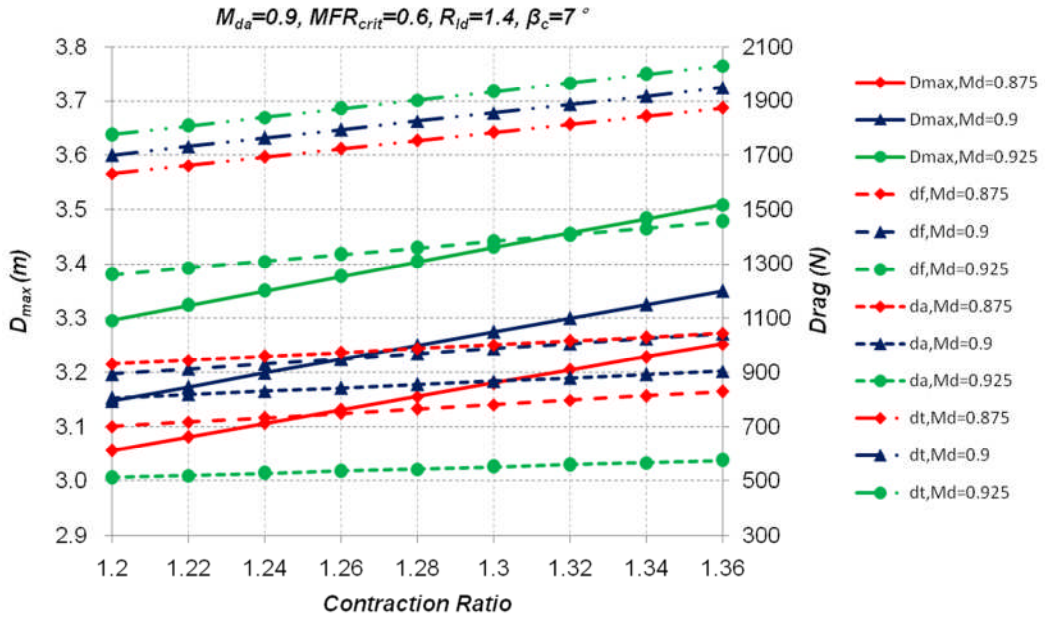

Figure 6-8 Effects of M_d on D_{max} and drags

Therefore, to minimize the D_{max} and nacelle drags, the MFR_{crit} has to be increased or/and the M_d has to be decreased. However, these will lead to the

reduction of margin of MFR, △MFR or/and margin of Much number, △M, which deteriorate the nacelle operating performance.

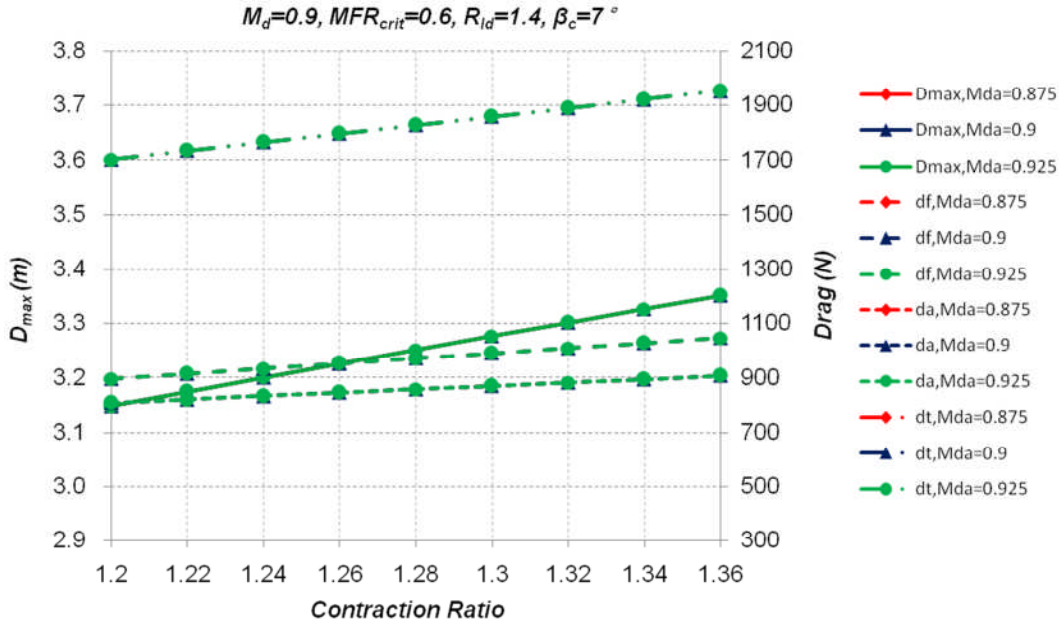

Figure 6-9 Effects of $M_{d,a}$ on D_{max} and drags

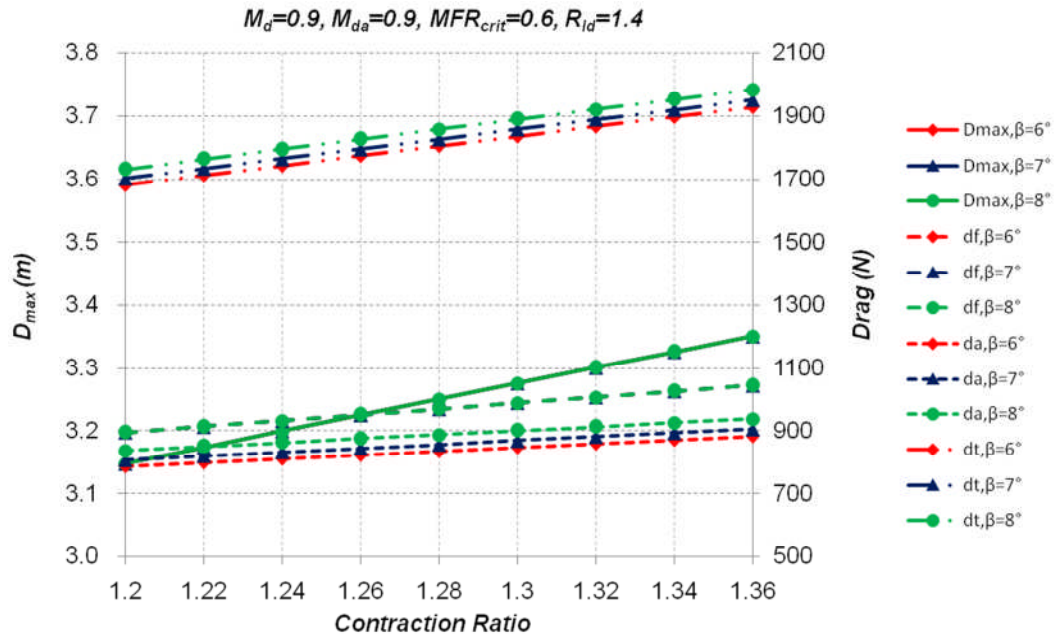

Figure 6-10 Effects of β_c on D_{max} and drags

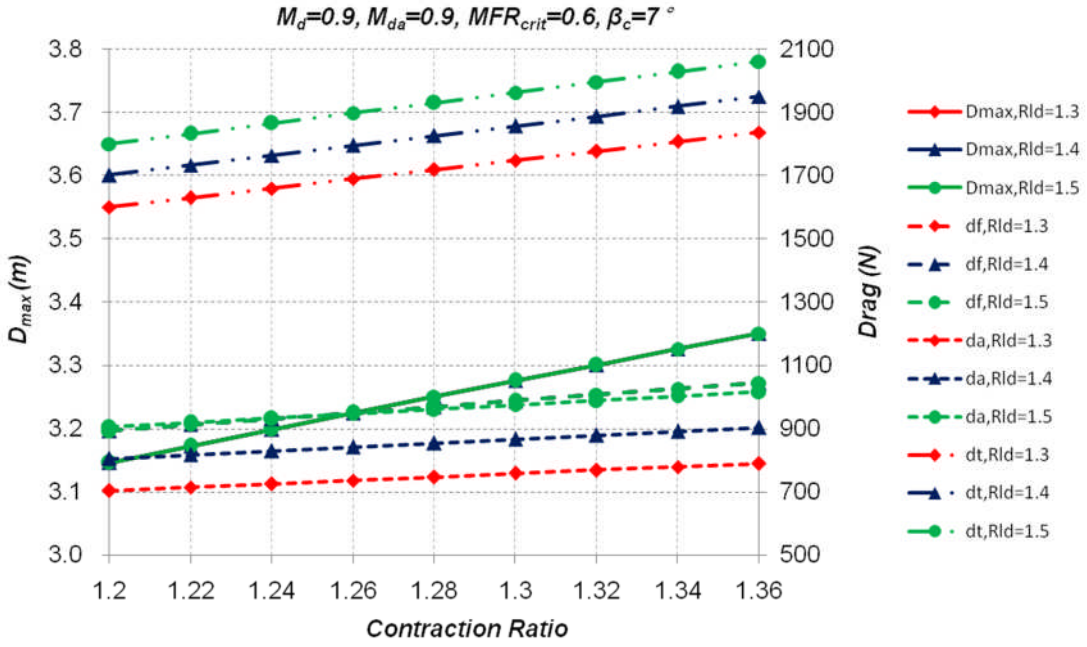

Figure 6-11 Effects of R_{ld} on D_{max} and drags

From Figure 6-9 to Figure 6-11, it can be found that the $M_{d,a}$, β_c and R_{ld} have no effects on the D_{max}. For nacelle drags, the effect of the $M_{d,a}$ is negligible in the range of study. The increase of the R_{ld} or/and β_c lead to the increase in nacelle drag, especially the after-body drag, d_a.

The sensitivity effects of the input variables on nacelle geometry and performance are summarized in Table 6-2.

Table 6-2 Sensitivity effects of input variables

	D_{max}	d_f	d_a	d_t	△MFR	△M
Contraction Ration↑	↑	↑	↑	↑	↓	—
M_D↑	↑	↑	↓	↑	—	↑
MFR_{crit}↑	↓	↓	↓	↓	↓	—
R_{ld}↑	—	—	↑	↑	—	—
β_c↑	—	—	↑	↑	—	—

6.6 Nacelle Design

6.6.1 Parameters Selection

Based on above analysis, the preliminary input variables for GTF-11 nacelle design can be selected as following:

1) Critical mass flow ratio, MFR_{crit}

Since the margin of the mass flow ratio, $\triangle$MFR, increases while the D_{max} and nacelle drag increase with the decrease of the MFR_{crit}, the MFR_{crit} is selected as 0.55 to obtain a compromise between these two factors.

2) Lip contraction ratio, A_{th}/A_{hl}

Some researchers suggested that increasing the radius of the inlet lip can improve the low speed characteristics of the nacelle while still remaining its high speed characteristics [39]. However, as presented in Figure 6-6 and Figure 6-7, the increase of contraction ratio will results in an increment in D_{max} and nacelle drag. Therefore, the contraction ratio is selected as 1.28 to balance this conflict.

3) Drag rise Mach number, M_d

Based on the values of MFR_{crit} and contraction ratio, it is reasonable to choose M_d of 0.9 for nacelle design. Meanwhile, assume that the after-body drag rise Mach number, $M_{d,a}$ equals the M_d.

4) Final boat-tail angle, β

Because the bypass exhaust always close to the maximum cross-section of the cowl for intermediate-cowl nacelle, the final boat-tail angle, β, for nacelle design are usually less than the maximum value of 16 degrees [33]. In present research, the final boat-tail angle of the nacelle is selected as 14 degrees and corresponding chord angle, β_c, is 7 degrees for preliminary design. Exact value of this parameter can be gained on the basis of CFD analysis or wind tunnel testing.

5) Overall length to maximum diameter ratio, R_{ld}

Finally, for nacelle overall length to maximum diameter ratio, R_{ld}, it is selected as 1.45 based on the measurement approach of the nacelle of Trent1000.

6.6.2 Nacelle Geometry of GTF-11

Then, the nacelle geometry of GTF-11 can be sized based on the above parameters. The detailed calculation process is presented in Appendix G.2 and the results are summarized in Table 6-3.

Table 6-3 Dimensions of GTF-11 nacelle

D_{hl}(m)	D_{th}(m)	D_{max}(m)	D_9(m)	L_f(m)	L_a(m)	L_{ov}(m)	R_a(m)	β(°)
2.658	2.349	3.321	2.750	2.488	2.327	4.815	13.28	7

Based on the dimensions, the profile of the nacelle can be plotted as shown in Figure 6-12.

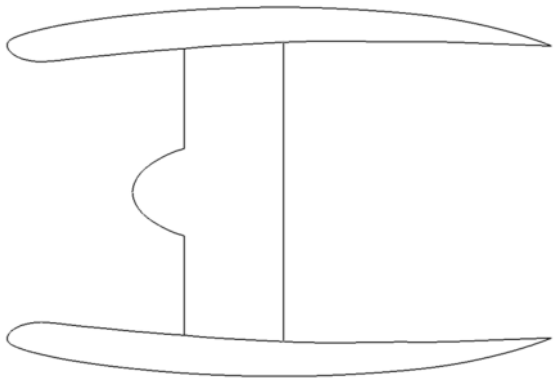

Figure 6-12 GTF-11 nacelle geometry

6.7 Nacelle Drag Coefficient Calculation

Knowing the nacelle geometry and for an accurate analysis, the nacelle drag coefficient of GTF-11 can be calculated using ESDU81024a, which provides comprehensive drag estimation methods for different engine operating conditions. Meanwhile, the nacelle drag coefficient of the conventional turbofan RB211-525B4 is calculated on the basis of measured nacelle dimensions, for a comparison with GTF-11.

6.7.1 Nacelle Drag Coefficient of GTF-11

Assuming left-off speed V_{LOF} is 1.1 times of stall speed at the maximum takeoff weight and approach speed V_A is 1.4 times of stall speed at maximum landing weight, therefore, the Mach number at takeoff and approach conditions are 0.184 and 0.217, respectively. Then, the nacelle drag coefficients of GTF-11 at different flight conditions are calculated using ESDU method. Detailed calculation results are presented in Appendix G.3.

The input parameters for calculation in ESDU are summarized in Table 6-4.

Table 6-4 Input variables for calculation in ESDU (M=0.82)

COWL GEOMETRY			
	Fore-body	Mid-body	After-body
Shape	NACA 1	Cylindrical	Circular arc
Length ratio	L_f/L_{ov} =0.5167	L_m/L_{ov} =0.0000	L_a/L_{ov} =0.4833
Fineness ratio	L_f/D_{max} = 0.7492	L_m/D_{max} =0.0000	L_a/D_{max} = 0.7007
Diameter ratio	D_{hl}/D_{max} =0.8004	---	D_9/D_{max} =0.8281
Inlet contraction ratio	A_{hl}/A_{th}=1.2800		
FLOW CONDITIONS			
R_e=0.3040E+08		M_0=0.82	

The nacelle drag coefficients of GTF-11 at different flight conditions are summarized in Table 6-5 and plotted in Figure 6-13.

Table 6-5 Drag coefficients of nacelle (GTF-11)

	MFR<MFR_{crit}			MFR>=MFR_{crit}			
MFR	0.3	0.4	0.5	0.53	0.6	0.7	0.8
M_d	0.8225	0.8375	0.8525	0.857	0.857	0.857	0.857
C_D(Cruise)	0.06800	0.03980	0.02280	0.01980	0.01910	0.01830	0.01760
C_D(Take-off)	0.08805	0.04674	0.02353	0.01960	0.01912	0.01846	0.01794
C_D(Landing)	0.08841	0.04689	0.02354	0.01960	0.01910	0.01840	0.01790

It can be found, from Table 6-5, the MFR_{crit} based on nacelle geometry is 0.53 and corresponding M_d is 0.857. Compared to the previous values estimated by empirical methods, the margin of mass flow ratio, △MFR, increases from 0.195

to 0.215 while the margin of Mach number, △M, decreases from 0.08 to 0.037. The reason might be that the ESDU method had taken account of the effect caused by the fore-body/after-body interference in calculation while empirical methods analyze the drags of fore-body and after-body separately.

Besides, it notes that the margin of Mach number, △M, is too small, which means the performance of nacelle at high speed may not meet the nacelle design requirement. Therefore, a further study and possible modifications should be developed in this field.

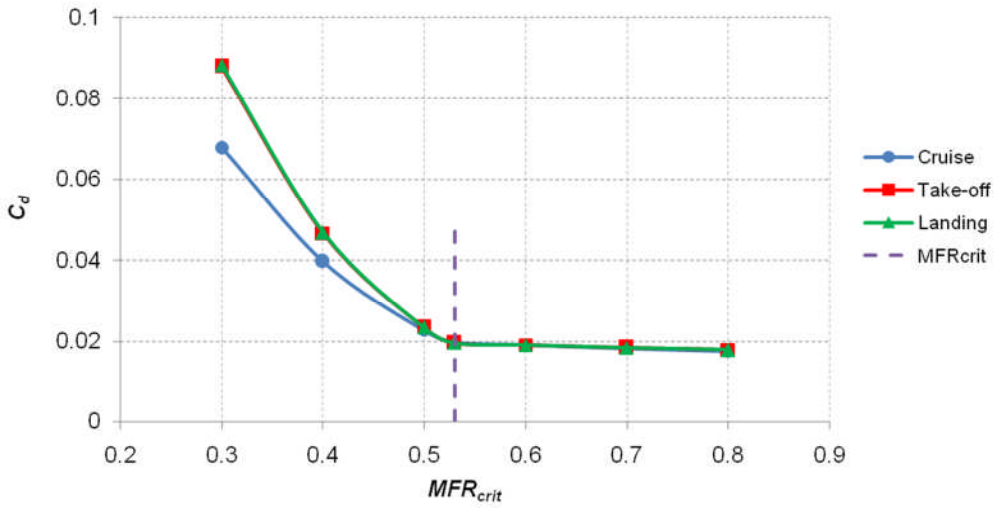

Figure 6-13 Drag coefficients of nacelle (GTF-11)

6.7.2 Nacelle Drag Coefficient of RB211-525B4

The dimensions of nacelle of RB211-525B4, as presented in Table 6-6, are obtained from aircraft characteristics airport planning of Boeing 747 [40] by measurement approach.

Table 6-6 Dimensions of nacelle (RB211-525B4)

D_{hl}(m)	D_{max}(m)	D_9(m)	L_f(m)	L_a(m)	L_m(m)	L_{ov}(m)
2.175	2.610	1.740	1.740	1.865	0.808	4.413

Similarly, the nacelle drag coefficients of RB211-525B4 at different flight conditions are calculated using ESDU. The results are summarized in Table 6-7

and plotted in Figure 6-14. It can be found that the MFR_{crit} of the nacelle of RB211-525B4 is 0.491 and corresponding M_d is 0.8651.

Table 6-7 Drag coefficients of nacelle (RB211-525B4)

	$MFR<MFR_{crit}$		$MFR>=MFR_{crit}$				
MFR	0.3	0.4	0.491	0.5	0.6	0.7	0.8
M_d	0.8364	0.8514	0.8651	0.8651	0.8651	0.8651	0.8651
C_D(Cruise)	0.06038	0.03707	0.02494	0.02483	0.02359	0.02245	0.02156
C_D(Take-off)	0.08002	0.04196	0.02363	0.02356	0.02279	0.02207	0.0215
C_D(Landing)	0.08031	0.04205	0.0236	0.02353	0.02277	0.02205	0.02148

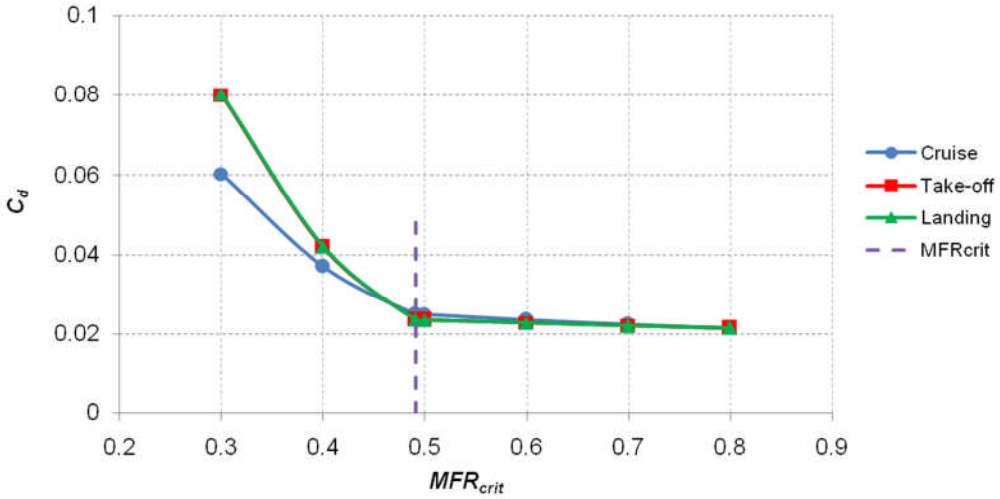

Figure 6-14 Drag coefficients of nacelle (RB211-525B4)

6.8 Effect of Nacelle Drag on Engine Performance

As the MFR of nacelle at cruise condition is 0.745 (refers to Appendix G.2), the nacelle drag coefficient for GTF-11 of 0.01795 and RB211-525B4 of 0.0220 can be obtained from Figure 6-13 and Figure 6-14, respectively. Then, the nacelle drag of two engines at cruise can be calculated using Equation 6-20. As presented in Table 6-8, the nacelle drags account for about 4.08% and 3.09% of net thrust for GTF-11 and RB211-525B4, respectively. It indicates that the nacelle drag would increase with the BPR increase, since a large fan is employed to get a reduction in fuel burn and noise. Obviously, this issue should be considered in engine selection.

Besides, according to Darrel William [33], the optimum nacelle drag should only accounts for about 3% of uninstalled engine thrust. Therefore, further studies in this field should be conducted.

Table 6-8 Effects of nacelle drag on engine performance

Engine	$F_{n\_uninstalled}$ (N)	D(N)	$F_{n\_installed}$(N)	Thrust Loss (%)
RB211-525B4	42790	1322	41468	3.09
GTF-11	42790	1745	41045	4.08

7 Engine Installation

7.1 Introduction

In aircraft design, many aspects, such as available space, safety, stability and control, maintainability, should be considered for engine installation. Comparing to most of conventional civil transport aircraft on which the engines are usually mounted under the wings, the FW aircraft requires a different solution for engine installation due to its unique configuration.

In this chapter, the considerations of engine installation are discussed at first. Then the preliminary disposition of GTF-11 on FW-11 is presented.

7.2 Number of Engines

The design of FW-11 with two engines was decided early in the GDP phase [3]. In this section, the factors that have to be considered when deciding the number of engines are discussed.

- Thrust required and thrust available
- Available space
- Reliability and safety
- Drag
- Simplicity
- Cost

Knowing the total thrust required of the aircraft, the number of engines can be obtained from current thrust available of the engines. For a given required total thrust, the number of engines can be reduced by employing more powerful engines.

As far as the available space is concerned, the fewer engines the better. Because the engines have to be separated enough to prevent each other from damaging by uncontained fragments of a failed engine. However, it should be noted that when deciding a reasonable distance between the engines, the effect of the power changes and power failure on aircraft stability and control should be considered as well.

The reliability and safety play important roles in engine number decision. Generally, the operational reliability and safety of the aircraft are enhanced by increasing the number of engines. This is the reason that the likelihood of catastrophic failure of the aircraft due to an engine failure will be reduced as more engines employed. However, since the more components the worse the maintenance reliability levels, the maintenance reliability of aircraft will be significantly degraded. Therefore, a balance should be achieved in these two aspects.

It also can be noted that a more streamlined body, as well as a reduction in the overall wetted area, can be obtained with fewer engines and pylon mountings protruding from the aircraft itself. These benefits allow the drag of the aircraft to be minimised and hence reductions in necessary thrust required and fuel burn of the aircraft. [41]

Since the number of systems, such as engine start system, fuel feed system and control system, is significantly affected by the number of engines, a simplicity design of these systems can be obtained as fewer engines used. It is obvious that simplicity leads to a more reliable, less expensive and lighter aircraft. From this point of view, it is sensible to keep the number of engines to a minimum.

According to reference [42], engines related costs can account for up to 19% of the aircraft production costs and 5% of the direct maintenance costs. Besides, a significant amount of man-hours will be demanded for a large number of engines maintenance as well. Consequently, it is desirable to use as few engines as possible.

7.3 Considerations of Engine Disposition

To decide the engine disposition, the following aspects should be considered.

- Space available
- Effect of engine failure on aircraft stability and control
- Drag
- Mass penalties

- Accessibility and maintainability
- Location of CG
- Engine inlet requirements
- Structure consideration
- Safety
- Noise

Based on the above factors, different locations of engines on a FW aircraft are discussed.

1) Under-wing installation

Usually, the engines are mounted under the wings for most of conventional civil transport aircraft. Despite this type of installation seems to be an effective solution, it may not be the case for a FW configuration aircraft.

For conventional aircraft with under-wing podded engines, one of the distinct advantages is that the engines produce a favourable bending relief and hence reduce the mass of the wing. However, since the FW configuration allows for a more favourable span-wise mass distribution, there is litter or nothing to be gained by implementing such a design.

Additionally, since the FW configuration features a whole wing and thick section, the available space under the wings of aircraft may not enough for engine installation. As presented in Figure 7-1, if the engines were located under the inner-wing, a longer and therefore heavier landing gear would be required to keep the necessary clearance from the ground. In turns, this requires more power for landing gear operating and increases the total mass of aircraft. The situation will become even worse when a very high BPR engine is used, for instance, GTF-11. With respect to outer-wing installation, there are some other problems. Since the engines are too far away from each other, the effect of power change and power failure of engines on aircraft stability and control will enlarge and burden the aircraft control system design. Moreover, putting such a heavier engine far away will increase the bending moment of the wing and

hence the structure has to be enhanced to support the engines. This in turn increases the mass of the aircraft.

One more aspect should be considered of this design is the noise problem. Since the engines are located near the ground, the airfield noise regulations should be introduced in aircraft design.

Finally, it should indicate that the under-wing installation will enhance the maintainability and accessibility of the engines, and also produce a favourable nose up pitching moment during take-off. However, based on previous issues, this type of installation has to be discarded in FW-11 design.

2) Over-wing installation

It is noted that the over-wing mounted could be an alternative solution for engine installation on a FW configuration, as which allow for short landing gear and reduce noise levels. Obviously, there are two options: front of the wing and rear of the wing.

Placing the engine in the front of the aircraft will contribute to a favourable CG distribution of the aircraft. However, this advantage is more than counteracted by many disadvantages.

Firstly, as presented in Figure 7-2, the front and centre area of the aircraft is cabin. Taking account of safety issue, if the engines are mounted on this area, it will be a hazard to the passengers, since the uncontained burst fragments from a failed engine would penetrate the fuselage. Meanwhile, the passengers will suffer from the noise and vibrations produced by overhead engines. Besides, the fuel pipes have to be routed around the cabin as well. Since there are already many electrical wires and air-conditioning ducts in this limited space, it leads to a potential fire hazard.

In addition, as be located too far forward, the engines and pylons will produce a detrimental effect upon the aerodynamic performance of the aircraft. The part of the flow that contributes most to the lift is disturbed and the lift produced by the trapezoidal wing will be degraded.

Consequently, the only suitable place for engine installation is the rear of the aircraft. As presented in Figure 7-2, this disposition can keep any uncontained hazard caused by failed engine away from the passengers. Meanwhile, the passengers comfort will be satisfied in addition to the safety consideration. Besides, since most of associated systems are located in the rear of the aircraft, it avoids the employment of long pipe and wires for connection, and hence simplifies the systems and reduces the overall mass of the aircraft.

One problem of this disposition is the effect on CG of the aircraft. The CG of the aircraft will be moved afterward and leads to a reduction in static stability margin. Therefore, this problem should be considered in aircraft design.

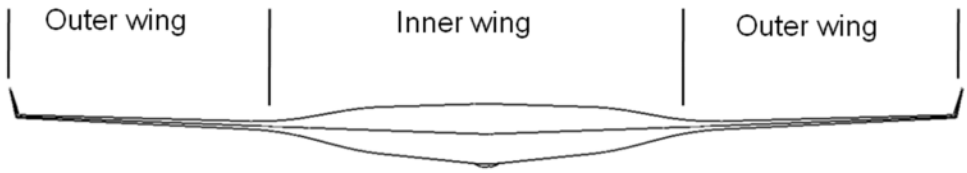

Figure 7-1 Rear view of FW-11

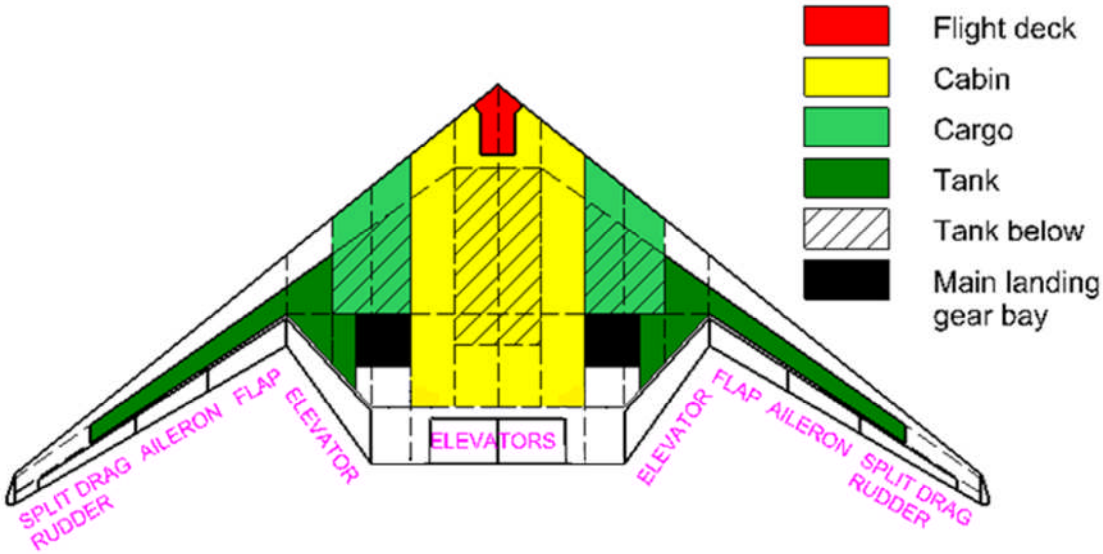

Figure 7-2 Over view of FW-11

7.4 Installation of GTF-11 on FW-11

Generally, there are three configurations for placing the engines at the rear of

the aircraft.

- Completely buried installation
- Partly buried installation
- Podded engines installation

According to FW-11 geometry, the length from the end of the cabin to the trailing edge is about 5.5m and the highest area of the rear space is about 2.6m. It is certain that the available space is not sufficient for completely buried or partly buried installation of GTF-11 which has a fan diameter of 2.56m and length of 3.52m.

Therefore, the two podded engines are axisymmetric mounted on the aircraft and the following parameters are estimated to determine the engines position on FW-11.

1) Longitude position

The longitude position is defined as the distance from the nose point of the aircraft to the CG of podded engines in X orientation. This parameter is mainly determined by the considerations of aircraft CG, structure and safety issues.

As discussed in previous section, from the points of passengers' safety and comfort, it favors the engines moved as afterward as possible. However, placing the engines afterward leads to the CG of the aircraft moved afterward that have a negative effect on aircraft static stability. It also increases the need to have an extensive and heavy structure in the relatively thin trailing space to support the engines.

Therefore, the engine longitude position is set of 22m to achieve a compromise between these factors. By calculation, the CG of aircraft with this disposition ranges from 30.68% to 37.09% and corresponding static stability margin ranges from 1.11% to 7.52%. It seems that the aircraft static stability is a bit weak. However, this result is acceptable for a FW configuration aircraft.

2) Spanwise position

The spanwise position is defined as the distance from the YZ plane of the

aircraft to the centerline of the engines.

As far as the safety issues are concerned, the two engines should be placed well apart. However, locating the engines far away from the centerline of the aircraft will burden the aircraft control system to trim the yaw deflection when one engine failure.

According to FW-11 geometry, the center area of the rear wing is the elevator which cannot be used for engine installation. Consequently, the engines are installed on the nearby aircraft frames as which have enough strength to support the engines. The corresponding spanwise distance is 5.8m and distance between the engines is 11.6m. Compared with conventional aircraft, as presented in Table 7-1, the value of spanwise position is acceptable for aircraft stability and control system design. Besides, based on BW-98 geometry [43] on which the distance between the engines is 7.5m, the value on FW-11 of 11.6m is reasonable.

Table 7-1 Spanwise position of engines on aircrafts

Aircraft	Spanwise Distance(mm)	Spanwise Position
A330-200	9,370	0.311
B767-200	7,920	0.333
FW-11	5,800	0.178

3) Vertical position

The vertical position is defined as the distance from XY plane of the aircraft to the centerline of the engines. The engines must be located at a height that would ensure required mass flow for engine operating into the inlet. Meanwhile, the vertical distance has to be large enough to prevent poor flow qualities in the gulley between the engine and aircraft.

However, since the engines are located on the top of the wing, it will introduce a nose down pitching moment and therefore a stabilizing effect. Hence, the vertical distance should be reduced to avoid very high pitch-down moments. Besides, from the viewpoints of the drag and the mass of structure, the length of the pylon should be kept to minimum as well.

Therefore, a balance has to be achieved between the above considerations when deciding the vertical position. Based on related research, the vertical distance is estimated to be 3.5m in conceptual design.

4) Incidence angle and toe-in angle

The incidence angle of engine installation is set to align the nacelle with the local flow. According to Raymer [44], a nose-up pitch of 2-4 deg is suggested for aft-mounting engines. In FW-11 conceptual design, a 3 deg incidence angle is selected for the preliminary engine installation; the over-wing engines are conformal to the wing. However, further investigation and modification of this value should be developed on the basis of CFD analysis and wind-tunnel testing.

There is no toe-in or toe-out for preliminary engine installation; the two engines point parallel to the chordline of the aircraft. It is deemed that since the engines are near the centre of the aircraft, and significantly raised above the upper surface of the airframe, that there would be a negligible velocity vector of the air in the spanwise direction.

The installation parameters of GTF-11 on the FW-11 are summarized in Table 7-2 and illustrated in Figure 7-3 and Figure 7-4.

Table 7-2 Installation parameters of GTF-11 on the FW-11

Longitude position	22.0m
Spanwise position	5.8m
Vertical position	3.5m
Incidence angle(nose-up)	3°

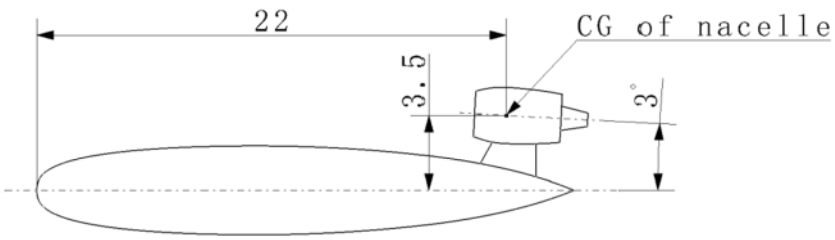

Figure 7-3 Cross section view of engine installation

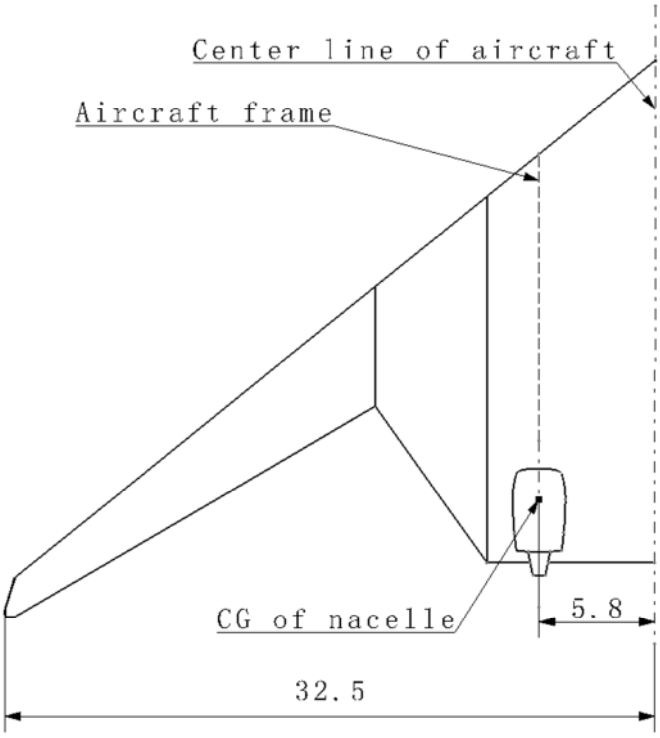

Figure 7-4 Over view of engine installation

8 Conclusion and Future Work

In this thesis, the characteristics of the new concept engine - GTF and relevant considerations of integration on a FW configuration aircraft were studied.

The associated works have done integrate the processes of engine modelling and performance simulation, aircraft performance calculation, aerodynamic design of nacelle and preliminary installation of engine. The objectives proposed in the Chapter 1 have been achieved; while there are still several works should be conducted in the future.

8.1 Conclusion

- Engine modelling and performance simulation

To investigate the characteristics of new concept engine, a preliminary engine model was constructed using TURBOMATCH software. The effects of main cycle parameters such as FPR, BPR, OPR, TET, on engine performance were analyzed.

Based on SFC target of 15.18mg/Ns and fan diameter constraint of 2.562m, FPR of 1.45, BPR of 12, OPR of 38.2 and TET of 1517K were selected as design point cycle parameters for GTF-11 engine.

Besides, the required take-off thrust was verified by SSC and take-off field length performance requirements of FW-11. According to the calculation results, the required take-off thrust was increased from 195.56kN to 212kN.

Finally, the off-design point performance at take-off, climb and cruise were simulated for further aircraft performance calculation. Meanwhile, the influences of ambient conditions on engine performance were also investigated to predicate the capacity of aircraft taking off from high altitude airport at hot day.

- Aircraft performance calculation

Based on empirical method, an aircraft performance spreadsheet calculation model was constructed and the performance of FW-11 with typical mission profile was analyzed.

The results indicated that the performance of aircraft, powered by GFT-11, can meet the requirements of FW-11 that are presented in the GDP specification. Meanwhile, the abilities of the aircraft beyond these requirements were also demonstrated, for instance, the capability of taking off from different altitude airports.

Besides, the benefits of GTF engine in aircraft performance improvement were investigated. The results showed that the geared concept can dramatically improve the aircraft fuel efficiency compared with conventional turbofan engine. A comparison between GTF-11 and RB211-524B4 indicated that the aircraft can achieve a 13.1% improvement in fuel efficiency by using new concept engine.

- Aerodynamic design of nacelle

In this section, a nacelle was designed for GTF-11 based on NACA 1-series and empirical method. Meanwhile, the installed thrust loss caused by nacelle drag was evaluated using ESDU.

The sensitivity analysis of key parameters indicated that the critical mass flow ratio, MFR_{crit}, and fore-body drag rise Mach number, M_d, have significant effect on nacelle dimension and drags. To achieve a compromise between the margin of the MFR, $\triangle$MFR, and the nacelle drags, the MFR_{crit} of 0.55 and M_d of 0.9 were selected for nacelle sizing.

To evaluate the installed thrust loss caused by nacelle drag, the nacelle drags of GTF-11 and conventional turbofan RB211-525B4 was calculated using ESDU81024a. The results showed that the nacelle drags account for about 4.08% and 3.09% of net thrust for GTF-11 and RB211-525B4, respectively.

- Preliminary installation of engine

In this section, the considerations of engine installation on a FW configuration aircraft were discussed. It was found that, from the analysis result, the podded engine over the rear wing can allow for a favourable overall aircraft design in terms of safety, location of CG, aerodynamic, stability and control, reliability and

maintenance. Then, a preliminary installation position of GTF-11 on FW-11 was presented.

8.2 Future Works

Based on the brief studies have done, several works are recommended to carry out in the future.

First of all, more detailed studies should be undertaken in engine modelling. For instance, the mechanical losses should be taken into account and the effect of cabin bleeding on engine performance could be analyzed. Meanwhile, the performance of components could be simulated for further components design. Furthermore, the increased take-off thrust requirement indicates that the maximum fan diameter may be less than the actual design value, which should be taken into consideration in further study.

With respect to aircraft performance calculation, the spreadsheet calculation model was just constructed using simply methods that are suitable for the preliminary study. Therefore, other approaches could be studied for deep investigation. In addition, the optimum mission profile could be scheduled for FW-11 based on engine performance simulation results.

Regarding the nacelle design and drags evaluation, only empirical method and ESDU method were employed. Therefore, the nacelle performance is proposed to be analyzed in depth using CFD-base method and possible modification of geometry may be made for the optimum aerodynamic performance. Besides, based on the preliminary design of the high bypass nacelle, the considerations of nacelle structure and subsystems design such as noise suppression, thrust reverser and de-icing could be studied.

Since the parameters for engine disposition were just estimated from related research, the interferences between nacelle, pylon and aircraft is suggested to be analyzed in depth using CFD-base method and/or wind tunnel testing. Besides, the effects of engine non-containment should be studied in further research as well.

Finally, the benefits of geared turbofan in reduction of noise and emission should be concerned. Moreover, the cost and reliability analysis could be inspected.

REFERENCES

[1] D. R. Kirk, Lecture note, Mechanical and Aerospace Engineering Department, Florida Institute of Technology

[2] "Jane's aero-engines", 9th ed, Jane's Information Group, 1996

[3] AVIC-4 GDP, FW-11 Specification, Flying Wing Aircraft Conceptual Design, Cranfield University, 2011

[4] Martin E. Eshelby, "Aircraft Performance Theory and Practice", Cranfiled University, UK, 2000

[5] Lloyd R. Jenkinson, Paul Simpkin, Darren Rhodes, "Civil Jet Aircraft Design", Arnold, Oxford, UK, 1999

[6] ESDU81024a, Drag of Axisymmetric Cowls at zero incidence for subsonic Mach numbers, 1994

[7] Alexander Martin Lippisch, "The delta wing – history and development", Iowa state University Press, AMES, 1981

[8] H. V. de Castro, "Flying and handling qualities of a fly-by wire blended-wing-bode civil transport aircraft", PhD thesis, School of Engineering, Cranfield University, 2003.

[9] A. L. Bolsunovsky, "Flying wing – problems and decisions", Aircraft Design 4 (2001), 193-219.

[10] R. H. Liebeck, "Design of the Blended Wing Body Subsonic Transport", Journal of Aircraft, Vol. 41, No. 1, 2004.

[11] "The Blended-Wing-Body", Langley Research Centre, NASA Facts, FS-1997-07-24-LaRC, 1997.

[12] http://en.wikipedia.org/wiki/Flying_wing

[13] Patrick H. Oosthuizen, "Environmental Effects of Civil Aviation", Department of Mechanical and Materials Engineering, Queen's University, Kingston, Ontario, Canada, 2010.

[14] C. Riegler, C. Bichlmaier, "The Geared Turbofan Technology – Opportunities, Challenges and Readiness Status", MTU Aero Engines GmbH, Germany

[15] Cumpsty, Nicholas, "Jet Propulsion", 2th ed. Cambridge University Press, Cambridge, UK, 2003.

[16] D. Crichton, E. de la Rosa Blanco, T. R. Law, J. I. Hileman, “Design and Operation for ultra low noise take-off”, AIAA 2007-0456, 2007.

[17] Dr. W. Waschka, Dr. K. Rüd, W. Humhauser, Dr. M. Metscher, Dr. A. Michel, “Design of a new 7 stage innovative compressor for 10 – 18 klbf thrust”, ISABE-2005-1266, MTU Aero Engines GmbH, Munich, Germany, 2005.

[18] http://www.pw.utc.com/products/commercial/purepower-pw1000g.asp

[19] H. Cohen, G.F.C. Rogers, H.I.H. Saravanamuttoo, “Gas Turbine Theory”, 4th ed. Longman Group Limited, UK, 1996

[20] Pachidis, V.A. “Gas Turbine Performance Simulation”, School of Engineering, Department of Power Propulsion and Aerospace Engineering, Cranfield University, UK, 1999

[21] V. A. Pachidis, “Gas Turbine Advanced Performance Simulation”, PhD thesis, School of Engineering, Cranfield University, 2006.

[22] Palmer, J.R. “The TURBOMATCH scheme for Gas-Turbine Performance Calculations: Users’ Guide”, School of Engineering, Department of Power and Propulsion, Cranfield University, UK, 1983

[23] Wang Faliang, AVIC-4 GDP Team, 2011.

[24] Zhang Jin, AVIC-4 GDP Team, 2011.

[25] FAR25, Airworthiness Standards: Transport Category Aircraft http://www.faa.gov/regulations_policies/faa_regulations/

[26] Civil Turbojet/Turbofan Specifications, Jet Engine Specification Database, http://www.jet-engine.net/

[27] Jack D. Mattingly, William H. Heiser, David T. Pratt, “Aircraft Engine Design”, 2th ed, AIAA Education Series. NY, US, 2002

[28] Jack D Mattingly et al, Elements of Propulsion Gas turbines and Rockets, AIAA Education Series. NY, US, 2006

[29] ESDU76011a, “First approximation to take-off field length of multi-engined transport aeroplanes”, 1985

[30] ESDU68046, “Atmospheric data for performance calculations”, 1992

[31] ESDU77022b “Equations for calculation of International Standard Atmosphere and associated off-standard atmospheres”, 1986

[32] “The Jet Engine”, 5th ed. The Technical Publication Department, Rolls-Royce plc, Derby, UK

[33] Darrel William, Lecture Notes, “Propulsion Systems Performance and Integration”, MSc Thermal Power, Cranfield University, UK, 2008

[34] Aimer, B. “Gas turbine intake design - peak Mach number response to changes of intake lip shape”, MSc Thesis, Cranfield University, 2005

[35] Albers, J. A., and Miller, B. A., “Effect of subsonic inlet lip geometry on predicted surface and flow Mach number distributions”, Technical Note NASA TN D-7446, NASA, December, 1973

[36] ESDU94013, “NACA 1-Series Geometry Representation for Computational Fluid Dynamics”, 1994

[37] Wang Qiang, “Gas Turbine Technology-Nacelle Design and Performance for Geared and Ungeared High Bypass Ratio Turbofans”, MSc Thesis, Cranfield University, 2009

[38] Leynaert, J., Surber, L. E. and Goldsmith, E. L., “Transport aircraft intake design”, AIAA, Washington DC, UNITED STATES,1993

[39] ESDU94014. “Wave drag coefficient for axisymmetric forecowls at zero incidence (M_∞<=1.5)”, 1994

[40] Boeing747 - Airplane Characteristics for Airport Planning, Boeing, 1984

[41] James Fincham, Ben Smiley, “G1F-BWB Final Engineering Definition Report”, Bristol University, 2008

[42] Panagiotis Laskaridis, “Integration of the Aft Fan Engine on a Blended Wing Body Configuration”, MSc Thesis, Cranfield University, 2000

[43] Anon, “BWB-98 Group Design Specifications”, Cranfield University, 1998

[44] Daniel P. Raymer, “Aircraft Design: A Conceptual Approach”, AIAA education series, 1992

APPENDICES

Appendix A Requirements for Engine Sizing

A.1 Thrust Requirements

A.1.1 Take-off Thrust Requirement

Detailed calculation process:

Total thrust required for take-off:

$$T_{req\_to} = 0.226 \times W_{to} = 0.226 \times 9.807 \times 176469 = 391122.7\text{N};$$

Thrust required per engine for take-off:

$$T'_{req\_to} = T_{req_{to}}/2 = 391122.7/2 = 195561.35\text{N} = 195.56\text{kN};$$

A.1.2 Second Segment Climb Thrust Requirement

The lift to drag ratio is estimated from the following equation:

$$L/D = C_L/C_D \quad \textbf{(A-1)}$$

Assuming that the climb speed is 1.2 times of the stall speed, the lift coefficient is the maximum take-off lift coefficient divided by 1.44:

$$C_L = \frac{C_{L\_max\_to}}{1.44} = \frac{1.35}{1.44} = 0.9375$$

Then, the drag coefficient can be got from the take-off drag polar:

$$C_D = 0.01443 + 0.05617 \times {C_L}^2 = 0.0638$$

Assuming that the aircraft weigh in second segment climb equals to W_{to}, the thrust required for 2.4% gradient of climb is:

$$T_{req\_sec} = \left(\frac{0.0638}{0.9375} + 0.024\right) \times 9.807 \times 176469 = 159307.00\text{N}$$

A.1.3 Maximum Climb Thrust Requirement

The cruise condition of FW-11 is altitude 35000ft and Mach number 0.82.

So, the true airspeed of aircraft in cruise is:

$$V = 0.82 \times 296.54 = 243.16 \mathrm{m/s}$$

Then:

$$\gamma = \frac{ROC}{V} = \frac{300 \times 0.3048/60}{243.16} = 0.00627$$

At the top of the climb, the aircraft approximately equals to weight.

$$L = W \times \cos\gamma \approx W \quad \textbf{(A-2)}$$

Also:

$$L = \frac{1}{2}\rho S V^2 C_L \quad \textbf{(A-3)}$$

So, the lift coefficient can be got as:

$$C_L = \frac{2L}{\rho S V^2} = \frac{2W}{\rho S V^2} \quad \textbf{(A-4)}$$

where,

W = aircraft weight at top of climb

ρ = air density at cruise altitude

S = reference wing area

V = true airspeed of aircraft

Thus,

$$C_L = \frac{2W}{\rho S V^2} = \frac{2 \times 9.807 \times 176469 \times 0.98}{0.3762 \times 647 \times (243.16)^2} = 0.2357$$

As the drag polar is$C_D = 0.00848 + 0.0535(C_L)^2$, the drag coefficient can be calculated.

$$C_D = 0.00848 + 0.0535 \times (0.2357)^2 = 0.01145$$

Then the required maximum climb thrust can be calculated as:

$$T_{req\_toc} = \left(\frac{0.01145}{0.2357} + 0.00627\right) \times 9.807 \times 176469 \times 0.98 = 93024.43 \mathrm{N}$$

The required maximum climb thrust for each engine:

$$T'_{req\_toc} = \frac{T_{req_{toc}}}{2} = \frac{93024.43}{2} = 46512.22N = 46.51kN$$

A.2 Engine Sizing

The maximum take-off thrust of Trent1000 is 241.14kN while the thrust required for GTF-11 is 195.56kN, so the SF can be got as:

$$SF = \frac{195.56}{241.14} = 0.811$$

Then the dimensions of candidate engine can be estimated from Trent1000 as following:

$$D_{req} = \sqrt{0.811} \times 2.845 = 2.562m$$

$$L_{req} = \sqrt{0.811} \times 3.912 = 3.523m$$

$$W_{req} = \sqrt{0.811} \times 5408.7 = 4870.8kg$$

Table A-1 Reference engine parameters [19, 20]

Engine	Engine Manufacturer	Application Aircraft	BPR	OPR	Take-off Thrust (N)	Fan Diameter (m)	Overall Length (m)	Weight (kg)
GE90-90B	GE	B777-200	8.5	38.7	400,347	3.124	7.290	7824.6
GE90-85B	GE	B777-200	8.3	36.9	376,771	3.124	7.290	7824.6
GE90-77B	GE	B777-200	8.7	34.4	339,850	3.124	7.290	7824.6
GP7270	Engine Alliance	A380-861	8.7	36.1	311,381	3.150	4.750	6085.5
Trent970	Rolls-Royce	A380	8.7	38.5	311,381	2.946	4.547	6436.6
Trent1700-63A1	Rolls-Royce	A350-800	10	-	280,243	2.845	4.064	5579.3
Trent1000	**Rolls-Royce**	**B787-3**	**11**	**47.7**	**241,143**	**2.845**	**3.912**	**5408.7**
GEnx-1B54	GE	B787-3	9.6	36.1	236,649	2.822	4.928	5642.3
PW1133G	P&W	A320neo	12	-	146,794	2.057	-	-
PW1521G	P&W	C-series	12	-	103,645	1.854	-	-
PW1215G	P&W	MRJ	9	-	75,621	1.422	-	-

Appendix B Engine Performance Simulation

B.1 Mass Flow Calculation

The one-dimensional isentropic equals are derived on following assumptions:

- The gas is thermally and calorically perfect.
- The flow is isentropic and adiabatic.
- The flow is uniform, and hence, one dimensional.

The relationships for mass flow calculation can be summarized as follows:

$$T_t = T\left(1 + \frac{\gamma - 1}{2} M^2\right) \quad \textbf{(B-1)}$$

$$P_t = P\left(1 + \frac{\gamma - 1}{2} M^2\right)^{\frac{\gamma}{\gamma - 1}} \quad \textbf{(B-2)}$$

$$\frac{\dot{m}\sqrt{T_t}}{P_t A} = M\sqrt{\frac{\gamma}{R}}\left(1 + \frac{\gamma - 1}{2} M^2\right)^{\frac{\gamma+1}{2(1-\gamma)}} \quad \textbf{(B-3)}$$

where:

T_t= total or stagnation temperature

T = standard atmosphere temperature

P_t = total or stagnation pressure

P = standard atmosphere pressure

A = area

M = Mach number

R = gas constant

$\dot{m}$ = mass flow rate

γ = ratio of specific heats

The equation for mass flow calculation can be conducted from Equation B-3.

$$\dot{m} = \frac{P_t A}{\sqrt{T_t}} M\sqrt{\frac{\gamma}{R}}\left(1 + \frac{\gamma - 1}{2} M^2\right)^{\frac{\gamma+1}{2(1-\gamma)}} \quad \textbf{(B-4)}$$

As the standard atmosphere temperature, pressure and Mach number was given in Chapter 4.2.1, and ratio of specific heats γ is 1.4 in this condition. The

total or stagnation temperature and pressure at intake face can be got.

$$T_t = 218.81 \times \left[1 + \frac{1.4-1}{2} \times (0.82)^2\right] = 248.2\text{K}$$

$$P_t = 23843.2 \times \left[1 + \frac{1.4-1}{2} \times (0.82)^2\right]^{\frac{1.4}{1.4-1}} = 37081.2\text{Pa}$$

As it shown in Equation B-4, the stagnation temperature and pressure, Mach number at fan face and fan area should be decided at first when calculate the mass flow rate. Assume that the stagnation temperature and pressure remains same as that at intake face. Besides, since the Mach number at fan face ranges between 0.55 and 0.65 for most current commercial engines, Mach number of 0.6 is chosen for calculation in this thesis. Also, the fan diameter is 2.562m refer to Chapter 3.4.2. Assume that the diameter of hub account for 30% of the fan diameter. Then the mass flow at design point is produced.

$$\dot{m} = \frac{37081.2 \times 4.645}{\sqrt{248.2}} \times 0.6 \times \sqrt{\frac{1.4}{286.71}} \times \left(1 + \frac{1.4-1}{2} \times 0.6^2\right)^{\frac{1.4+1}{2(1-1.4)}} = 372.1\text{kg/s}$$

B.2 Engine Model

B.2.1 GTF-11 Engine Model Scheme

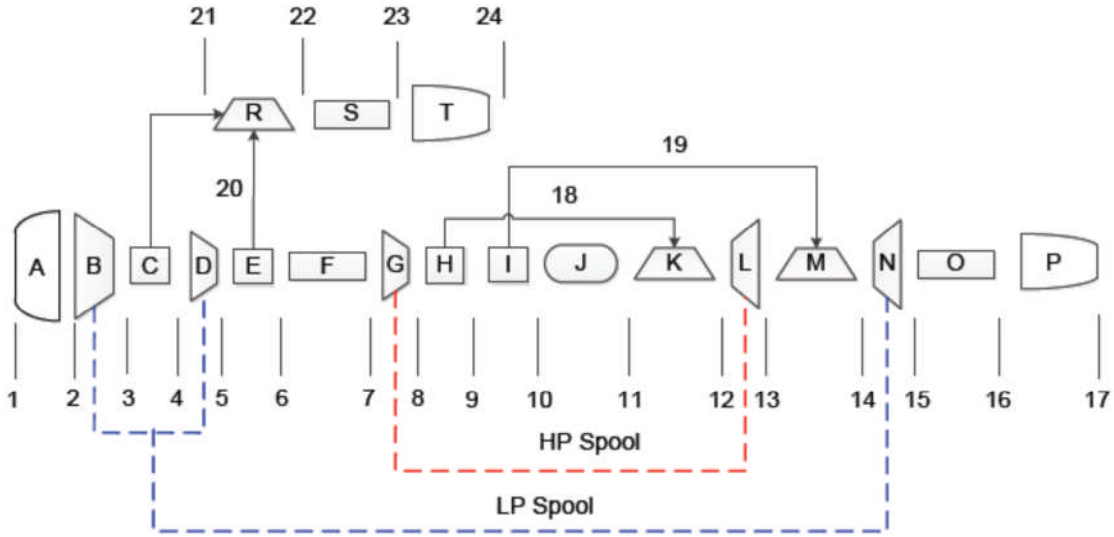

Figure B-1 Two spools GTF-11 engine model scheme

B.2.2 Definition of Engine Model Bricks and Stations

Table B-1 GTF-11 engine model bricks and stations

Brick Name	Symbol	Station Inlet	Station Outlet
Intake	A	1	2
Fan	B	2	3
Bypass Flow	C	3	21,4
Boost	D	4	5
Air Bleed into Bypass Duct	E	5	20,6
Core Duct	F	6	7
HPC	G	7	8
Cooling Air to HPT Blade	H	8	18,9
Cooling Air to LPT Blade	I	9	19,10
Combustion Chamber	J	10	11
Air Flow Mixer	K	11,18	12
HPT	L	12	13
Air Flow Mixer	M	13,19	14
LPT	N	14	15
Core Nozzle Duct	O	15	16
Core Nozzle	P	16	17
Air Flow Mixer	R	20,21	22
Bypass Nozzle Duct	S	22	23
Bypass Nozzle	T	23	24

B.2.3 Engine Model Codes

GTF-11 Engine (2 Spools)

Design Point: Cruise (H=10668m, M=0.82)

////

DP SI KE CT FP

-1

-1

INTAKE S1,2 D1-4 R400

COMPRE	S2,3	D5-10	R410	V5 V6
PREMAS	S3,21,4	D12-15		V12
ARITHY		D100-104		
COMPRE	S4,5	D16-21	R420	V16
PREMAS	S5,20,6	D23-26		
MIXEES	S21,20,22			
DUCTER	S22,23	D27-30	R430	
NOZCON	S23,24,1	D31	R440	
DUCTER	S6,7	D32-35	R450	
COMPRE	S7,8	D36-41	R460	V36 V37
PREMAS	S8,18,9	D50-53		
PREMAS	S9,19,10	D55-58		
BURNER	S10,11	D59-61	R470	
MIXEES	S11,18,12			
TURBIN	S12,13	D62-69,460		V63
MIXEES	S13,19,14			
ARITHY		D105-111		
TURBIN	S14,15	D70-77,480		V71
DUCTER	S15,16	D78-81	R490	
NOZCON	S16,17,1	D82	R500	
PERFOR	S1,0,0	D83-86,400,500,470,440,0,0,0,0,0		
CODEND				

BRICK DATA///

! INLET

1 10668.0

2 0.0

3 0.82

4 0.995

! FAN

5 0.85

6 1.0
7 1.45
8 0.915
9 0.0
10 1.0

! BYPASS
12 0.916667
13 0.0
14 1.0
15 0.0

! BOOSTER
16 0.85
17 1.0
18 1.69
19 0.91
20 1.0
21 2.0

! AIR BLEED
23 0.00
24 0.0
25 1.0
26 0.0

! BYPASS-DUCT
27 0.0
28 0.01
29 0.0
30 0.0

! BYPASS NOZZLE
31 -1.0

! CORE DUCT
32 0.0
33 0.01
34 0.0
35 0.0

! HPC COMPRESSOR
36 0.85
37 1.0
38 15.589
39 0.9
40 1.0
41 5.0

! COOLING AIR
50 0.08
51 0.0
52 1.0
53 0.0

! COOLING AIR
55 0.014
56 0.0
57 1.0
58 0.0

! BURNER
59 0.045
60 0.999

61 -1.0

! HPT TURBINE
62 0.0
63 -1.0
64 -1.0
65 0.91
66 -1.0
67 3.0
68 1.0
69 -1.0

! LPT TURBINE
70 0.0
71 -1.0
72 -1.0
73 0.93
74 -1.0
75 1.0
76 5.0
77 -1.0

! CORE DUCT
78 0.0
79 0.0
80 0.0
81 0.0

! CONVERGENT NOZZLE
82 -1.0

! PERFORMANCE

```
83 -1.0
84 -1.0
85 0.0
86 0.0

! ARITHY: BOOSTER SPEED = FAN SPEED
100 5.0
101 -1.0
102 17.0
103 -1.0
104 6.0

! ARITHY: LPTWORK = BOOSTERWORK + FANWORK
105 1.0
106 -1.0
107 480.0
108 -1.0
109 410.0
110 -1.0
111 420.0
-1
1 2 372.1
11 6 1517.0
-1
-3
```

B.3 Parameter Analysis

More simulation results for parameter analysis are presented in the following figures.

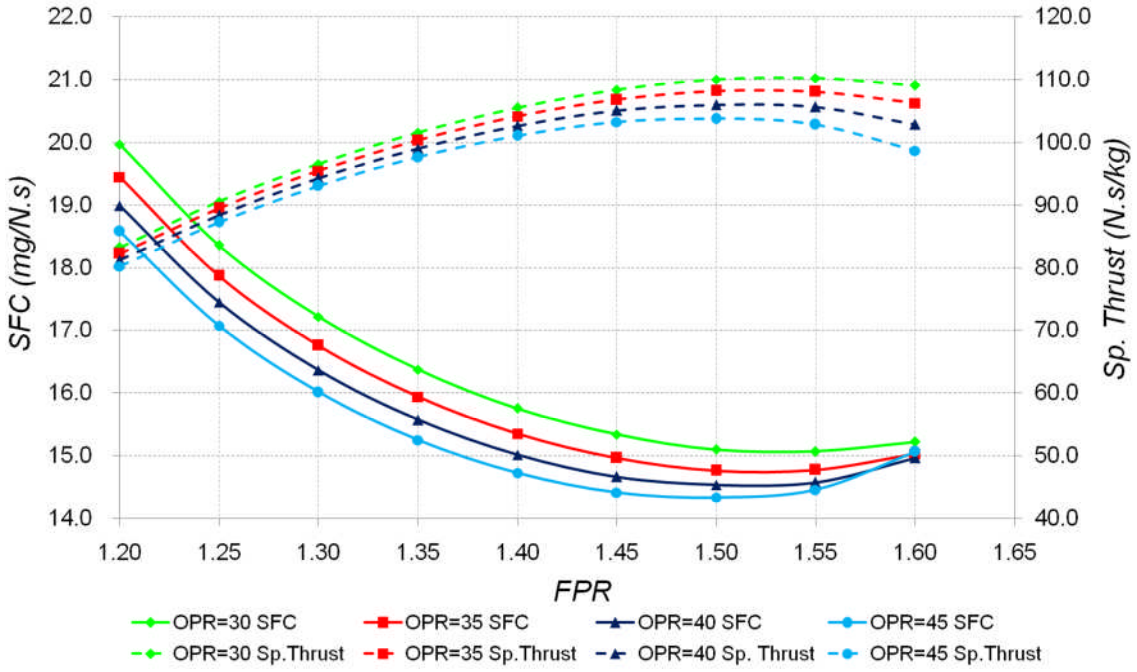

Figure B-2 Effects of OPR onengine performance (BPR=11, TET=1450K)

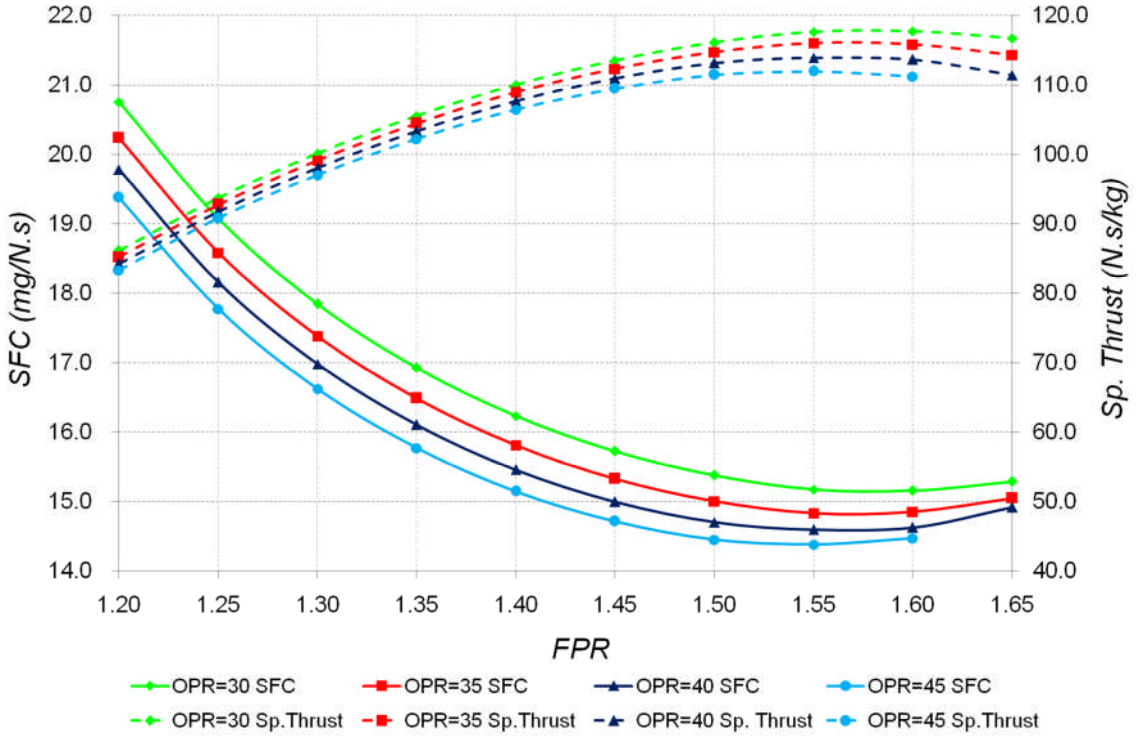

Figure B-3 Effects of OPR onengine performance (BPR=11, TET=1500K)

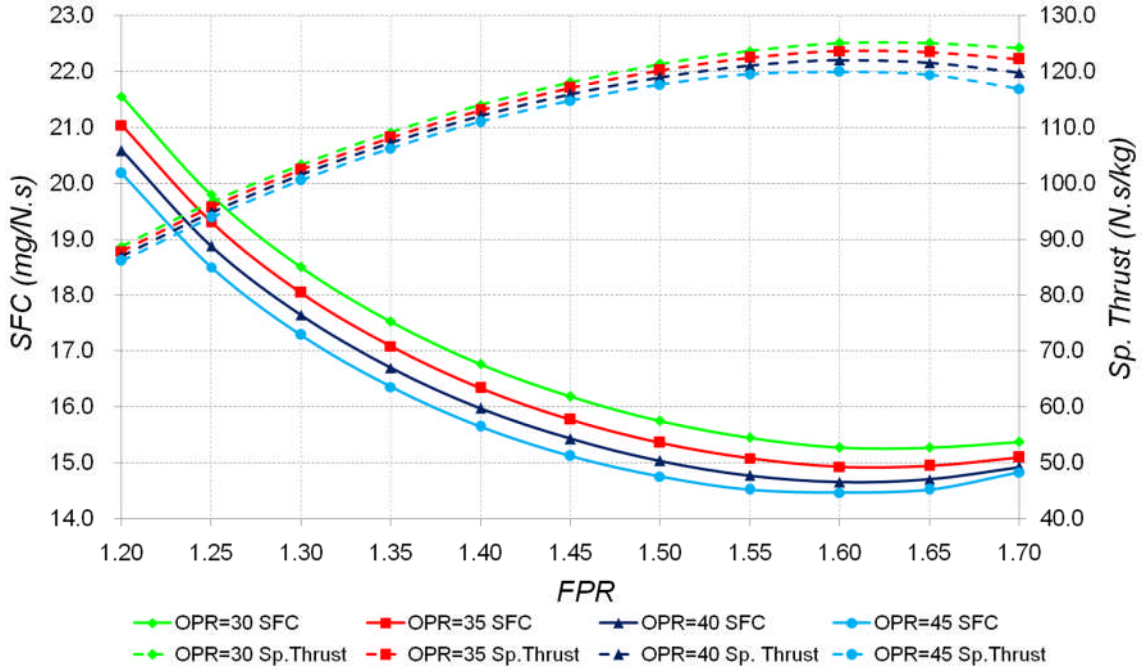

Figure B-4 Effects of OPR onengine performance (BPR=11, TET=1550K)

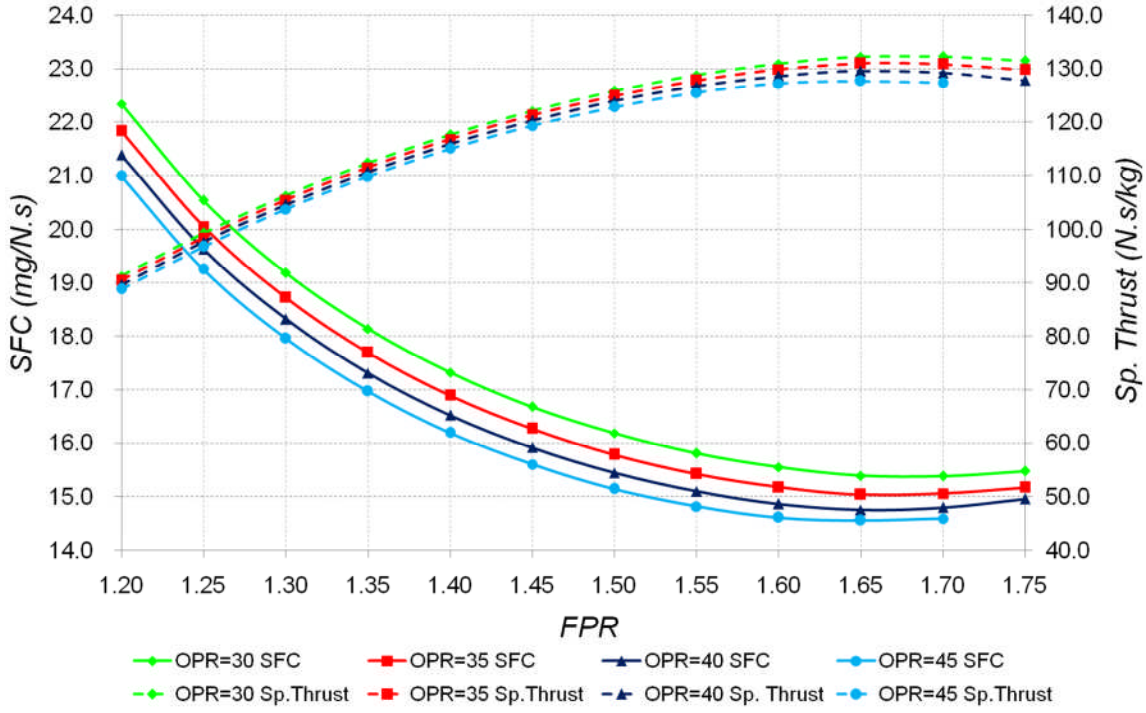

Figure B-5 Effects of OPR onengine performance (BPR=11, TET=1600K)

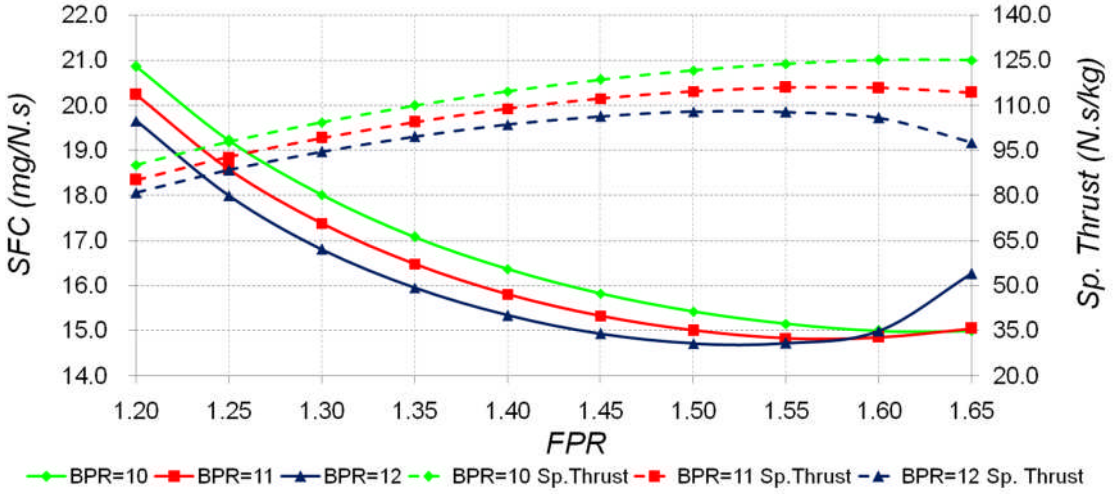

Figure B-6 Effects of BPR onengine performance (OPR=35, TET=1500K)

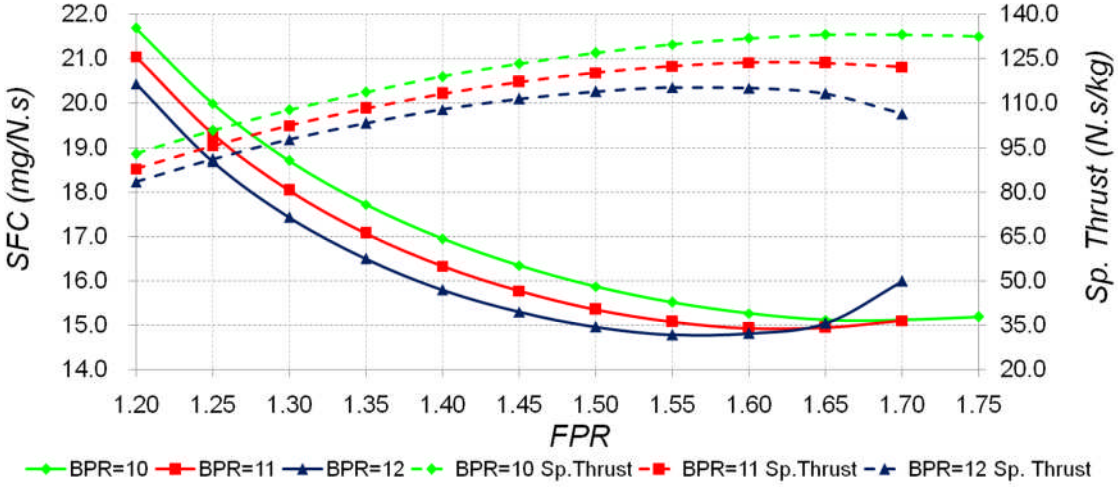

Figure B-7 Effects of BPR onengine performance (OPR=35, TET=1550K)

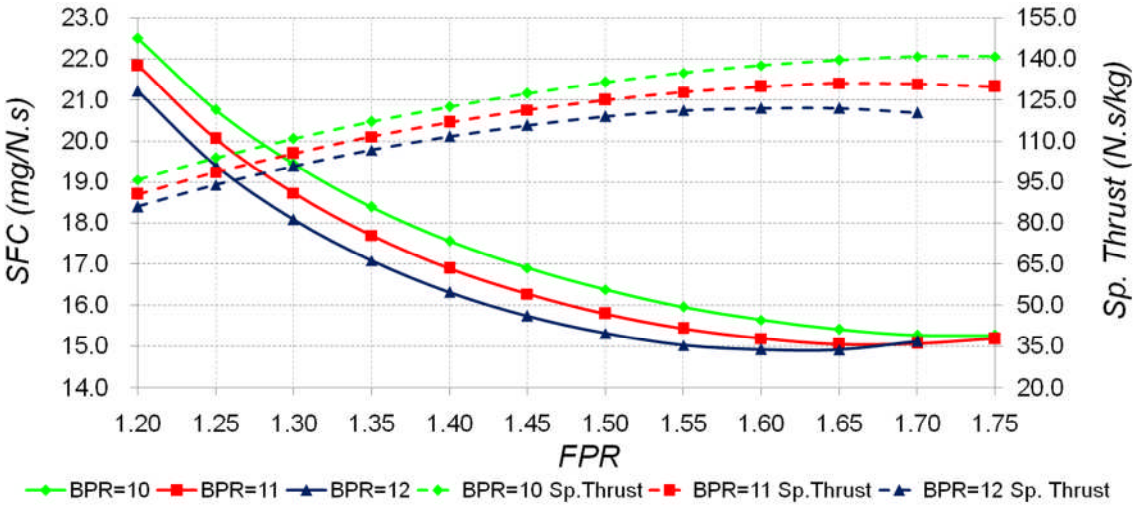

Figure B-8 Effects of BPR onengine performance (OPR=35, TET=1600K)

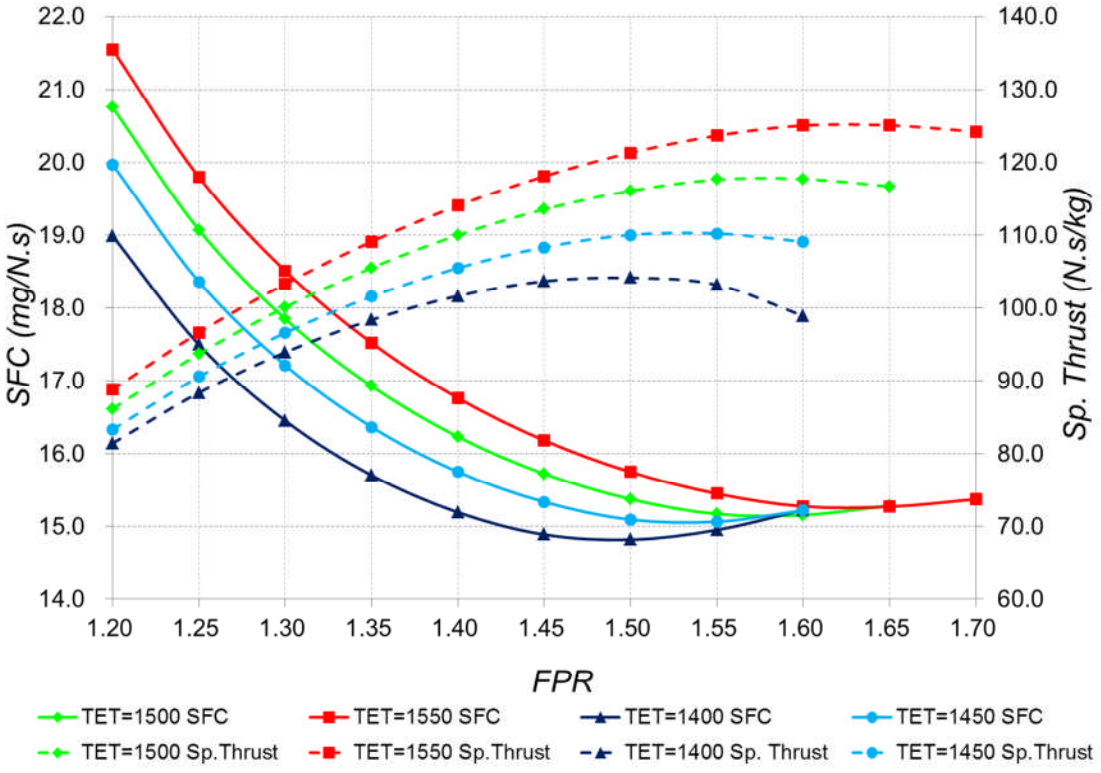

Figure B-9 Effects of TET on engine performance (BPR=11, OPR=30)

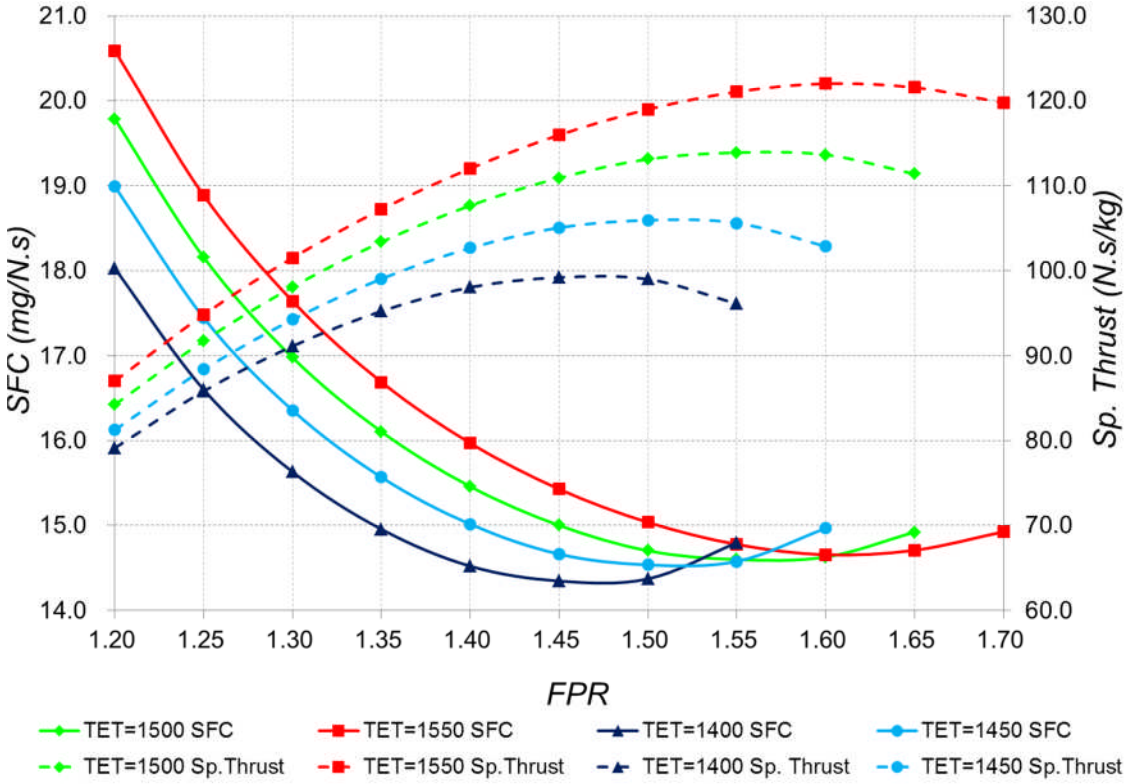

Figure B-10 Effects of TET on engine performance (BPR=11, OPR=40)

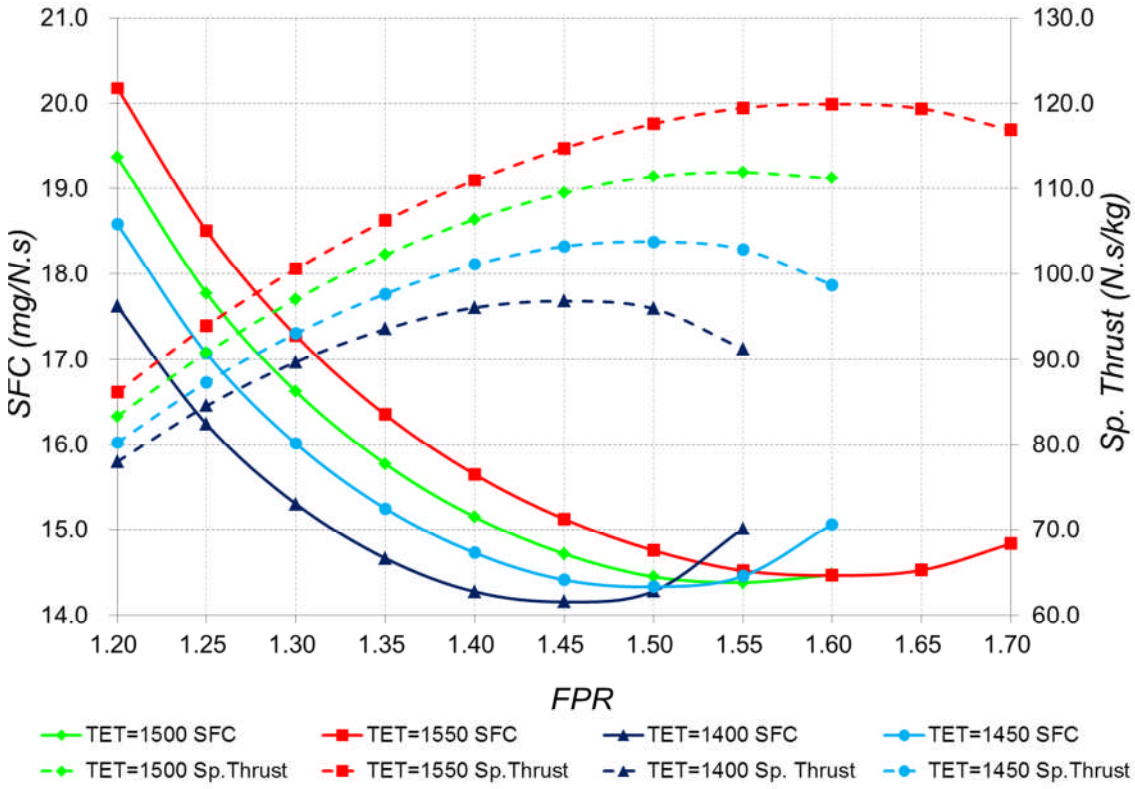

Figure B-11 Effects of TET on engine performance (BPR=11, OPR=45)

Appendix C Take-off Thrust Verification

C.1 Take-off Safety Speed

According to the aerodynamic team in GDP, the maximum take-off lift coefficient is 1.35. Then the stall speed of FW-11 can be estimated by follow equation.

$$\mathrm{L} = \frac{1}{2}\rho \mathrm{S} V_s^{\,2} \mathrm{C}_{\mathrm{L\_max}} = W \tag{C-1}$$

Where W is the maximum take-off weight of 176469 kg and S is the wing area of 647m^2, then:

$$\mathrm{V_s} = \sqrt{\frac{2W}{\rho \mathrm{S C_{L\_max}}}} = \sqrt{\frac{2 \times 176469 \times 9.807}{1.221 \times 647 \times 1.35}} = 56.97\mathrm{m/s}$$

Assume that the safety speed at take-off V_2 is 1.2 times of the stall speed V_s, then:

$$V_2 = 1.2\mathrm{V_s} = 68.36\mathrm{m/s}$$

And corresponding Mach number is 0.201.

C.2 Take-off Field Length Estimation

According to the ESDU76011a, the “basic parameter” for field-length data estimation is:

$$\frac{\mathrm{W}^2}{\mathrm{C_{L_2}} \mathrm{n f_{N_{0.7}}} \mathrm{S}\sigma} \tag{C-2}$$

where:

W = aircraft take-off weight;

C_{L2} = lift coefficient at V_2;

n = number of engine;

$f_{N0.7}$ = installed thrust at $0.7V_2$;

S = reference wing area;

σ = relative density.

The lift coefficient at take-off safety speed V_2 can be got as:

$$C_{L_2} = \frac{C_{L\_max\_to}}{1.44} = \frac{1.35}{1.44} = 0.9375$$

The drag coefficient is conducted by take-off drag polar.

$$C_{D_2} = 0.01443 + 0.05617 \times (0.9375)^2 = 0.0638$$

From Figure C-1, when take-off thrust is 209.08kN, the installed thrust at $0.7V_2$ is 174.79kN and corresponding installed thrust is 169.55kN. Thus, the basic parameter can be calculated as following:

$$\frac{W^2}{C_{L_2} n f_{N_{0.7}} S\sigma} = \frac{(176469 \times 9.80665)^2}{0.9375 \times 2 \times 169546 \times 647 \times 1} = 12409.8$$

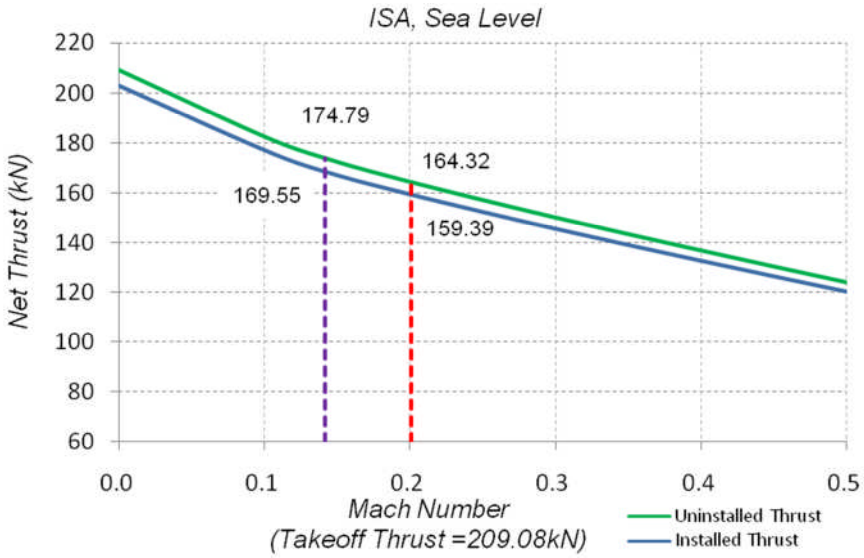

Figure C-1 Engine thrust at take-off thrust of 209.08kN

From Figure C-1, the installed thrust at V_2 is 159.39kN. Then, the gradient of SSC can be calculated using ESDU 76011a.

$$\tan\gamma_{seg2} = \frac{(n-1)T}{W} - \left(\frac{L}{D}\right)^{-1}_{@V_2} = \frac{(2-1) \times 159390}{176469 \times 9.80665} - \left(\frac{0.9375}{0.0638}\right)^{-1} = 0.024$$

Based on $\tan\gamma_{seg2}$ of 0.024 and basic parameter of 12409.8, the unfactored take-off distance of 1640m and BLF of 1940m can be gained from figure-1a and figure-2a of ESDU76011a, respectively. The factored take-off distance of 1886m is then conducted by 1.15 times of unfactored distance. Since the field length is defined as the longer one of factored take-off distance and BFL, it is 1940m when take-off thrust is 209.08kN. Obviously, it cannot meet the required take-off field length of 1900m. Then, more cases with take-off thrust of 212kN and 215kN are calculated to seek a correct value.

Appendix D Aircraft Performance Calculation Method

The method for aircraft performance calculation mainly from Jenkinson's Civil Jet Aircraft Design and Eshelly's Aircraft Performance: Theory and Practice.

D.1 Take-off Performance

D.1.1 Take-off Distance - All Engines Operating (AEO)

The take-off distance calculation of the aircraft with all engines operating can be divided into three parts: ground roll, transition and climb.

1. Ground roll

Based on the analysis of the forces acting on aircraft during ground roll, the ground roll distance can be estimated as below.

$$S_G = \frac{1}{2gK_A} \ln\left[\frac{\left(K_T + K_A V_{LOF}^2\right)}{K_T}\right] \quad \textbf{(D-1)}$$

The two constants K_T and K_A are defined as follows:

$$K_T = (T/W) - \mu \quad \textbf{(D-2)}$$

$$K_A = \rho\left(-C_{D0} - KC_L^2 + \mu C_L\right)/(2W/S) \quad \textbf{(D-3)}$$

where,

W = aircraft weight
S = reference wing area
T = aircraft thrust at 0.707times V_{LOF}
V_{LOF} = lift-off speed
C_L = aircraft lift coefficient
μ = runway coefficient of friction
ρ = air density

Typical value of μ in take-off would be 0.02.

2. Transition

The aircraft flight path can be simplified as an arc, as shown in Figure D-1. During transition the aircraft accelerates from V_{LOF} to the take-off safety speed V_2. The ground distance of transition can be estimated as below.

$$S_T = r \cdot \gamma \quad \textbf{(D-4)}$$

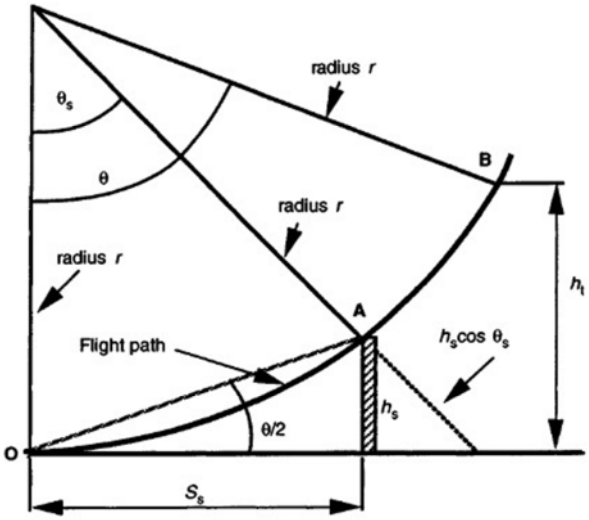

Figure D-1 Transition flight path geometry

Where r is the radius of the arc and γ is the climb gradient at the end of transition. The two parameters can be estimated as following:

$$r = V_T^2/[g(n-1)] \quad \textbf{(D-5)}$$

$$\gamma = (T - D)/W \quad \textbf{(D-6)}$$

Typically, V_T = 1.15 V_S and n = 1.2. The drag and thrust for final climb gradient calculation is estimated at take-off climb speed V_2.

Then height at end of transition is:

$$h_T = r \cdot \gamma \cdot \gamma/2 \quad \textbf{(D-7)}$$

If h_T exceeds the screen height h_S which is defined as 35ft (10.7m) in FAR 25 and CS25 during the transition, the distance to the screen height can be approximated to:

$$S_S = [(r + h_S)^2 - r^2]^{0.5} \quad \textbf{(D-8)}$$

3. Climb

The ground distance from the end of transition to the screen height is given by:

$$S_C = (h_S - h_T)/\tan\gamma_C \quad \textbf{(D-9)}$$

For small climb angles tan $\gamma_C = \gamma$.

Then the total distance is calculated by summing these three parts. For FAR25 and CS25 certifications, the take-off field length is then factored by 1.15 for safety margin.

D.1.2 Balanced Field Length – One Engine Inoperative (OEI)

In the event of one engine inoperative the distances are determined for two possible actions: continued take-off after engine failure and rejected take-off, as shown in Figure D-2.

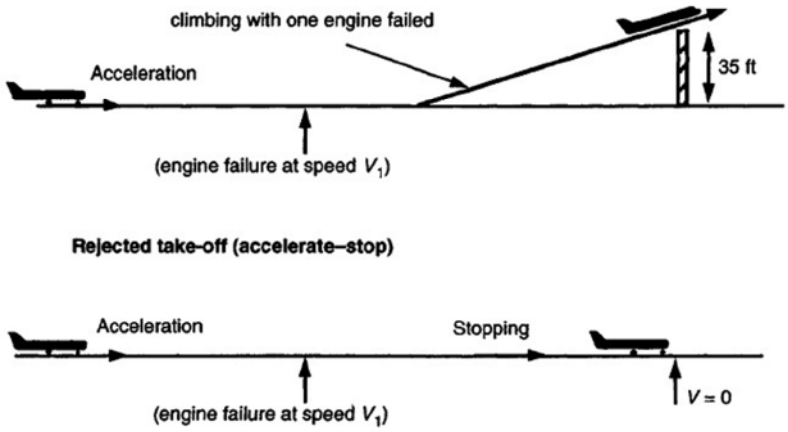

Figure D-2 Take-off options with one engine failure

The BLF refers to the balance between the distances required for these two options, as shown in Figure D-3. Aircraft speed for this balance is defined as decision speed V_1.

The BFL can be estimated as following three segments:

- Distance of accelerate to engine failure speed with AEO
- Distance of continued take-off with OEI after engine failure
- Distance of stop with OEI after engine failure

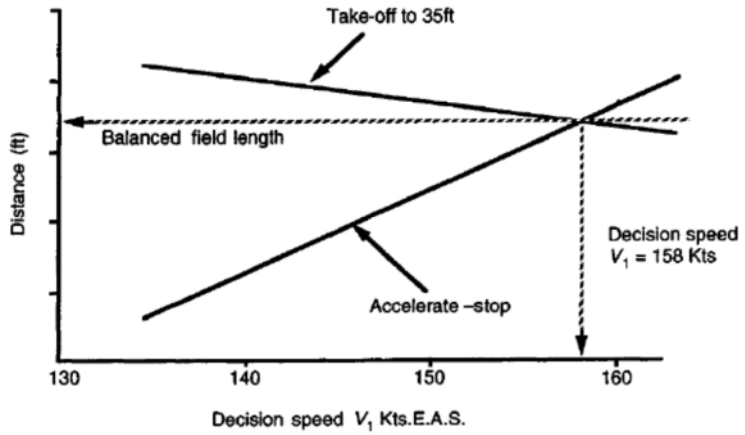

Figure D-3 Definition of BFL

For latter two segments, the drag caused by failed engine and additional trim should be taken into account in calculation. The windmilling drag caused by failed engine may be estimated by Equation D-10 and the additional trim drag ΔC_{Dt} is assumed as 5% of basic profile drag at take-off.

$$\Delta C_{Dw} = 0.3A_f/S \quad \textbf{(D-10)}$$

Where A_f is the fan cross-sectional area.

D.2 Landing Performance

The landing distance is estimated in a similar manner to take-off. It can be divided into three segments: approach, flare and ground roll, as shown in Figure D-4.

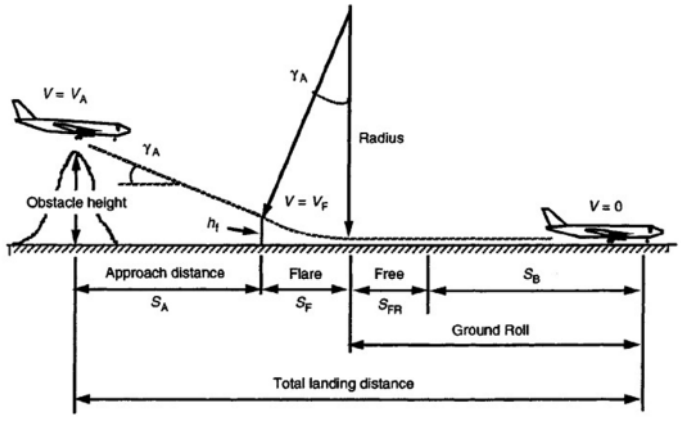

Figure D-4 Approach and lading definition

1. Approach

According to FAR and CS certification, the approach starts at an obstacle height h_O of 50ft (15.2m) and ends at the flare height h_F. The flare height can be estimated by:

$$h_F = r \cdot \gamma_A \cdot \gamma_A/2 \quad \textbf{(D-11)}$$

Where r is the flare radius and γ_A is the approach gradient. Then the approach distance can be conducted by:

$$S_A = (h_O - h_F)/\tan\gamma_A \quad \textbf{(D-12)}$$

2. Flare

During this phase, the aircraft decelerates from the approach speed V_A to the touch-down speed V_{TD}. The average speed during flare, V_F, can be estimated as:

$$V_F = (V_A + V_{TD})/2 \quad \textbf{(D-13)}$$

The radius of flare manoeuvre is given by:

$$r = V_F^2/[g(n-1)] \quad \textbf{(D-14)}$$

Typically, $V_{TD} = 1.15V_S$ and n=1.2.

Then, the ground distance covered during the flare can be calculated as:

$$S_F = r \cdot \gamma_A \quad \textbf{(D-15)}$$

3. Ground roll

The ground roll distance consists of two parts: free roll distance and breaking distance.

For free roll distance, it can be approximated using:

$$S_{FR} = t \cdot V_{TD} \quad \textbf{(D-16)}$$

Where, t is duration of free roll.

For breaking distance, it is estimated by following equation:

$$S_B = [1/(2gK_A)]\ln\left[\left(K_T + K_T V_{TD}^2\right)/K_T\right] \quad \textbf{(D-17)}$$

where,

$$K_A = -\rho C_{D0}/(2W/S) \quad \textbf{(D-18)}$$

$$K_T = -\mu \quad \textbf{(D-19)}$$

Typical value of friction coefficient μ in landing would be 0.3. Then, the total landing distance can be gained by summing of above three parts. For FAR25 and CS25 certification rules, it is then multiplied by 1.66 for operational variability.

D.3 Climb Performance

Based on aircraft equilibrium equations in climb phase, the rate of climb with no acceleration is expressed as:

$$(ROC)_0 = [(T - D)/W]V \quad \textbf{(D-20)}$$

And the rate of climb with acceleration is given by:

$$(ROC)_a = (ROC)_0/[1 + (V/g)(dV/dh)] \quad \textbf{(D-21)}$$

Then, the climb performance can be estimated using a step by step method on the basis of engine data at climb phase.

D.4 Cruise Performance

In cruise phase, fuel is burned and fuel mass flow will determine the rate of change of mass of the aircraft. Assume the total aircraft thrust is T and engine SFC is a constant value c, the change of aircraft weight can be expressed as:

$$dW/dt = c \cdot T \quad \textbf{(D-22)}$$

As T=D and L=W in level flight, therefore:

$$dW/dt = -cD(W/L) \quad \textbf{(D-23)}$$

And,

$$dt = (1/c)(L/D)\ln(dW/W) \quad \textbf{(D-24)}$$

Integrating between an initial cruise weight W_i and the final cruise weight W_f gives:

$$t = (1/c)(L/D)\ln(W_i/W_f) \quad \textbf{(D-25)}$$

Then, for a given cruise speed, V, the range can be estimated as:

$$R = V \cdot t = (V/c)(L/D)\ln(W_i/W_f) \quad \textbf{(D-26)}$$

D.5 Descent Performance

The descent performance calculation is similar to the climb except that in this phase the thrust is less than the drag. The rate of descent is given by:

$$(ROC)_a = [(T - D)/W]V/[1 + (V/g)(dV/dh)] \quad \textbf{(D-27)}$$

Appendix E Field Performance Calculation

E.1 Take-off Performance Calculation

In present research, assuming that the V_{LOF} is 1.1 times and V_2 is 1.2 times of stall speed V_s during take-off, respectively. The aircraft speeds during take-off are presented in Table E-1.

Table E-1 Aircraft speed during take-off

Speeds	Symbol	Value (m/s)	M
Stall Speed	V_S	56.88	0.167
Lift-off Speed	$V_{LOF}=1.1V_S$	62.56	0.184
Take-off Safety Speed	$V_2=1.2V_S$	68.25	0.201
Transition Speed	$V_T=0.5(V_{LOF}+V_2)$	65.41	0.192

E.1.1 Take-off Performance - AEO

The engine data during take-off are summarized in Table E-2.

Table E-2 Engine data during take-off

Altitude (m)	0	0
Aircraft Speed (m/s)	62.563	68.25
Mach	0.184	0.201
0.707M	0.130	0.142
Engine Thrust (N)	179970	177110
Engine Fuel Flow (kg/s)	1.5340	1.5355
SFC (mg/Ns)	8.8134	8.9567
Aircraft Thrust (N)	359940	354220
Aircraft Fuel Flow (kg/s)	3.068	3.071

The results of take-off performance calculation with AEO are summarized in Table E-3. It should notes that the height at the end of transition is greater than the obstacle height and the unfactored total take-off distance of 1332m is the summation of the ground roll distance and the ground distance in transition.

Besides, as the time allowance for take-off is 2 minutes, the fuel consumption during take-off can be estimated as: $3.068 \times 2 \times 60 = 368.16\text{kg}$

Table E-3 Take-off performance calculation of AEO

Phase1: Ground Roll					
Input Parameters					
W (kg)	S (m^2)	C_L	C_{D0}	K	T (N)
176469	647	0.21	0.02193	0.05617	359940
Output Parameters					
K_A	K_T	S_G (m)			
0.1879893	-4.62727E-06	**1116.2**			
Phase2: Transition					
Input Parameters					
W (kg)	S (m^2)	C_L	C_{D0}	K	T (N)
176469	647	0.938	0.01443	0.05617	354220
Output Parameters					
r	γ	h_T (m)	S_T (m)	S_S (m)	
2181	0.137	20.36	298	**216**	
Total Take-off Distance - AEO					
Unfactored Distance (m)			Factored Distance (m)		
1332			**1532**		

E.1.2 Balanced Field Length– OEI

In order to get the balanced field length and decision speed V_1, take-off distances are calculated at different engine failure speed V_{EF}. The segment calculations of balance filed length are presented from Table E-4 to Table E-8.

Table E-4 Distance of ground roll to engine failure

V_{EF} (m/s)	50.050	56.875	59.719	62.563
Mach	0.147	0.167	0.175	0.184
0.707M	0.104	0.118	0.124	0.130
Engine Thrust (N)	184200	180760	181420	179970
Aircraft Thrust (N)	368400	361520	362840	359940
K_T	0.193	0.189	0.190	0.188
K_A	-4.627E-06			
S_G (m)	**682.9**	**909.6**	**1003.0**	**1116.2**

Table E-5 Distance of pilot reaction

V_{EF} (m/s)	50.050	56.875	59.719	62.563
Reaction Time (s)	2	2	2	2
Reaction Distance (m)	**100.1**	**113.8**	**119.4**	**125.1**

Table E-6 Distance from end of reaction to aircraft lift-off

Mean speed during this period is given by: $V_m=0.5(V_1+V_{LOF})$				
V_m (m/s)	56.3	59.7	61.1	62.6
M	0.165	0.175	0.180	0.184
0.707M	0.117	0.124	0.127	0.130
Engine Thrust (N)	181000	181420	180690	179970
Aircraft Thrust (N)	181000	181420	180690	179970
ΔC_{Df}	0.00239			
ΔC_{Dt}	0.00122			
C_L	0.21			
C_{D0}	0.02554			
(1)=T/W-μ	0.08459	0.08483	0.08441	0.08400
(2)=$\mu C_L-C_{D0}-KC_L^2$	-0.02382			
(3)=$\rho V_m^2/(2W/S)$	0.726	0.81667	0.85602	0.89630
(4)=(2)(3)	-0.01729	-0.01945	-0.02039	-0.02135
(5)=(1)+(4)	0.06730	0.06538	0.06402	0.06265
dv/dt (m/s^2)	0.65997	0.64117	0.62784	0.61436
Δt (s)	18.959	8.871	4.529	0.000
ΔS (m)	**1067.5**	**529.7**	**276.9**	**0.0**

Table E-7 Distance of transition and climb

$V_{m,t}=0.5(V_{LOF}+V_2)$ (m/s)	65.4
R (m)	2181
V_2 (m/s)	68.3
M	0.201
0.707M	0.142
Engine Thrust (N)	177110
Aircraft Thrust (N)	177110
C_L	0.93750
C_D	0.06938

Drag (N)	128069
γ	0.02834
S_T (m)	**61.8**
h_T (m)	0.88
∆h to screen height (m)	9.79
S_C (m)	**345.5**

Table E-8 Stop distance from engine failure

V_{EF} (m/s)	50.1	56.9	59.7	62.6
K_T	-0.3			
K_A	0.000006534			
S_{st} (m/s)	**437.8**	**570.1**	**630.9**	**695.3**

Then, the accelerate-go distances and accelerate-stop distances are obtained by summing of corresponding segments distances. The results are presented in Table E-9 and Figure.

Table E-9 Distances of accelerate-go and accelerate-stop

V_{EF}^2 (m^2/s^2)	2505	3235	3566	3914
Distances of accelerate-go (m)	2258	1960	1807	1649
Distances of accelerate-stop (m)	1221	1593	1753	1937

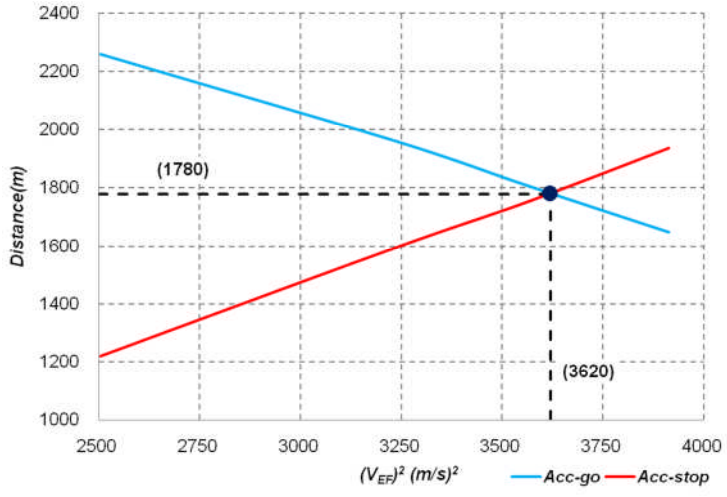

Figure E-1 Balanced field length

From Figure E-1, it can be found that the balance field length of OEI is 1780m and corresponding decision speed is 60.2m/s.

E.2 Landing Performance Calculation

In present research, assuming that the V_{TD} is 1.15 times and V_A is 1.4 times of stall speed V_s during landing, respectively. The aircraft speeds during landing are presented in Table E-10.

Table E-10 Aircraft speed during landing

Speeds	Symbol	Value (m/s)	M
Stall Speed	V_S	52.64	0.155
Touch-down Speed	$V_{TD}=1.15V_S$	60.53	0.178
Approach Speed	$V_A=1.4V_S$	73.69	0.217
Flare Speed	$V_F=0.5(V_A+V_{TD})$	67.11	0.197

The result of landing distance calculation is summarized in Table E-11.

Table E-11 Landing distance calculation

Input Parameters					
V_A (m/s)	V_{TD} (m/s)	V_F (m/s)	Approach Angle (degree)		Free Roll Time (s)
73.7	60.5	67.11	3		2
Output Parameters					
r (m)	h_F (m)	S_A (m)	S_F (m)	S_{FR} (m)	S_B (m)
2297	3.148	230.7	120.2	121.1	572.4
Total Landing Distance					
Unfactored Distance (m)			Factored Distance (m)		
1044			**1734**		

It can note that, from Table E-11, the unfactored landing distance is 1044m and factored landing distance is 1734m, respectively. Besides, as the time allowance for landing is 6 minutes and the aircraft fuel flow is 1.69kg/s, the fuel consumption during take-off can be estimated as: $1.69 \times 6 \times 60 = 608.4\text{kg}$

Appendix F En-route Performance Calculation

F.1 Climb Performance Calculation

1500~10000ft: EAS=250Kt; 10000~26460ft: EAS=320Kt; 26460~35000ft: EAS=0.82

Alt (ft)	Weight (kg)	TAS (m/s)	EAS (Kt)	M	C_L	C_D	Drag (N)	Thrust (N)	ROC_0 (m/s)	ROC_a (m/s)	FF (kg/s)	Δt (s)	$\sum\Delta t$ (s)	ΔF (kg)	$\sum\Delta F$ (kg)	Δs (km)	$\sum\Delta s$ (nm)
1500	176101	131.48	250	0.388	0.26346	0.01206	79055	318140	18.202	16.689	3.5948	0.0	0.0	0.0	0.0	0.0	0.0
2000	176068	132.46	250	0.392	0.26341	0.01205	79010	314400	18.058	16.999	3.5622	9.0	9.0	32.4	32.4	1.2	0.6
3000	176005	134.44	250	0.399	0.26332	0.01204	78917	306580	17.733	16.134	3.4976	18.4	27.4	64.9	97.3	2.4	2.0
4000	175939	136.47	250	0.407	0.26322	0.01202	78823	299260	17.436	15.776	3.4320	19.1	46.5	66.2	163.5	2.6	3.3
5000	175874	138.55	250	0.414	0.26312	0.01201	78726	291700	17.109	15.388	3.3664	19.6	66.1	66.5	230.0	2.7	4.8
6000	175808	140.67	250	0.422	0.26302	0.01200	78628	284020	16.759	14.976	3.3000	20.1	86.2	66.9	296.9	2.8	6.3
7000	175741	142.84	250	0.430	0.26292	0.01198	78528	276340	16.395	14.822	3.2338	20.5	106.6	66.8	363.8	2.9	7.8
8000	175675	145.07	250	0.439	0.26282	0.01196	78426	269100	16.056	14.736	3.1692	20.6	127.3	66.0	429.8	3.0	9.4
9000	175610	147.34	250	0.447	0.26273	0.01195	78322	261700	15.689	14.324	3.1360	21.0	148.2	66.1	495.9	3.1	11.1
10000	175544	149.66	250	0.456	0.26263	0.01193	78215	254320	15.310	14.571	3.1044	21.1	169.3	65.8	561.7	3.1	12.8
10000	175415	191.57	320	0.583	0.16018	0.00952	102269	230060	14.231	13.139	3.0762	48.4	217.7	149.6	711.3	8.3	17.2
11000	175344	194.61	320	0.595	0.16011	0.00950	102073	223860	13.783	11.538	3.0400	24.7	242.4	75.5	786.9	4.8	19.8
12000	175264	197.73	320	0.607	0.16004	0.00949	101874	217780	13.334	11.217	3.0174	26.8	269.2	81.1	868.0	5.2	22.6
13000	175183	200.92	320	0.619	0.15996	0.00947	101673	211820	12.882	10.369	2.9596	28.2	297.5	84.4	952.4	5.6	25.7
14000	175096	204.19	320	0.631	0.15989	0.00945	101471	206800	12.525	10.312	2.9020	29.5	327.0	86.4	1038.8	6.0	28.9
15000	175011	207.53	320	0.644	0.15981	0.00943	101272	201180	12.081	10.840	2.8458	28.8	355.8	82.8	1121.6	5.9	32.1
16000	174932	210.96	320	0.657	0.15974	0.00941	101080	195688	11.634	9.348	2.7908	30.2	386.0	85.1	1206.7	6.3	35.5

17000	174842	214.47	320	0.671	0.15965	0.00939	100897	190336	11.187	8.870	2.7368	33.5	419.4	92.5	1299.2	7.1	39.3
18000	174749	218.06	320	0.685	0.15957	0.00938	100732	184800	10.698	9.387	2.6840	33.4	452.8	90.5	1389.7	7.2	43.2
19000	174663	221.75	320	0.699	0.15949	0.00937	100598	179766	10.249	8.918	2.6320	33.3	486.1	88.5	1478.2	7.3	47.2
20000	174574	225.53	320	0.714	0.15941	0.00936	100512	174826	9.790	7.420	2.5810	37.3	523.4	97.3	1575.4	8.3	51.7
21000	174469	229.40	320	0.729	0.15931	0.00936	100501	170000	9.318	7.958	2.5310	39.6	563.1	101.3	1676.8	9.0	56.6
22000	174373	233.38	320	0.744	0.15923	0.00937	100613	165186	8.813	7.449	2.4816	39.6	602.6	99.2	1775.9	9.2	61.5
23000	174272	237.45	320	0.761	0.15913	0.00940	100914	160408	8.266	6.910	2.4326	42.5	645.1	104.3	1880.3	10.0	66.9
24000	174166	241.63	320	0.777	0.15904	0.00945	101512	155216	7.598	6.277	2.3824	46.2	691.3	111.3	1991.5	11.1	72.9
25000	174051	245.92	320	0.794	0.15893	0.00955	102576	150790	6.947	5.667	2.3358	51.0	742.4	120.4	2111.9	12.4	79.6
26000	173927	250.32	320	0.812	0.15882	0.00972	104373	146024	6.113	4.920	2.2886	57.6	799.9	133.1	2245.1	14.3	87.3
26460	173862	252.39	320	0.820	0.15876	0.00983	105554	144058	5.700	4.558	2.2680	29.6	829.5	67.4	2312.5	7.4	91.3
26460	173862	252.38	320	0.820	0.15876	0.00983	105553	144058	5.700	5.700	2.2680	0.0	829.5	0.0	2312.5	0.0	91.3
27000	173797	251.81	316	0.820	0.16254	0.00989	103741	141912	5.640	6.484	2.2330	27.0	856.5	60.8	2373.3	6.8	95.0
28000	173694	250.75	309	0.820	0.16985	0.01002	100521	137972	5.513	5.513	2.1688	50.8	907.3	111.8	2485.1	12.8	101.9
29000	173575	249.68	302	0.820	0.17754	0.01017	97473	134122	5.376	6.181	2.1058	52.1	959.5	111.4	2596.5	13.0	108.9
30000	173473	248.60	296	0.820	0.18566	0.01032	94600	130082	5.185	5.185	2.0398	53.6	1013.1	111.2	2707.7	13.4	116.1
31000	173355	247.52	289	0.820	0.19421	0.01050	91894	125932	4.956	5.698	1.9751	56.0	1069.1	112.4	2820.2	13.9	123.6
32000	173251	246.44	282	0.820	0.20326	0.01069	89359	121938	4.726	5.433	1.9116	54.8	1123.9	106.4	2926.6	13.5	130.9
33000	173146	245.35	276	0.820	0.21281	0.01090	86992	118032	4.485	5.157	1.8495	57.6	1181.5	108.3	3034.8	14.2	138.6
34000	173038	244.26	269	0.820	0.22290	0.01114	84793	114218	4.235	4.870	1.7890	60.8	1242.3	110.6	3145.4	14.9	146.6
35000	172928	243.16	263	0.820	0.23357	0.01140	82761	110484	3.975	3.975	1.7298	68.9	1311.2	121.3	3266.7	16.8	155.7

F.2 Cruise Performance Calculation

Step-climb cruise: 35000ft-39000ft; M=0.82

Alt (ft)	W_i (kg)	W_f (kg)	TAS (m/s)	EAS (m/s)	M	C_L	C_D	Drag (N)	Δt (s)	$\sum\Delta t$ (s)	ΔFF (kg)	$\sum\Delta FF$ (kg)	ΔR (nm)	$\sum\Delta R$ (nm)
35000	172928	171974	243.16	135.36	0.82	0.23357	0.01140	82761	0	0	954.2	954.2	100	100
35000	171974	171022	243.16	135.36	0.82	0.23228	0.01137	82527	761.6	761.6	951.5	1905.7	100	200
35000	171022	170073	243.16	135.36	0.82	0.23100	0.01133	82296	761.6	1523.3	948.8	2854.6	100	300
35000	170073	169127	243.16	135.36	0.82	0.22971	0.01130	82067	761.6	2284.9	946.2	3800.8	100	400
35000	169127	168184	243.16	135.36	0.82	0.22844	0.01127	81839	761.6	3046.6	943.6	4744.3	100	500
35000	168184	167243	243.16	135.36	0.82	0.22716	0.01124	81614	761.6	3808.2	941.0	5685.3	100	600
35000	167243	166304	243.16	135.36	0.82	0.22589	0.01121	81390	761.6	4569.9	938.4	6623.7	100	700
35000	166304	165369	243.16	135.36	0.82	0.22462	0.01118	81168	761.6	5331.5	935.8	7559.5	100	800
35000	165369	164435	243.16	135.36	0.82	0.22336	0.01115	80948	761.6	6093.1	933.3	8492.7	100	900
35000	164435	163505	243.16	135.36	0.82	0.22210	0.01112	80730	761.6	6854.8	930.7	9423.5	100	1000
35000	163505	162576	243.16	135.36	0.82	0.22084	0.01109	80514	761.6	7616.4	928.2	10351.7	100	1100
35000	162576	161651	243.16	135.36	0.82	0.21959	0.01106	80299	761.6	8378.1	925.8	11277.5	100	1200
35000	161651	160727	243.16	135.36	0.82	0.21834	0.01103	80087	761.6	9139.7	923.3	12200.8	100	1300
35000	160727	159806	243.16	135.36	0.82	0.21709	0.01100	79876	761.6	9901.4	920.9	13121.6	100	1400
35000	159806	158888	243.16	135.36	0.82	0.21585	0.01097	79667	761.6	10663.0	918.4	14040.0	100	1500
35000	158888	157972	243.16	135.36	0.82	0.21461	0.01094	79459	761.6	11424.7	916.0	14956.1	100	1600
35000	157972	157058	243.16	135.36	0.82	0.21337	0.01092	79254	761.6	12186.3	913.7	15869.7	100	1700
35000	157058	156147	243.16	135.36	0.82	0.21214	0.01089	79050	761.6	12947.9	911.3	16781.0	100	1800
35000	156147	155238	243.16	135.36	0.82	0.21090	0.01086	78847	761.6	13709.6	909.0	17690.0	100	1900
35000	155238	154331	243.16	135.36	0.82	0.20968	0.01083	78647	761.6	14471.2	906.6	18596.6	100	2000

35000	154331	153427	243.16	135.36	0.82	0.20845	0.01080	78448	761.6	15232.9	904.3	19501.0	100	2100
35000	153427	152525	243.16	135.36	0.82	0.20723	0.01078	78251	761.6	15994.5	902.1	20403.0	100	2200
35000	152525	151625	243.16	135.36	0.82	0.20601	0.01075	78055	761.6	16756.2	899.8	21302.8	100	2300
35000	151625	150728	243.16	135.36	0.82	0.20480	0.01072	77861	761.6	17517.8	897.5	22200.4	100	2400
35000	150728	149832	243.16	135.36	0.82	0.20358	0.01070	77669	761.6	18279.4	895.3	23095.7	100	2500
35000	149832	148939	243.16	135.36	0.82	0.20238	0.01067	77478	761.6	19041.1	893.1	23988.8	100	2600
35000	148939	148048	243.16	135.36	0.82	0.20117	0.01065	77289	761.6	19802.7	890.9	24879.7	100	2700
35000	148048	147160	243.16	135.36	0.82	0.19997	0.01062	77102	761.6	20564.4	888.8	25768.5	100	2800
35000	147160	146273	243.16	135.36	0.82	0.19877	0.01059	76916	761.6	21326.0	886.6	26655.0	100	2900
35000	146273	145389	243.16	135.36	0.82	0.19757	0.01057	76731	761.6	22087.7	884.5	27539.5	100	3000
35000	145389	144506	243.16	135.36	0.82	0.19637	0.01054	76548	761.6	22849.3	882.3	28421.9	100	3100
35000	144506	143626	243.16	135.36	0.82	0.19518	0.01052	76367	761.6	23611.0	880.2	29302.1	100	3200
35000	143626	142748	243.16	135.36	0.82	0.19399	0.01049	76187	761.6	24372.6	878.2	30180.3	100	3300
35000	142748	141872	243.16	135.36	0.82	0.19281	0.01047	76009	761.6	25134.2	876.1	31056.4	100	3400
39000	141872	141083	241.96	122.97	0.82	0.23218	0.01136	68097	761.6	25895.9	789.0	31845.4	100	3500
39000	141083	140296	241.96	122.97	0.82	0.23089	0.01133	67905	765.4	26661.3	786.8	32632.2	100	3600
39000	140296	139511	241.96	122.97	0.82	0.22960	0.01130	67715	765.4	27426.7	784.6	33416.8	100	3700
39000	139511	138729	241.96	122.97	0.82	0.22831	0.01127	67527	765.4	28192.2	782.4	34199.2	100	3800
39000	138729	137949	241.96	122.97	0.82	0.22703	0.01124	67340	765.4	28957.6	780.2	34979.4	100	3900
39000	137949	137171	241.96	122.97	0.82	0.22576	0.01121	67154	765.4	29723.0	778.1	35757.5	100	4000
39000	137171	136395	241.96	122.97	0.82	0.22448	0.01118	66971	765.4	30488.4	775.9	36533.4	100	4100
39000	136395	135621	241.96	122.97	0.82	0.22321	0.01115	66788	765.4	31253.8	773.8	37307.2	100	4200
39000	135621	134849	241.96	122.97	0.82	0.22195	0.01112	66608	765.4	32019.3	771.7	38078.9	100	4300
39000	134849	134079	241.96	122.97	0.82	0.22068	0.01109	66428	765.4	32784.7	769.6	38848.6	100	4400
39000	134079	133312	241.96	122.97	0.82	0.21942	0.01106	66251	765.4	33550.1	767.6	39616.2	100	4500

39000	133312	132546	241.96	122.97	0.82	0.21817	0.01103	66074	765.4	34315.5	765.5	40381.7	100	4600
39000	132546	131783	241.96	122.97	0.82	0.21692	0.01100	65900	765.4	35081.0	763.5	41145.2	100	4700
39000	131783	131021	241.96	122.97	0.82	0.21567	0.01097	65726	765.4	35846.4	761.5	41906.6	100	4800
39000	131021	130262	241.96	122.97	0.82	0.21442	0.01094	65555	765.4	36611.8	759.5	42666.1	100	4900
39000	130262	129504	241.96	122.97	0.82	0.21318	0.01091	65384	765.4	37377.2	757.5	43423.6	100	5000
39000	129504	128749	241.96	122.97	0.82	0.21194	0.01088	65215	765.4	38142.7	755.5	44179.1	100	5100
39000	128749	127995	241.96	122.97	0.82	0.21070	0.01086	65048	765.4	38908.1	753.6	44932.7	100	5200
39000	127995	127244	241.96	122.97	0.82	0.20947	0.01083	64882	765.4	39673.5	751.7	45684.4	100	5300
39000	127244	126494	241.96	122.97	0.82	0.20824	0.01080	64717	765.4	40438.9	749.7	46434.1	100	5400
39000	126494	125746	241.96	122.97	0.82	0.20701	0.01077	64554	765.4	41204.3	747.8	47181.9	100	5500
39000	125746	125000	241.96	122.97	0.82	0.20579	0.01075	64392	765.4	41969.8	746.0	47927.9	100	5600
39000	125000	124256	241.96	122.97	0.82	0.20457	0.01072	64231	765.4	42735.2	744.1	48672.0	100	5700
39000	124256	123514	241.96	122.97	0.82	0.20335	0.01069	64072	765.4	43500.6	742.2	49414.2	100	5800
39000	123514	122773	241.96	122.97	0.82	0.20213	0.01067	63914	765.4	44266.0	740.4	50154.6	100	5900
39000	122773	122035	241.96	122.97	0.82	0.20092	0.01064	63757	765.4	45031.5	738.6	50893.2	100	6000
39000	122035	121298	241.96	122.97	0.82	0.19971	0.01061	63602	765.4	45796.9	736.8	51630.0	100	6100
39000	121298	120563	241.96	122.97	0.82	0.19851	0.01059	63448	765.4	46562.3	735.0	52364.9	100	6200
39000	120563	119830	241.96	122.97	0.82	0.19731	0.01056	63295	765.4	47327.7	733.2	53098.1	100	6300
39000	119830	119098	241.96	122.97	0.82	0.19611	0.01054	63144	765.4	48093.1	731.4	53829.6	100	6400
39000	119098	118369	241.96	122.97	0.82	0.19491	0.01051	62994	765.4	48858.6	729.7	54559.3	100	6500
39000	118369	117641	241.96	122.97	0.82	0.19371	0.01049	62845	765.4	49624.0	728.0	55287.2	100	6600
39000	117641	116915	241.96	122.97	0.82	0.19252	0.01046	62698	765.4	50389.4	726.2	56013.5	100	6700
39000	116915	116190	241.96	122.97	0.82	0.19133	0.01044	62552	765.4	51154.8	724.5	56738.0	100	6800
39000	116190	115467	241.96	122.97	0.82	0.19015	0.01041	62407	765.4	51920.3	722.9	57460.8	100	6900
39000	115467	114746	241.96	122.97	0.82	0.18897	0.01039	62263	765.4	52685.7	721.2	58182.0	100	7000

F.3 Descent Performance Calculation

Alt (ft)	Weight (kg)	TAS (m/s)	EAS (m/s)	M	C_L	C_D	Drag (N)	Thrust (N)	ROD_0 (m/s)	ROD_a (m/s)	FF (kg/s)	Δt (s)	$\sum\Delta t$ (s)	ΔF (kg)	$\sum\Delta F$ (kg)	Δs (km)	$\sum\Delta s$ (nm)
39000	114746	241.79	239	0.819	1.03107	0.06536	71328	6039	14.029	10.176	0.1183	0	0	0	0	0	0
38000	114743	237.67	241	0.805	1.01698	0.06381	70606	6380	13.566	10.058	0.1234	30.1	30.1	3.6	3.6	7.2	3.9
37000	114741	233.04	242	0.790	1.00815	0.06286	70154	6683	13.146	8.021	0.1284	33.7	63.8	4.2	7.9	7.9	8.2
36000	114738	228.93	243	0.776	0.99647	0.06160	69561	7046	12.719	8.009	0.1338	38.0	101.9	5.0	12.9	8.8	12.9
35000	114734	224.81	243	0.758	0.99405	0.06134	69436	7263	12.422	8.037	0.1370	38.0	139.9	5.1	18.0	8.6	17.6
34000	114731	220.70	243	0.741	0.99261	0.06119	69362	7521	12.130	8.055	0.1405	37.9	177.7	5.3	23.3	8.4	22.1
33000	114727	217.10	244	0.726	0.98754	0.06065	69103	7778	11.833	8.042	0.1439	37.9	215.6	5.4	28.7	8.3	26.6
32000	114724	212.98	244	0.709	0.98808	0.06071	69128	8035	11.565	8.049	0.1474	37.9	253.5	5.5	34.2	8.1	31.0
31000	114720	209.38	244	0.694	0.98483	0.06037	68963	8303	11.289	8.025	0.1510	37.9	291.4	5.7	39.8	8.0	35.3
30000	114716	205.78	245	0.679	0.98251	0.06012	68843	8578	11.023	7.996	0.1545	38.0	329.5	5.8	45.6	7.9	39.6
29000	114711	202.69	245	0.666	0.97614	0.05946	68521	8861	10.750	7.939	0.1581	38.3	367.7	6.0	51.6	7.8	43.8
28000	114707	199.60	246	0.653	0.97054	0.05887	68237	9143	10.486	7.878	0.1618	38.5	406.3	6.2	57.8	7.7	48.0
27000	114702	196.52	247	0.640	0.96574	0.05838	67994	9432	10.231	7.813	0.1655	38.9	445.1	6.4	64.2	7.7	52.1
26000	114697	193.43	247	0.627	0.96174	0.05796	67792	9700	9.990	7.748	0.1691	39.2	484.3	6.6	70.7	7.6	56.2
25000	114692	190.34	248	0.615	0.95852	0.05763	67628	9974	9.757	7.680	0.1727	39.5	523.8	6.8	77.5	7.6	60.3
24000	114686	187.26	248	0.602	0.95608	0.05738	67504	10234	9.535	6.914	0.1762	41.8	565.6	7.3	84.7	7.9	64.6
23000	114681	184.17	248	0.590	0.95444	0.05722	67419	10513	9.319	7.539	0.1799	42.2	607.8	7.5	92.3	7.8	68.8
22000	114675	181.08	248	0.578	0.95362	0.05713	67374	10800	9.110	7.464	0.1835	40.6	648.4	7.4	99.6	7.4	72.8
21000	114668	178.00	248	0.565	0.95362	0.05713	67371	11079	8.910	6.809	0.1873	42.7	691.1	7.9	107.6	7.7	77.0
20000	114662	174.91	248	0.553	0.95443	0.05722	67407	11364	8.718	7.313	0.1910	43.2	734.3	8.2	115.7	7.6	81.1
19000	114655	171.82	248	0.542	0.95612	0.05739	67487	11655	8.532	7.235	0.1948	41.9	776.2	8.1	123.8	7.3	85.0
18000	114648	168.74	248	0.530	0.95867	0.05765	67610	11924	8.357	7.161	0.1987	42.3	818.5	8.3	132.1	7.2	88.9

17000	114641	166.17	248	0.520	0.95617	0.05739	67481	12240	8.165	7.058	0.2027	42.9	861.4	8.6	140.7	7.2	92.8
16000	114633	163.59	248	0.510	0.95438	0.05721	67388	12547	7.981	6.958	0.2065	43.5	904.9	8.9	149.6	7.2	96.6
15000	114625	161.02	248	0.500	0.95332	0.05710	67330	12817	7.809	6.471	0.2102	45.4	950.3	9.5	159.1	7.4	100.6
14000	114617	158.45	248	0.490	0.95296	0.05707	67308	13105	7.641	6.400	0.2138	47.4	997.6	10.0	169.1	7.6	104.7
13000	114608	155.88	248	0.480	0.95335	0.05710	67322	13354	7.485	6.334	0.2174	47.9	1045.5	10.3	179.5	7.5	108.7
12000	114599	153.82	249	0.472	0.94810	0.05657	67057	13616	7.314	6.245	0.2210	48.5	1094.0	10.6	190.1	7.5	112.8
11000	114590	151.76	250	0.464	0.94345	0.05610	66821	13884	7.149	6.454	0.2246	48.0	1142.0	10.7	200.8	7.3	116.7
10000	114581	149.70	250	0.454	0.94588	0.05635	66936	14169	7.006	6.086	0.2283	48.6	1190.6	11.0	211.8	7.3	120.7
9000	114570	147.13	250	0.446	0.94246	0.05600	66761	14445	6.851	5.996	0.2320	50.5	1241.1	11.6	223.4	7.5	124.7
8000	114560	145.07	250	0.437	0.94634	0.05639	66947	14714	6.721	5.930	0.2357	51.1	1292.2	12.0	235.4	7.4	128.7
7000	114549	142.50	249	0.429	0.94418	0.05617	66833	14987	6.577	6.068	0.2395	50.8	1343.0	12.1	247.4	7.3	132.7
6000	114538	140.44	250	0.421	0.94264	0.05602	66751	15275	6.436	5.755	0.2436	51.6	1394.5	12.5	259.9	7.3	136.6
5000	114526	138.39	250	0.414	0.94171	0.05592	66698	15580	6.298	5.667	0.2476	53.4	1447.9	13.1	273.0	7.4	140.6
4000	114514	136.33	250	0.406	0.94138	0.05589	66675	15819	6.174	5.770	0.2516	53.3	1501.2	13.3	286.3	7.3	144.6
3000	114502	134.27	250	0.399	0.94169	0.05592	66683	16045	6.055	5.681	0.2557	53.2	1554.4	13.5	299.8	7.2	148.5
2000	114489	132.21	250	0.391	0.94264	0.05602	66722	16308	5.937	5.431	0.2598	54.9	1609.3	14.1	313.9	7.3	152.4
1000	114475	130.15	249	0.382	0.95175	0.05694	67165	16573	5.842	5.375	0.2639	56.4	1665.7	14.8	328.7	7.4	156.4
0	114462	128.61	250	0.378	0.93896	0.05565	66525	16820	5.695	5.259	0.2681	57.3	1723.0	15.2	343.9	7.4	160.4

Appendix G Nacelle Design

G.1 Reynolds Number

The Reynolds number per foot run, Re_{ft} at a cruise condition can be estimated using Equation G-1[33].

$$\mathrm{Re_{ft}} = 7.086\mathrm{M}[1-(1.98\mathrm{H}/288)]^{4.016} \times 10^{6} \quad \textbf{(G-1)}$$

Where, H is the flight altitude in thousands of feet.

Then, the Reynolds number, Re, for a chosen reference length, L, can be obtained as Re_{ft} multiply the length L in feet.

$$\mathrm{Re} = \mathrm{Re_{ft}} \times \mathrm{L} \quad \textbf{(G-2)}$$

G.2 Nacelle Dimensions Calculation

1) Throat diameter, D_{th}, and highlight diameter, D_{hl}

The top of the climb (TOC) conditions of GTF-11 is summarized in Table G-1.

Table G-1 Conditions at top of the climb

Altitude (m)	10668
Mach Number	0.82
ISA Deviation (℃)	0
TET (K)	1660
Mass Flow (kg/s)	381.83

Assume that throat Mach number, M_{th}, is 0.72, the throat area, A_{th}, can be calculated using Equation G-3 [27].

$$\frac{\dot{\mathrm{m}}\sqrt{\mathrm{T_t}}}{\mathrm{P_t A_{th}}} = \mathrm{M}\sqrt{\frac{\gamma}{\mathrm{R}}}\left(1+\frac{\gamma-1}{2}\mathrm{M}^2\right)^{\frac{\gamma+1}{2(1-\gamma)}} \quad \textbf{(G-3)}$$

Therefore, the throat diameter, D_{th}, is 2.349m. As the contraction ratio, A_{hl}/A_{th}, is 1.28, the nacelle highlight area, A_{hl}, of 5.549m^2 and highlight diameter, D_{hl}, of 2.658m can be obtained.

Similarly, the capture area A_0 at cruise condition can be calculated as 4.134m^2. Then, the mass flow ratio, MFR, at cruise condition can be conducted as:

$$\mathrm{MFR} = \mathrm{A_0/A_{hl}} = 4.134/5.549 = 0.745$$

2) Fore-body length, L_f, and maximum diameter, D_{max}

As MFR_{crit} is 0.55 and M_d is 0.9, D_{hl}/D_{max} of 0.80 and L_f/D_{max} of 0.75 can be obtained from Figure 6-3. Then, L_f is 2.489m and D_{max} is 3.321m.

3) The shape of inlet lip

For ellipse sharp inlet lip:

$$\mathrm{b} = (\mathrm{D_{hl}} - \mathrm{D_{th}})/2 = 0.154\mathrm{m}$$

$$\mathrm{a} = 2\mathrm{b} = 0.308\mathrm{m}$$

The corresponding equation is:

$$(\mathrm{x}/0.308)^2 + (\mathrm{y}/0.154)^2 = 1 \qquad \textbf{(G-4)}$$

4) External contour

In which, $\mathrm{X} = \mathrm{L_f} = 2.489\mathrm{m}$; $\mathrm{Y} = (\mathrm{D_{max}} - \mathrm{D_{hl}})/2 = 0.331\mathrm{m}$.

5) Boat-tail radius, R_a, and

Knowing the after-body drag rise Mach number, $M_{d,a}$, is 0.9 and D_{max} is 3.321m, the boat-tail radius, R_a, can be obtained as:

$$\mathrm{R_a} = 0.04\mathrm{D_{max}}/\left(1 - \mathrm{M_{d,a}}\right)^2 = 13.28\,\mathrm{m}$$

6) After-body length, L_a, and nozzle-exit diameter, D_9

As R_{ld} is 1.45, the overall length of nacelle, L_{ov}, of 4.815m can be got and corresponding after-body length, L_a, is 2.327m. Then the nozzle-exit diameter, D_9, is 2.750m based on after-body chord angle, β_c, is 7°

$$\mathrm{D_9} = \mathrm{D_{max}} - 2\mathrm{L_a} \times \tan\beta_c = 2.750\mathrm{m}$$

G.3 Nacelle Drag Coefficient Calculation

Table G-2 Nacelle drag coefficient calculation of GTF-11(M=0.82)

QUANTITIES INDEPENDENT OF M_0 AND MFR							
Factor used in evaluation of MFR_{crit}, S				1			
Critical flow area ratio, MFR_{crit}				0.5302			
Fore-body surface area coefficient, CSf				0.9651			
After-body surface area coefficient, CSa				0.952			
Parameter, A_{sur}/A_{max}				5.5603			
K0=1.0157		K1=0.6665		K2=1.0000			
K3=0.1712		K7=0.6808		K10 =1.0000			
R_a/D_{max}=2.8985		Δ MDf=0.0509		MDfdash =0.9080			
M_0= 0.8200							
QUANTITIES DEPENDENT ON M_0 AND INDEPENDENT OF MFR							
Choking flow area ratio, MFR_{ch}				0.8051			
Flat plate mean skin friction coefficient, CF				0.0024			
$MFR<MFR_{crit}$				$MFR>=MFR_{crit}$			
MFR	0.300	0.400	0.500	0.530 *	0.600	0.700	0.800
M_d	0.8225	0.8375	0.8525	0.857	0.857	0.857	0.857
K	2.4892	2.4892	2.4892	2.4892	2.1933	1.777	1.4379
λ0	1.3694	1.3694	1.3694	1.3694	1.321	1.2541	1.2007
λ1	1.2462	1.2462	1.2462	1.2462	1.214	1.1694	1.1337
K4	1.0957	1.0957	1.0957	1.0957	1.0803	1.0609	1.0464
Δλ	0.1786	0.1786	0.1786	0.1786	0.1761	0.1729	0.1706
K5	1.0746	0.8497	0.6934	0.6558	0.6558	0.6558	0.6558
λ3	1.5636	1.5346	1.5144	1.5095	1.4619	1.3972	1.3464
λ2	1.5636	1.5346	1.5144	1.5095	1.4619	1.3972	1.3464
CDp	0.0205	0.0201	0.0198	0.0197	0.0191	0.0183	0.0176
K6	0.3158	0.1700	0.0354				
K8	0.5341	0.5341	0.5341				
K9	1.0000	1.0000	1.0000				
Cpφ	0.6457	0.4979	0.3658				
ΔCDs	0.0475	0.0197	0.0030	0.0000	0.0000	0.0000	0.0000
ΔCDw	0.0000	0.0000	0.0000	0.0000	0.0000	0.0000	0.0000
CD	0.0680	0.0398	0.0228	0.0198	0.0191	0.0183	0.0176
*Critical value							

Table G-3 Nacelle drag coefficient calculation of GTF-11(M=0.184)

QUANTITIES INDEPENDENT OF M_0 AND MFR							
Factor used in evaluation of MFR_{crit}, S				1			
Critical flow area ratio, MFR_{crit}				0.5302			
Fore-body surface area coefficient, CSf				0.9651			
After-body surface area coefficient, CSa				0.952			
Parameter, A_{sur}/A_{max}				5.5603			
K0=1.0157		K1=0.6665		K2=1.0000			
K3=0.1712		K7=0.6808		K10=1.0000			
R_a/D_{max}=2.8985		∆ MDf=0.0509		MDfdash=0.9080			
M_0=0.1840							
QUANTITIES DEPENDENT ON M_0 AND INDEPENDENT OF MFR							
Choking flow area ratio, MFR_{ch}				2.5074			
Flat plate mean skin friction coefficient, CF				0.0025			
$MFR<MFR_{crit}$				$MFR>=MFR_{crit}$			
MFR	0.300	0.400	0.500	0.530 *	0.600	0.700	0.800
M_d	0.8225	0.8375	0.8525	0.857	0.857	0.857	0.857
K	2.4892	2.4892	2.4892	2.4892	2.1933	1.777	1.4379
λ0	1.3694	1.3694	1.3694	1.3694	1.321	1.2541	1.2007
λ1	1.2462	1.2462	1.2462	1.2462	1.214	1.1694	1.1337
K4	1.0957	1.0957	1.0957	1.0957	1.0803	1.0609	1.0464
Δλ	0.1786	0.1786	0.1786	0.1786	0.1761	0.1729	0.1706
K5	0.0000	0.0000	0.0000	0.0000	0.0000	0.0000	0.0000
λ3	1.4248	1.4248	1.4248	1.4248	1.3901	1.3423	1.3043
λ2	1.4248	1.4248	1.4248	1.4248	1.3901	1.3423	1.3043
CDp	0.0196	0.0196	0.0196	0.0196	0.0191	0.0185	0.0179
K6	0.3158	0.1700	0.0354				
K8	1.0000	1.0000	1.0000				
K9	1.0000	1.0000	1.0000				
Cpφ	0.4971	0.3660	0.2548				
ΔCDs	0.0684	0.0271	0.0039	0.0000	0.0000	0.0000	0.0000
ΔCDw	0.0000	0.0000	0.0000	0.0000	0.0000	0.0000	0.0000
CD	0.08805	0.04674	0.02353	0.01960	0.01912	0.01846	0.01794
*Critical value							

Table G-4 Nacelle drag coefficient calculation of GTF-11(M=0.217)

QUANTITIES INDEPENDENT OF M_0 AND MFR							
Factor used in evaluation of MFR_{crit}, S				1			
Critical flow area ratio, MFR_{crit}				0.5302			
Fore-body surface area coefficient, CSf				0.9651			
After-body surface area coefficient, CSa				0.952			
Parameter, A_{sur}/A_{max}				5.5603			
K0=1.0157		K1=0.6665		K2=1.0000			
K3=0.1712		K7=0.6808		K10=1.0000			
R_a/D_{max}=2.8985		∆ MDf=0.0509		MDfdash=0.9080			
M_0= 0.217							
QUANTITIES DEPENDENT ON M_0 AND INDEPENDENT OF MFR							
Choking flow area ratio, MFR_{ch}				2.1429			
Flat plate mean skin friction coefficient, CF				0.0025			
$MFR<MFR_{crit}$				$MFR>=MFR_{crit}$			
MFR	0.300	0.400	0.500	0.530 *	0.600	0.700	0.800
M_d	0.8225	0.8375	0.8525	0.857	0.857	0.857	0.857
K	2.4892	2.4892	2.4892	2.4892	2.1933	1.777	1.4379
λ0	1.3694	1.3694	1.3694	1.3694	1.321	1.2541	1.2007
λ1	1.2462	1.2462	1.2462	1.2462	1.214	1.1694	1.1337
K4	1.0957	1.0957	1.0957	1.0957	1.0803	1.0609	1.0464
Δλ	0.1786	0.1786	0.1786	0.1786	0.1761	0.1729	0.1706
K5	0.0000	0.0000	0.0000	0.6558	0.6558	0.6558	0.6558
λ3	1.4248	1.4248	1.4248	1.5095	1.4619	1.3972	1.3464
λ2	1.4248	1.4248	1.4248	1.5095	1.4619	1.3972	1.3464
CDp	0.0196	0.0196	0.0196	0.0197	0.0191	0.0183	0.0176
K6	0.3158	0.1700	0.0354				
K8	1.0000	1.0000	1.0000				
K9	1.0000	1.0000	1.0000				
Cpφ	0.4998	0.3684	0.2567				
ΔCDs	0.0688	0.0273	0.0040	0.0000	0.0000	0.0000	0.0000
ΔCDw	0.0000	0.0000	0.0000	0.0000	0.0000	0.0000	0.0000
CD	0.08841	0.04689	0.02354	0.0196	0.0191	0.0184	0.0179
*Critical value							